ELECTROCHEMICAL PROMOTION OF GOLD NANOPARTICLES SUPPORTED ON YTTRIA-STABILIZED ZIRCONIA

By

Jong Min Kim

A thesis submitted to the Faculty of Graduate and Postdoctoral Studies in partial fulfillment of the requirements for the degree of

Master of Applied Science

In

Department of Chemical and Biological Engineering

Faculty of Engineering

University of Ottawa

© Jong Min Kim, Ottawa, Canada, 2011

Acknowledgements

I would like to thank my supervisors, Dr. Elena Baranova for the great mentorship and continued encouragement through my research. Without her guidance, I could not be able to complete my thesis - she has provided inspiring suggestions and the best research environment.

There are many people to thank for their help on characterizations of materials and diagnosis of my experiments: Dr. Yun Liu for SEM, TEM and EDX and Dr. Sadok Lataief for TGA, Sander Mommers for XPS from the Center for Catalysis Research and Innovation (CCRI) uOttawa and the staffs at NRC for the additional characterizations of SEM, TEM and XRD.

Many thanks are sent to my colleagues at the Laboratory of Electrochemical Engineering in University of Ottawa. Chae-Ho introduced me to Dr. Baranova to do my Masters program as well as provided me with continuous guide on my research physically and emotionally. Holly has done a part of the CO oxidation experiments on Au nanoparticles in Institut de Recherches sur la Catalyse et l'Environnement de Lyon (IRCELYON), France. I would also like to thank colleagues from IRCELYON, Lyon France: Dr. Philippe Vernoux and Dr. Leonardo Lezarraga for help with CO oxidation measurements. I would like to thank Rima Isafan for XRD, Alexandra Tavasoli for gold nanoparticle synthesis and Michelle Fee, Daniel Martin, Audrey Calley, Thegy Lomosco, and Jihad Arafa for open discussion on electrochemistry. All the experimental setups would not have been installed without the assistance from Louis Tremblay, Gérard Nina and Franco Ziroldo. Their continuous support is highly appreciated.

This thesis would not be possible without the financial support from NSERC (Natural Science and Engineering Research Council Canada).

Without my family, I could not be doing what I am doing. They have been supportive of everything that I do and have always been there for me – 'loving wife' Mira Kim, 'best parents in the world' Sang Bog Kim and In Young Kim, and 'forever friendly rivalry and mentor' Jong Ho Kim.

Finally, I thank God for protecting me and believing in me.

나를 위해 늘 곁에서 웃어주는 나의 사랑하는 아내, 모든것을 아낌없이 주실줄만 아는 나의 사랑하는 부모님, 인생의 선배이자 제일 친한 친구인 형, 친부모님처럼 대해주시는 장인, 장모님께 이 논문을 바칩니다.

Abstract

The feasibility of highly dispersed gold nanocatalyst supported on yttria-stabilized zirconia (YSZ) for the model reactions of C_2H_4 and CO oxidation is demonstrated for the first time. Gold nanoparticles are synthesized on YSZ powder by chemical reduction of the precursor salt in the mixture of ethanol, water and polyvinylpyrrolidone (PVP). Resulting metal loading of the catalysts are 1 wt.% with average particle sizes ranging from 6 to 9 nm. Results of CO and C_2H_4 oxidation display catalytic activity at 65 ^{0}C and 25 ^{0}C for CO and C_2H_4 oxidation, respectively. The catalytic properties of the catalysts are different due to their average particle size. Electrochemical Promotion of Catalysis (EPOC) of C_2H_4 oxidation is demonstrated. Application of constant potential difference between two electrodes in the bipolar electrochemical cell led to increase in C_2H_4 conversion. A proposed mechanism explains the bipolar EPOC phenomenon through formation of O^{2-} flux across the electrochemical cell, resulting in the change of Work Function of gold nanoparticles placed in between the electrodes and is electronically isolated.

TABLES OF CONTENTS

ACKNOWLEDGEMENTS ..... **II**

ABSTRACT ..... **IV**

LIST OF FIGURES ..... **VIII**

LIST OF TABLES ..... **XII**

CHAPTER 1 INTRODUCTION **1**

1.1 REFERENCE 3

CHAPTER 2 LITERATURE REVIEW **4**

2.1 HETEROGENEOUS CATALYSIS 4

2.1.1 Langmuir-Hinshelwood Reaction Mechanism *5*

2.1.2 Catalysis by Nanoparticles *7*

2.1.3 Gold as Nanocatalyst *9*

2.1.4 Metal Support Interaction *14*

2.2 ELECTROCHEMICAL PROMOTION 19

2.2.1 Definitions and basic quantities involved *19*

2.2.2 The mechanism of electrochemical promotion *23*

2.2.3 Electrochemical cell types *29*

2.2.4 Solid Electrolyte *32*

2.3 COMPLETE OXIDATION OF ETHYLENE 35

2.3.1 Mechanism of complete oxidation of ethylene in open circuit condition *36*

2.3.2 Mechanism of complete oxidation of ethylene using O^{2-} conductors in closed circuit condition *38*

2.4 RESEARCH OBJECTIVES 38

2.5 REFERENCES 40

CHAPTER 3 EXPERIMENTAL **47**

3.1 INTRODUCTION 47

3.2 SYNTHESIS OF GOLD NANOCATALYST 47

3.2.1 Synthesis Method *47*

3.2.2 Removal of PVP *49*

3.3 CHARACTERIZATIONS OF GOLD NANOPARTICLES 49

3.3.1 Scanning Electron Microscopy (SEM) *50*

3.3.2 Transmission Electron Microscopy (TEM) *50*

3.3.3 X-ray Diffraction (XRD) *51*

3.3.4 X-ray Photoelectron Spectroscopy (XPS) *51*

3.3.5 Thermogravimetric Analysis (TGA) *52*

3.4 CATALYTIC MEASUREMENT UNITS 52
3.5 ELECTROCHEMICAL CELLS 56
3.5.1 Bipolar cell configuration of gold nanoparticles 56
3.6 REFERENCES 59

CHAPTER 4 PHYSIOCHEMICAL CHARACTERIZATIONS OF GOLD NANOPARTICLE CATALYSTS 60

4.1 INTRODUCTION 60
4.2 CHARACTERIZATIONS OF AU/YSZ-P 60
4.2.1 TGA 60
4.2.2 SEM 62
4.2.3 TEM 66
4.2.4 XRD 68
4.2.5 XPS 71
4.3 CONCLUSION 75
4.4 REFERENCES 77

CHAPTER 5 CO OXIDATION REACTION ON GOLD NANOPARTICLE CATALYSTS 78

5.1 INTRODUCTION 78
5.2 EXPERIMENTAL 79
5.3 RESULTS AND DISCUSSION 80
5.3.1 Treatment comparison 80
5.3.2 Particle size and stability comparison 82
5.4 CONCLUSION 87
5.5 REFERENCES 88

CHAPTER 6 ETHYLENE OXIDATION ON GOLD NANOPARTICLE CATALYST 90

6.1 INTRODUCTION 90
6.2 EXPERIMENTAL 91
6.2.1 PFR Reaction 91
6.2.2 CSTR Reaction 92
6.3 RESULTS AND DISCUSSION 93
6.3.1 Preliminary PFR Reaction 93
6.3.2 CSTR Reaction 98
6.4 CONCLUSION 101
6.5 REFERENCES 103

CHAPTER 7 ELECTROCHEMICAL PROMOTION OF C_2H_4 COMPLETE OXIDATION WITH GOLD NANOPARTICLE CATALYST 105

7.1 INTRODUCTION 105
7.2 EXPERIMENTAL 107
7.3 RESULTS AND DISCUSSION 108
7.3.1 Experiment at 200 ml min^{-1} 108
7.3.2 Experiment at 80 ml min^{-1} 114
7.3.3 Effect of flow rates 117
7.4 CONCLUSION 122
7.5 REFERENCES 124

CHAPTER 8 CONCLUSIONS AND RECOMMENDATIONS 126

8.1 SYNTHESIS AND PHYSIOCHEMICAL CHARACTERIZATIONS OF GOLD NANOPARTICLE CATALYST 127
8.2 CO OXIDATION REACTION ON GOLD NANOPARTICLE CATALYST 129
8.3 ETHYLENE OXIDATION ON GOLD NANOPARTICLE CATALYST 130
8.4 ELECTROCHEMICAL PROMOTION OF C_2H_4 COMPLETE OXIDATION WITH GOLD NANOPARTICLE CATALYST 131
8.5 REFERENCE 132

LIST OF ABBREVIATIONS AND SYMBOLS 134

List of Figures

Figure 2-1 Surface atomic ratios of terrace and edge together with metal dispersion as a function of particle diameter [2]. 8
Figure 2-2 Electron potentials related to metal electron structure 15
Figure 2-3 Electron potentials related to semiconductor electron structure 17
Figure 2-4 Basic setup of EPOC for ethylene oxidation, using O^{2-} conductor as solid electrolyte. 20
Figure 2-5 Transient effect of EPOC 21
Figure 2-6 Schematic representation of the mechanism of electrochemical promotion by an applied anodic current via back spillover of charged promoting species (O^{2-}). 24
Figure 2-7 Reaction network for oxygen species associated with an electron conductor catalyst (c) on an oxygen-ion (O^{2-})-conducting solid-electrolyte support (s) in contact with an oxygen (O_2)-containing gas phase (g) 25
Figure 2-8 Conventional cell configuration. The catalyst functions as working electrode [96]. 30
Figure 2-9 Examples of single-disk type bipolar configuration [96] 31
Figure 2-10 Electron, hole, and ion conductivities in yttria-stabilized zirconia 33
Figure 2-11 The face centered cubic structure of the zirconia lattice 34
Figure 3-1 Schematics of the synthesis method of Au nanoparticles supported on YSZ-p 48
Figure 3-2 Flow diagram of the experimental setup 53
Figure 3-3 plug flow reactor (A) for heterogeneous catalysis measurements and continuously stirred tank reactor (B) for electrochemical promotion measurements. 55
Figure 3-4 Dimension of the single-disk type bipolar electrochemical cell configuration. A) top view, b) bottom view, c) and d) side view 57
Figure 4-1 TGA of 1 wt. % Au1/YSZ-p prepared at Au:PVP ratio of 3:1 61
Figure 4-2 SEM (BS detector) micrographs of Au1/YSZ-p sample before treatment (A) and after 600 ^{0}C calcination treatment (B) 63
Figure 4-3 (Continued) SEM (BS detector) micrographs of Au1/YSZ-p sample after oxygen plasma etching at 112 RF for 10 minutes (C) 64

Figure 4-4 SEM (BS detector) micrographs of different calcined Au/YSZ-p samples (left) and their particle size distributions (right) 65
Figure 4-5 TEM of calcined Au1/YSZ-p, (A) and Au after support removal using replica technique, (B) (left) and corresponding histograms (right) Molar ratio of Au:PVP = 1:3. 67
Figure 4-6 XRD patterns in the broad range from 28 to 65 $^{0}2\theta$ 68
Figure 4-7 X-ray diffraction patterns of calcined Au1/YSZ-p (a), Au2/YSZ-p (b) and Au3/YSZ-p (c) around Au (111) peak. The numbers indicate the values of the calculated FWHM. 69
Figure 4-8 Representative XPS survey spectrum for Au1/YSZ-p catalyst 71
Figure 4-9 XPS spectra at the gold core level electrons 4f for calcined Au1/YSZ-p (A-1). Thin purple lines correspond to the experimental spectra and other lines correspond to the deconvoluted spectra. 73
Figure 4-10 (Continued) XPS spectra at the gold core level electrons 4f for oxygen plasma etched Au1/YSZ-p (A-2) and calcined Au3/YSZ-p (B). Thin purple lines correspond to the experimental spectra and other lines correspond to the deconvoluted spectra. 74
Figure 5-1 CO oxidation on Au1/YSZ-p (3:1 molar ratio of PVP to Au) after different catalyst treatments. 81
Figure 5-2 Catalytic performance for CO oxidation of Au1/YSZ-p (A, 3:1 molar ratio of PVP to Au) and Au3/YSZ-p (B, 10:1 molar ratio of PVP to Au). 83
Figure 5-3 (Continued) Catalytic performance for CO oxidation of Au4/YSZ-p (C, 20:1 molar ratio of PVP to Au). 84
Figure 5-4 Comparison of catalytic performance for CO oxidation of Au1/YSZ-p, Au3/YSZ-p and Au4/YSZ-p to commecial gold nanocatalyst (Au/γ-Al_2O_3). The second run is compared. 85
Figure 6-1 Open circuit ethylene conversion (black lines) and TOF (grey lines) of Au1/YSZ-p (solid lines) and Au3/YSZ-p (dotted lines) as a function of the partial pressure ratio of ethylene to oxygen at various reaction temperature (A = 25 ^{0}C, B = 100 ^{0}C, C = 200 ^{0}C, D = 250 ^{0}C). Vertical dashed lines indiate critical partial pressure ratio where ethylene conversion changes significantly. Flow rate = 200 ml min^{-1}. 94
Figure 6-2 (Continued) Open circuit ethylene conversion (black lines) and TOF (grey lines) of Au1/YSZ-p (solid lines) and Au3/YSZ-p (dotted lines) as a function of the partial pressure

ratio of ethylene to oxygen at various reaction temperature (E = 275 ^{0}C, F = 300, G = 350 ^{0}C). Vertical dashed lines indiate critical partial pressure ratio where ethylene conversion changes significantly. Flow rate = 200 ml min^{-1}. 95
Figure 6-3 Open circuit ethylene conversion of Au1/YSZ-p and Au3/YSZ-p as a function of the partial pressure of ethylene to oxygen. T = 300, 350 and 400 ^{0}C. Flowrate = 80 ml min^{-1}. 99
Figure 6-4 Open circuit ethylene conversion and turnover frequency of Au1/YSZ-p as a function of the partial pressure ratio of ethylene to oxygen at various temperatures. Flowrate = 200 ml/min. 100
Figure 7-1 Effects of reaction temperature on ethylene conversion and turnover frequency at different potential applications. Gas composition: $P_{C_2H_4}$ = 0.1 kPa and P_{O_2} = 3 kPa. Flow rate: 200 ml min^{-1}. 109
Figure 7-2 Rate enhancement ratio, ρ, as a function of the applied potential. Gas composition: $P_{C_2H_4}$ = 0.1 kPa and P_{O_2} = 3 kPa. Flow rate: 200 ml min^{-1}. 110
Figure 7-3 Response of current on different potential applications as a function of temperature. Gas compositions: $P_{C_2H_4}$ = 0.1 kPa and P_{O_2} = 3 kPa. Flow rate: 200 ml/min. 111
Figure 7-4 Transient effect of applied potential on the ethylene conversion (green points) and catalyst potential (red line) at ethylene partial pressure of 0.1 kPa (A). T = 350℃, P_{O_2} = 3 kPa, flow rate = 200 ml min^{-1} 113
Figure 7-5 (Continued) Transient effect of applied potential on the ethylene conversion (green points) and catalyst potential (red line) at different partial pressure of ethylene (B = 0.2, C = 0.5 kPa). T = 350℃, P_{O_2} = 3 kPa, flow rate = 200 ml min^{-1} 113
Figure 7-6 C_2H_4 conversion of Au1/YSZ-p as function of temperature under (A) fuel-rich and (B) stoichiometry condition. Flow rate = 80 ml min^{-1}. $P_{C_2H_4}$ / P_{O_2} = 1, 0.333 and 0.125, respectively. 115
Figure 7-7 (Continued) C_2H_4 conversion of Au1/YSZ-p as function of temperature under fuel-lean condition (C). Flow rate = 80 ml min^{-1}. $P_{C_2H_4}$ / P_{O_2} = 1, 0.333 and 0.125, respectively. 116

Figure 7-8 Turnover frequency as function of flow rates at different applied potentials. T = 350 ^{0}C. $P_{C_2H_4}$ = 0.1 kPa, P_{O_2} = 3 kPa. 117

Figure 7-9 Proposed mechanism by Xia et al. In-plane polarization of Pt particles result in a bipolar system and leads to the formation of a large number of galvanic cells partially or completely polarized. 119

Figure 7-10 Proposed mechanism of induced bipolar EPOC of gold nanoparticles in complete oxidation of ethylene. Portion of the transported oxygen ions would polarize the gold nanoparticles. 120

List of Tables

Table 2-1 Properties of YSZ 35
Table 3-1 Properties of synthesized Au/YSZ-p catalysts 49
Table 4-1 FWHM, average particle size and dispersion of Au/YSZ-p catalysts from XRD .. 70
Table 4-2 Average particle sizes and dispersions of Au/ YSZ-p samples from SEM, TEM and XRD analysis 76
Table 6-1 Varying parameters for ethylene oxdiation experiment with plug flow reactor. Mass of catalyst = 50 mg. 91
Table 6-2 Varying parameters for ethylene oxdiation experiment with the CSTR reactor. Mass of catalyst = 12 mg. 93
Table 6-3 Calculated activation energy at different reactant partial pressures 97
Table 7-1 EPOC Experimental summary 108

Chapter 1 Introduction

A significant number of heterogeneous catalytic processes are performed by transition-metal catalysts supported on metal oxides. Several of these metals belong to the platinum group and they have been applied to industry for quite some time. However, due to the limited availability of such metals, discovering alternative catalysts has been an ongoing research project for scientists and engineers. Recent development in nanotechnology has opened up a possibility of reducing the amount of catalyst used for improved catalytic activity. In addition, the discovery of electrochemical promotion of catalysis (EPOC) or non-Faradaic electrochemical modification of catalytic activity (NEMCA) effect by Vayenas and co-workers in the end of the 1980s has demonstrated numerous possibilities of improving heterogeneous catalytic performance.

EPOC is an alteration of the catalytic properties of heterogeneous catalyst, which usually functions as the working electrode in an electrochemical cell. The catalytic activity of metal in contact with solid electrolyte is strongly affected by applying electrical current or potential between the catalyst, working electrode, and a counter electrode deposited on the solid electrolyte. The effect of electrochemical promotion is a powerful means of altering the catalytic properties of metal or metal oxide interfaced with a wide variety of solid electrolytes.

In the late 1980s, Haruta et al. discovered that gold nanoparticles are very active for CO oxidation [1, 2]. This opened up a new research area in the world of heterogeneous catalysis. Since then, supported gold catalysts have been extensively studied due to their

superior catalytic activity [3-13]. The exact catalytic mechanism of gold nanoparticles deposited on various oxide supports is still being investigated.

There have been no reports on complete ethylene oxidation on gold nanoparticles supported on YSZ. Also, the bipolar configuration of the EPOC experiment has not been used with gold nanoparticles. Catalytic performance of gold nanoparticles deposited on YSZ for complete ethylene oxidation is compared between open circuit (conventional heterogeneous catalysis) and closed circuit (electrochemical promotion of catalysis) conditions. Catalytic performances at these two distinct conditions allow determination of the behaviour and characteristics of the gold nanocatalysts.

1.1 **Reference**

[1] T. Kobayashi, *et al.*, "A selective CO sensor using Ti-doped α-Fe2O3 with coprecipitated ultrafine particles of gold," *Sensors and Actuators,* vol. 13, pp. 339-349, 1988.

[2] M. Haruta, *et al.*, "Gold catalysts prepared by coprecipitation for low-temperature oxidation of hydrogen and of carbon monoxide," *Journal of Catalysis,* vol. 115, pp. 301-309, 1989.

[3] M. Haruta, "Size- and support-dependency in the catalysis of gold," *Catalysis Today,* vol. 36, pp. 153-166, 1997.

[4] G. C. Bond and D. T. Thompson, "Catalysis by Gold," *Catalysis Reviews - Science and Engineering,* vol. 41, pp. 319-388, 1999.

[5] M. A. P. Dekkers, *et al.*, "Supported gold/MOx catalysts for NO/H2 and CO/O2 reactions," *Catalysis Today,* vol. 54, pp. 381-390, 1999.

[6] D. Thompson, "A golden future for catalysis," *Chemistry in Britain,* vol. 37, pp. 43-44, 2001.

[7] M. Haruta, "When gold is not noble: Catalysis by nanoparticles," *Chemical Record,* vol. 3, pp. 75-87, 2003.

[8] N. Lopez, *et al.*, "On the origin of the catalytic activity of gold nanoparticles for low-temperature CO oxidation," *Journal of Catalysis,* vol. 223, pp. 232-235, 2004.

[9] H. G. Ahn, *et al.*, "Complete oxidation of ethylene over supported gold nanoparticle catalysts," *Journal of Nanoscience and Nanotechnology,* vol. 6, pp. 3599-3603, 2006.

[10] M. Jia, *et al.*, "Preparation of Au/CeO2 catalyst and its catalytic performance for HCHO oxidation," *Journal of Rare Earths,* vol. 26, pp. 528-531, 2008.

[11] L. Q. Nguyen, *et al.*, "Performance of nano-sized Au/TiO2 for selective catalytic reduction of NOx by propene," *Applied Catalysis A: General,* vol. 347, pp. 94-99, 2008.

[12] M. Chun Yan, *et al.*, "Mesoporous co3o4 and AU/CO3o4 catalysts for low-temperature oxidation of trace ethylene," *Journal of the American Chemical Society,* vol. 132, pp. 2608-2613, 2010.

[13] Y. Zhang, *et al.*, "Gold catalysts supported on the mesoporous nanoparticles composited of zirconia and silicate for oxidation of formaldehyde," *Journal of Molecular Catalysis A: Chemical,* vol. 316, pp. 100-105, 2010.

Chapter 2 Literature Review

Catalytic reactions under electrochemically promoted conditions use concepts and techniques from two distinct areas of chemistry: heterogeneous catalysis and electrochemistry. However, scientists and engineers in the field of catalysis are seldom acquainted with the terms and experimental methods applied in electrochemistry, and vice versa. The literature review is divided into three sections and the main goal is to summarize important concepts from both heterogeneous catalysis and electrochemistry and relate the two. The first section is dedicated to the transition metal in heterogeneous catalysis. The focus is on gold nanoparticles as heterogeneous catalysts, particularly when supported on metal oxides. The second section deals with the state of the art in electrochemical promotion. The third section is dedicated to ethylene oxidation in the gas phase, which is the main reaction studied.

2.1 Heterogeneous Catalysis

A typical heterogeneous catalyst consists of combinations of nanometer-sized particles with a specific surface of up to 1000 $m^2\ g^{-1}$ and exposes different crystal faces with various structural defects. In most cases a catalyst consists of more than one component. Then, the surface composition will usually be different from that of the bulk material and may even differ between the different crystal planes. These complications,

along with the variability in parameters of actual catalyst behaviours and actual reaction environment make this field of science a long time reputation of a "blackart". As a consequence industrial catalysis even at present is largely governed by empirical experience. However, the development of the surface science approach has enabled closer insights into the elementary steps involved in catalysis and directed the research towards real science.

2.1.1 Langmuir-Hinshelwood Reaction Mechanism

Most commonly used approach is the *Langmuir approach,* which is the most frequently applied attempt to describe the kinetics of a catalytic reaction. It starts with the assumption of a possible reaction mechanism, possibly supported by various experimental data on reaction intermediates. The various steps are then formulated in terms of rate equations for adsorption, desorption, and surface reaction steps. If adsorption/desorption steps are fast compared to the rate of surface reaction, these can be considered to be in equilibrium and the coverage for the different surface species are related to the respective partial pressures through adsorption isotherms. Adsorption isotherms are determined experimentally, and require careful measurement due to the complexity of the kinetic and energetic adsorption of the coverage, even for a single, uniform crystal surface, apart from the additional complications due to coadsorption. If the non-ideal surfaces are considered with the various structural elements, the situation gets even more complicated. Nevertheless, the Langmuir adsorption isotherm with its crude underlying assumptions provides satisfactory results, because several effects are able to compensate for each other. Dumesic

et al. [1] argue that the actual presence of different surface sites and the effects of surface coverage may well be responsible for the robustness of a catalyst for operation over a wide range of reaction conditions. At a certain set of reactions conditions, an optimal set of surface sites will dominate the reactivity that may change into another subset if the temperature and pressure conditions are varied.

The rate of a surface reaction of the type,

$$A_{ad} + B_{ad} \xrightarrow{k} C \qquad \text{(Eq. 2-1)}$$

is then formulated as

$$r = k\Theta_A\Theta_B \qquad \text{(Eq. 2-2)}$$

where the fractional coverages Θ_A and Θ_B are related with the respective partial pressures P_A and P_B through

$$\Theta_A = \frac{k_A P_A}{1 + k_A P_A + k_B P_B} \qquad \text{(Eq. 2-3)}$$

$$\Theta_B = \frac{k_B P_B}{1 + k_A P_A + k_B P_B} \qquad \text{(Eq. 2-4)}$$

This modification of the original Langmuir isotherm is based on the assumption that an adsorption site may either be occupied by A or B and that the product molecule is so weakly adsorbed that its surface concentration is negligible. (Eq. 2-2) then becomes

$$r = k\Theta_A\Theta_B = \frac{kk_A k_B P_A P_B}{\left(1 + k_A P_A + k_B P_B\right)^2} \qquad \text{(Eq. 2-5)}$$

For constant T and P_B, the rate will pass through a maximum upon variation of P_A that is reached when $\Theta_A = \Theta_B$. If $k_AP_A << k_BP_B + 1$, the rate will increase linearly with P_A, while in the opposite case $r \approx (kk_BP_B/k_AP_A)$, that is, further increase in P_A lowers the rate since the adsorption of A blocks sites for adsorption of B.

2.1.2 Catalysis by Nanoparticles

One of the areas of catalysis that is developing at a rapid place is nano-catalysis. Nano-catalysis can be considered as a bridge between homogeneous and heterogeneous catalysis. Because of nano-size, i.e. high surface area, the contact between reactants and catalyst increases dramatically and they can operate in the same manner as homogeneous catalysts (close to homogeneous catalysis), at the same time, due to their insolubility in the reaction solvent, they may be separated out from the reaction mixture. Thus, Nano-materials can combine the advantage of both the system, and can offer unique activity with high selectivity. In order to harness the power of these nanocatalysts, a detailed understanding of the origin of their enhanced performance is needed.

2.1.2.1 Transition Metal Nanoparticles

The unique physical and chemical properties of transition metal nanoparticles (TMNPs), which are distinct from those of the bulk metal have brought many engineers' and scientists' attention. TMNPs have attracted great interest in scientific research and industrial application, due to their unique large surface to volume ratios, which makes

TMNPs good heterogeneous catalyst. Different transition metals and/or their oxidation states are used in the field of nanocatalysis.

2.1.2.2 Properties

Some properties of supported metal nanoparticles that directly affect their catalytic activities are size, shape, support and the oxidation state, which are not scalable from bulk properties. Some of the important properties for the interest of this thesis (i.e. gold nanoparticles) are further discussed below.

2.1.2.2.1 Size

One of the properties that governs the activity of the catalyst is the size of metal crystallites. For instance, Figure 2-1 shows that a decrease in the diameter of metal particles increases the fractions of edges, corners, and surface exposed atoms.

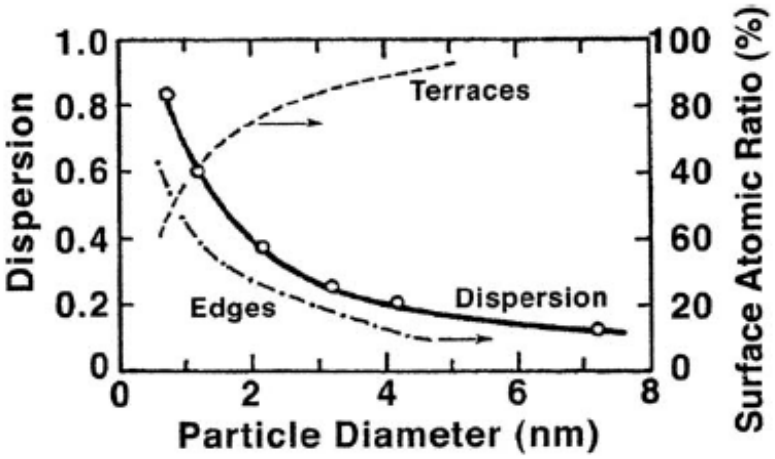

Figure 2-1 Surface atomic ratios of terrace and edge together with metal dispersion as a function of particle diameter [2].

A review article by Lopez et al. [2] compiling available experimental data on CO oxidation by gold has concluded that the particle size is the determining factor controlling the catalyst's performance. The author pointed out that the density of low-coordinated sites strongly affects the chemical activity, and proposed a $\sim 1/d^3$ scaling law for the activity, with d being the particle diameter. However, the underlying origin of the distinct changes observed in the catalytic reactivity of nanoparticles as function of the size is still an open question.

2.1.2.2.2 Oxidation state effects

Although the majority of industrially viable reactions are conducted on nanoparticles oxidized under the reaction conditions, not much information is currently available on how the oxidation states of these catalysts affect their reactivity. This problem has generated renewed interest after recent findings of superior catalytic performance of metal oxides over neutral metals [3-5]. Recent work by Friend's group on O-covered Au (111) demonstrates the enhanced reactivity of the pre-oxidized gold surface [6, 7].

While the effects of pre-oxidation on the catalytic activity of metal surfaces are the subject of extensive studies, much less is known about such phenomena on supported nanoparticles. Experimentally, this is largely due to the challenge of fabricating reproducible samples with consistent particle size, shape and oxide stoichiometry.

2.1.3 Gold as Nanocatalyst

Platinum, palladium, iridium, copper, silver and other transition noble metals are highly active, promoting many different types of organic reactions including hydrogenation,

oxidations, C-C bond formation, etc [8, 9]. In contrast to the high catalytic activity of Pt (Z=78) or Ir (Z=77), Au (Z=79) as a metal has been largely considered devoid of interesting catalytic activity. This assumption of considering gold catalytically inert changed, however, in the late 1990s after the seminal contribution of Haruta, who has reported that gold nanoparticles are extremely active in promoting the low-temperature, aerobic oxidation of CO to CO_2 [10] . Moreover, Haruta and coworkers have shown that the catalytic activity of a few nanometer sized gold, there being a direct relationship between activity and particle diameter [11-14].

Since this breakthrough, research has been aimed at determining the reaction types that can be efficiently catalyzed by gold nanoparticles. The focus has been dedicated to increasing the catalytic activity of gold by stabilizing nanoparticles against agglomeration, understanding the role of the solid support in the catalytic activity and also demonstrating the similarities and distinctive properties of gold catalysis with respect to catalysis by other noble metals.

2.1.3.1 Properties of Gold Catalysts

Properties of supported Au nanocatalysts are dependent on the preparation, pre-treatment, and calcination procedures used [15]. This section discusses the most important properties of catalytic gold nanoparticles.

2.1.3.1.1 Activity

The importance of parameters described in section 2.1.2.2 is also valid for gold nanocatalysts. Although, the reasons for the catalytic activity of gold are not as yet fully

understood, the presence of gold as well-dispersed nanoparticles (< 10 nm) is one of the best established requirements for preparing active catalysts [10, 12-20]. Nevertheless, unsupported powdered gold (mean diameter, 76 nm) has proved to be active for CO oxidation [21, 22] under mild conditions. There are suggestions that there is an optimal Au particle size between 2 and 5 nm, although under the right circumstances particles as large as 10 nm, or even more, can exhibit high activity [23], and smaller particles, not always visible under the electron microscope, could also be effective.

Haruta states that strong contact is necessary between gold and the underlying support [14], and that this may be achieved via the calcination procedure. Since calcination at high temperatures generally leads to agglomeration of particles, which is undesirable, calcinations at mild temperatures (373−573 K) have been preferred by several authors [24-27]. Consequently, the challenge consists in selecting a temperature for calcining the sample to produce good contact between the gold particles and the support, without producing too much sintering of particles. Some investigators report highest activities for untreated catalysts [28].

2.1.3.1.2 Selectivity

Gold nanoparticles show extraordinary selectivity in a large number of reactions. One remarkable example is in the oxidation of propene to the corresponding epoxide. A notable selectivity of above 99% has been reported from early investigations over an Au/TiO_2 catalyst, using a combination of H_2 and O_2 in the gas stream, and the yield of propene oxide can be increased by optimizing the support composition [29, 30].

Selective dehydrochlorination of chlorofluorocarbons (CFCs) is a very important environmental issue, and the need to replace these detrimental, ozone depleting compounds by benign hydrochlorofluorocarbons (HCFCs) and/or hydrofluorocarbons (HFCs) has also stimulated intensive work on the subject [31-34].

2.1.3.1.3 Durability

From Tammann temperature considerations, gold would be expected to sinter at around 773−823 K (half of the melting point of metallic gold). Small Au nanoparticles might well sinter at much lower temperatures than this, as their melting temperature would be expected to decrease drastically with decreasing particle size due to the drastic altering in their thermodynamic and thermal properties. However, there is increasing evidence that gold catalysts are much more durable than would be expected from these considerations [35].

An example is a catalyst consisting of gold on cobalt oxide particles supported on a mechanical mixture of zirconia-stabilised ceria, zirconia and titania, that survived 773 K for 157 h, with some deactivation [23]. Datye and co-workers [36] have also shown that Au/Al_2O_3 is hydrothermally stable at 873 K for 96 h. Since 873 K is higher than the Tamman temperature for gold, these results point to the fact that the active gold species are produced by interaction between the gold and the support. These catalytically active gold-metal oxide mixtures are much less likely to sinter than metallic gold and these results, therefore, indicate a much higher potential for practical applications than if the catalyst is metallic gold itself [37].

2.1.3.1.4 Poison Resistance

One feature of particular interest is the resistance that gold-based systems might display against sulfur poisoning. Only a little work has been carried out in this area to date, but gold on titania catalyses the Claus reaction and is 5 to 10 times more effective than titania itself, indicating that gold can be sulfur-tolerant:

$$SO_2 + 2H_2S \rightarrow 2H_2O + 3S_{solid} \qquad \text{(Eq. 2-6)}$$

In addition, the reduction of SO_2 by CO using Au/TiO_2 is also 5 to 10 times more active than with pure titania [38]. Also, Marsh and co-workers [23] have shown that gold on cobalt oxide particles, supported on a mechanical mixture of zirconia-stabilized ceria, zirconia and titania remains active in a gas stream containing 15 ppm of SO_2. Haruta and co-workers [39] have found that although the low-temperature CO oxidation activity of TiO_2-supported Au can be inhibited by exposure to SO_2, the effect on the activity for the oxidation of H_2 or propane is quite small.

2.1.3.2 Gold nanoparticles synthesis methods

Supported nanoparticles have received more attention than naked or colloidal gold because the supported catalysts have more viable commercial application. However, using naked or colloidal gold to study the surface science provides useful fundamental information relevant to reaction mechanisms and the nature of active centres of supported gold catalysts. There are many established chemical methods to prepare colloidal and supported gold nanoparticles.

Colloidal gold nanoparticles synthesis methods include reduction method using alcohol, sodium citrate, tetrakis(hydroxymethyl)phosphonium chloride (THPC), borohydride, and toluene [40-43]. A stabilizing agent is often used, for instance, polyvinylpyrolidone (PVP), polyvinyl alcohol (PVA) and poly(methylvinylether) (PMVE) [44-47]. Synthesis parameters that are known to influence the product are reaction temperature and concentrations of reactants.

Well known methods for synthesizing supported gold nanoparticles include co-precipitation [10], deposition precipitation [18], impregnation [48, 49], vapour-phase [15], grafting, ion-exchange [50], and sol-gel [51].

2.1.4 Metal Support Interaction

Metal-support interactions are a phenomenon responsible for changes which occur in the catalytic activity or selectivity of catalytically active phase when varying the catalyst support [52]. An explanation frequently offered for the nature of metal support interaction is electronic-type interactions between support and catalyst particles. A concept of electronic interactions originating from the bulk electronic properties of the two phases in contact (metal crystallites and support materials) has been first proposed by Schwab [53] and Solymosi [54]. This concept is based on the metal-semiconductor boundary-layer theory, according to which crystallites-support of the two solids is at equal height. In order for this to be achieved, charge must be transferred from one material to the other. In cases where the work function of electrons of the metal is higher than the work function of the semiconductor, charge will flow from the semiconductor to the metal, until the Fermi level

at the interface is equilibrated. The charge transfer process, which is due to the difference in electrochemical potential, causes significant alterations in the catalyst properties and selectivity of the dispersed metal particles.

2.1.4.1 The electron structure of metal and semiconductors

The electron potentials related to the electron structure of a metal is shown schematically in Figure 2-2.

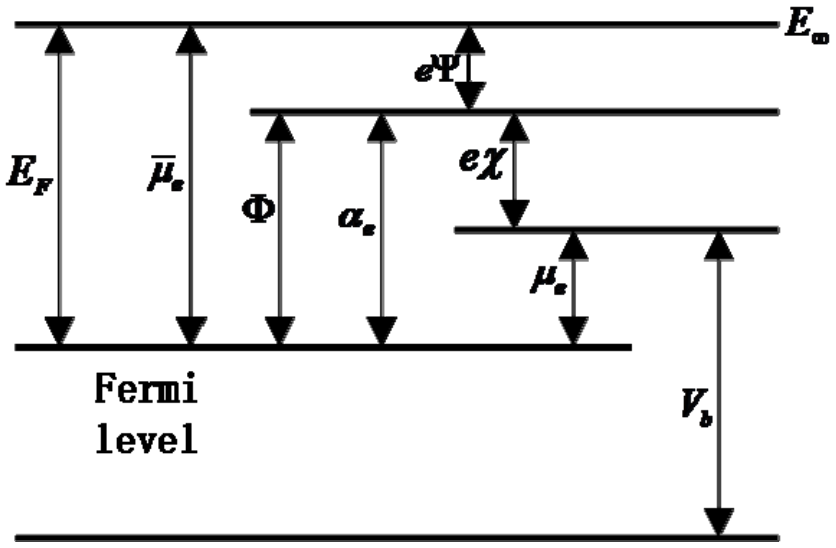

Figure 2-2 Electron potentials related to metal electron structure

Free electrons inside the metal possess kinetic energy, and the energy of the highest occupied level is defined as the Fermi energy, E_F. Electrons are bound inside the bulk by the action of an attractive potential, named V_b. The net stabilizing energy corresponds to the chemical potential of the electrons, μ_e [55, 56].

$$\mu_e = E_F + V_b \qquad \text{(Eq. 2-7)}$$

A metal surface is characterized by the presence of a dipole layer with its negative end pointing away from the surface. The potential due to this dipole is called surface potential χ. The real potential, α_e, of the electron is defined as

$$\alpha_e = \mu_e - e\chi \qquad \text{(Eq. 2-8)}$$

while the minimum energy required for transferring an electron out of the metal, namely the work function, Φ, is [55, 56]

$$\Phi = -\alpha_e = -\mu_e + e\chi \qquad \text{(Eq. 2-9)}$$

The work function incorporates the contribution of a term related to the bulk, μ_e, and a term related to the surface, $e\chi$. If the metal surface contains a net macroscopic charge, there is an electrostatic (or outer) potential, Ψ, corresponding to this charge. The energy binding the electrons inside the metal in this general case is called the electrochemical potential of the electron, $\overline{\mu_e}$ [55]

$$\overline{\mu_e} = \alpha_e - e\Psi = \mu_e - e\chi - e\Psi \qquad \text{(Eq. 2-10)}$$

The electron potentials relating to the electronic structure of a semiconductor are shown schematically in Figure 2-3. The upper edge of the valence band is of energy E_v, while the lower edge of the conduction band is of energy E_C. Thus, semiconductors are characterized by the existence of an energy gap, E_g, between the highest occupied energy level (valence band) and the lowest unoccupied empty level (conduction band). The magnitude of this energy gap is used to differentiate metal oxides as semiconductors and insulators. If the magnitude of E_g is such that thermal excitation is capable of transferring

an appreciable number of electrons into the conduction band, the solid is considered to be a semiconductor, otherwise insulator. Generally, solids whose band gap is less than 4eV are classified as semiconductors.

Electrons in a solid are distributed in available energy states following the Fermi-Dirac statistics. The Fermi energy, E_F, is defined as the energy at which the probability of occupancy is 0.5. For intrinsic or ionic conducting solids, the Fermi level is located at the center of the energy gap and shifts toward the empty zone for an n-type semiconductor or the filled band for a p-type semiconductor. As in the case of metals, the Fermi energy is equal to the electrochemical potential ($E_F = \bar{\mu}_e$) as shown in Figure 2-2 and Figure 2-3 for both metals and semiconductors.

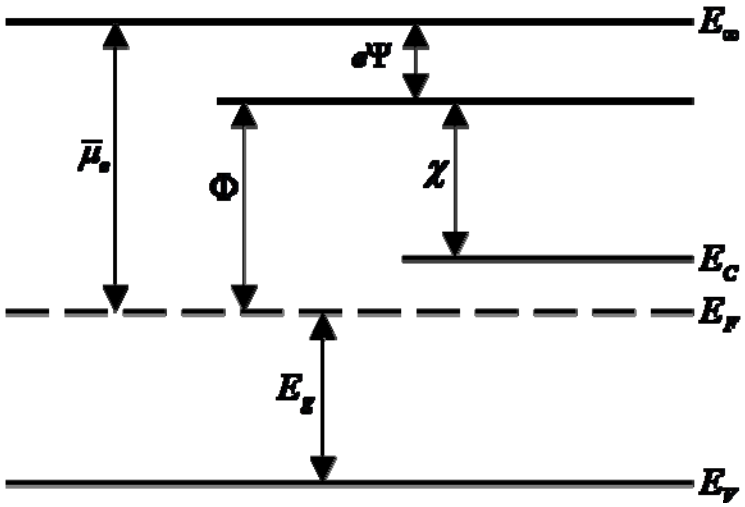

Figure 2-3 Electron potentials related to semiconductor electron structure

The work function, Φ, is defined as the average work needed to move an electron from the solid and place it at a distance x from the surface where the classical image-force

potential, $-e^2/4x$, is just negligible. A distance of 10^{-6} m is sufficient to meet this requirement. Its value is equal to the difference between the Fermi level and the electrostatic potential, Ψ**,** just outside of the semiconductor. (The vacuum level is the energy level of an electron just outside of semiconductor with zero kinetic energy.)

$$\Phi = \overline{\mu_e} - e\Psi \qquad \text{(Eq. 2-11)}$$

Another important parameter is the electron affinity, χ_s, which is defined as the difference between the lower end of the conduction band and the electrostatic potential just outside the semiconductor:

$$\chi_S = -E_C - e\Psi \qquad \text{(Eq. 2-12)}$$

2.1.4.2 Boundary Layer Theory

The condition of thermodynamic equilibrium at a metal-semiconductor contact implies that the electrochemical potential should be uniform throughout the system. If, prior to contact, the metal and the semiconductor have different electrochemical potentials, then upon contact, charge will flow to the material with the smaller potential until the potentials reach equilibrium. When the two materials carry no net charge, then $\overline{\mu_e}^M = \Phi_M$ and $\overline{\mu_e}^S = \Phi_S$, where M and S denote the metal and semiconductor, respectively. For $\Phi_M > \Phi_S$ the electron flux will be toward the metal. At equilibrium, the common electrochemical potential will be:

$$\overline{\mu_e} = -\Phi_M - e\Psi_M = -\Phi_S - e\Psi_S \qquad \text{(Eq. 2-13)}$$

and

$$\Delta\Phi = e\left(\Delta\Psi\right) \qquad \text{(Eq. 2-14)}$$

That is, a contact potential difference to the work function difference has developed. Quantities Ψ_M and Ψ_S are the outer potential of the metal and the semiconductor, respectively. For instance, in a situation where $\Phi_M > \Phi_S$, charge is transferred from the semiconductor to the metal. Electrons transferred to the metal are associated with the interface atoms, while the more extended region in the semiconductor that is depleted of electrons is characterized by a bending of the valence and conduction bands.

2.2 **Electrochemical Promotion**

During the last 15 years, a similar phenomenon to metal-support interaction, named electrochemical promotion of catalysis (EPOC) [57, 58], or non-Faradaic electrochemical modification of catalytic activity, NEMCA effect [57, 58], has been discovered and studied for numerous reactions [59]. The goal of this section is to summarize the concept of this EPOC phenomenon and how it can be used with gold nanoparticles to increase the catalytic activity of oxidation of ethylene, which is the main reaction of interest.

2.2.1 **Definitions and basic quantities involved**

EPOC is a unique phenomenon observed in heterogeneous catalysis that is discovered relatively recently and it has made a strong impact on modern electrochemistry and surface science [58-63].

Vayenas, who is one of the pioneers of this phenomenon, defines EPOC as *"distinct and reversible changes in the catalytic properties of metal or metal oxide catalysts deposited on solid electrolytes as a result of small electrical current or potential application [58, 61, 64]"*

The basic setup used to observe this effect on an O^{2-} conducting solid electrolyte is shown in Figure 2-4 for the case of complete ethylene oxidation and its effect is shown in Figure 2-5. The porous, electropromoted catalyst film also serves as the working electrode in the solid-electrolyte cell. Upon application of potential or current, oxygen from the atmosphere gets reduced to O^{2-} ions in the cathode side. Then, the ion starts to flow across the solid electrolyte and migrates over to the surface of the working electrode to change its work function.

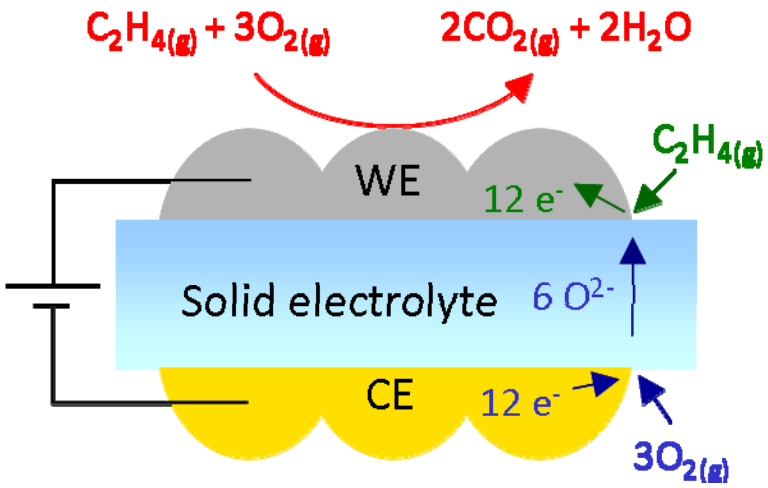

Figure 2-4 Basic setup of EPOC for ethylene oxidation, using O^{2-} conductor as solid electrolyte.

The catalytic rate can be altered by applying current or potential. Under open-circuit condition, where I = 0 (e.g. no electrochemical contribution), a catalytic rate r_0 is measured.

Application of an electrical current, I, or potential difference between the working and counter electrode gives rise to very pronounced changes in the catalytic rate, r, and quite often in product selectivity [59]. The increase in the reaction rate well surpasses the expected increase in reaction rate, the Faradaic rate (e.g. $\Delta r >> I/2F$).

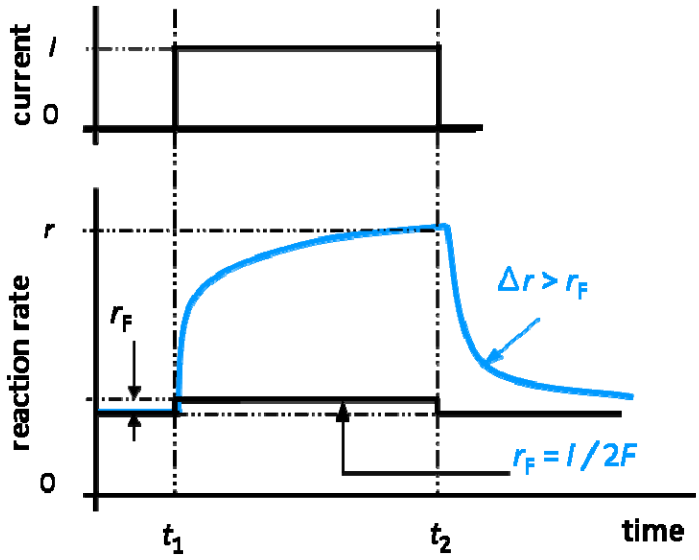

Figure 2-5 Transient effect of EPOC

The rate of the catalytic reaction, r, can become up to 200 times larger than the open-circuit rate, r_0, and up to $3x10^5$ times larger than the Faradaic rate (I/2F for O^{2-}) [59, 65, 66]. The increase in the catalytic reaction rate as well as the enhancement of product selectivity is entirely reversible in most cases. The steady-state open-circuit catalytic reaction rate after current interruption typically relaxes within 10 to 30 minutes to the value observed prior to application of the current.

The phenomenon of electrochemical promotion can be described by:

a) The rate enhancement ratio, ρ, defined as [59]:

$$\rho = \frac{r}{r_o} \qquad \text{(Eq. 2-15)}$$

where r_0 is the catalytic rate at open circuit, and r is the catalytic rate observed under polarization by an applied current or potential difference.

b) The apparent Faradaic efficiency, Λ, is defined as the ratio of the observed rate increase to the highest possible electrochemical rate [59]:

$$\Lambda = \frac{r - r_o}{\left(\frac{I}{2F}\right)} = \frac{\Delta r}{r_F} \qquad \text{(Eq. 2-16)}$$

where I is the applied current, F is the Faraday constant, and $r_F = I/2F$ is the rate of O^{2-} supply to the catalyst.

The transport of specific promoting species, such as O^{2-}, are thought to be the main cause of the electrochemical promotion effect [52, 59]. These species are reacted electrochemically at the three-phase boundaries (tpd) between solid electrolyte, catalyst, and gas phase, and then spread out over the gas-exposed catalyst surface.

The overall parameters of the complex phenomenon in electrochemical promotion are readily investigated by phenomenological techniques such as catalytic rate measurements [59, 65, 67-71], solid-state cyclic voltammetry [72, 73], catalyst work function measurements [58, 74], and AC impedance spectroscopy [75, 76], while more sophisticated techniques such as XPS [59, 77, 78], UPS, TPD [64, 79-81], PEEM[64] [82, 83], or STM [69-71, 74, 84] are used to identify and monitor particular promotion species.

The phenomenon of electrochemical promotion may be of great importance in present and future industrial applications. The industrial focus lies in the development of reactors for bipolar cell configurations [66, 85-90] and monolithic electropromoted reactor.

In the following, a demonstration of electrochemical promotion will be outlined using classical electrochemical promotion configuration using thin platinum film, and bipolar cell configurations [85-90] using gold nanoparticles under electrochemical conditions.

2.2.2 The mechanism of electrochemical promotion

The fundamentals involved in electrochemical promotion of catalysis are similar to those of chemical promotion and metal-support interaction in a sense that they all involve spillover-backspillover phenomena. The latter can be described as *"the mobility of adsorbed species from one phase on which they easily adsorb (donor) to another phase where they do not directly adsorb (acceptor)."* [59] By this mechanism, an inert material can portray some catalytic activity. In addition, spillover may lead to an improvement of catalytic activity or selectivity and also the lifetime.

The most plausible mechanism of electrochemical promotion is illustrated in Figure 2-6, which is similar but not the same as the spillover mechanism in heterogeneous catalysis. Anodic polarization of the catalyst allows the solid electrolyte to work as a donor supplying O^{2-} ions to the catalyst working as an acceptor. This migration from the support to the catalyst may be called backspillover, in order to distinguish from the migration in the opposite direction, which is quite common in catalysis and is called spillover.

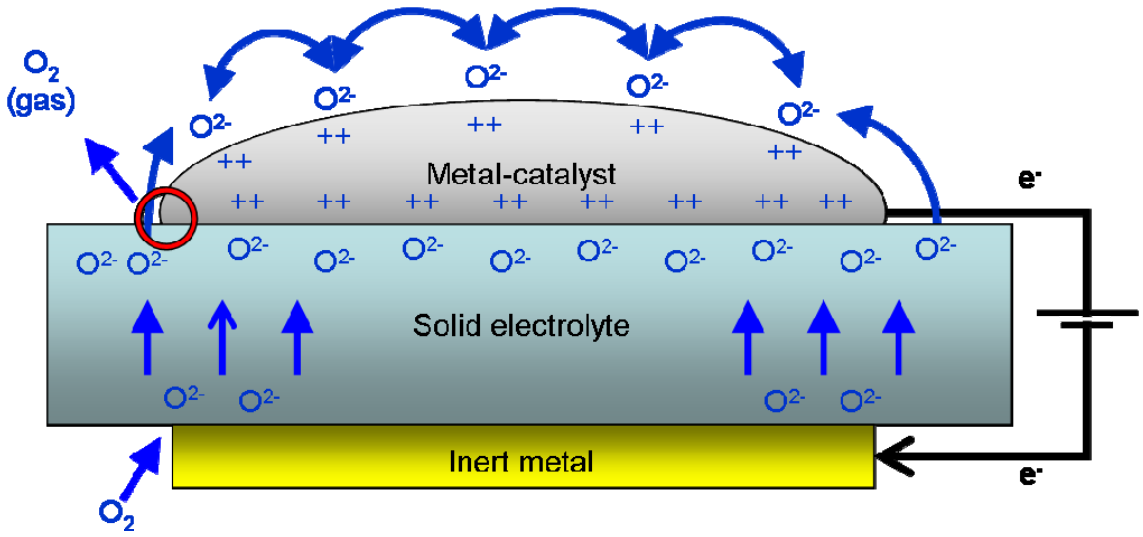

Figure 2-6 Schematic representation of the mechanism of electrochemical promotion by an applied anodic current via back spillover of charged promoting species (O^{2-}).

The O^{2-} ions are released from the solid electrolyte at the three-phase boundaries. By a thermodynamic analysis of electrochemical promotion involving O^{2-} conductors, it is demonstrated that two types of adsorbed oxygen species exist [91]: one type is the catalytically active species adsorbed from the gas phase and the other is backspillover oxygen from the solid electrolyte, which acts as a sacrificial promoter [59, 66, 77]. The rate of consumption of the promoter is slow relative to the kinetics of migration (backspillover) from the electrolyte to metal/gas interface.

There are different pathways for the species experiencing the backspillover. They can either be consumed in electrochemical reactions (oxygen evolution and/or oxidation of adsorbed reactants) occurring along or close to the tpb, obeying the Faraday's law, or they may migrate over to the gas-exposed catalyst surface.

The presence of backspillover at gas-exposed catalyst surface is demonstrated by XPS measurements [92]. No charged oxygen species could be detected under open-circuit conditions, but the abundance of them are found after anodic polarization of the catalyst/solid electrolyte interface. During the migration of oxygen ions, the ions are accompanied by their compensating image charges in the catalyst, with which they form surface dipoles. When these dipoles spread out, an over neutral, effective double layer is built up at the gas-exposed catalyst surface. Simultaneously, there is a change in the catalyst's work function, which modifies the binding strength of chemisorbed reactants and intermediates, and thus gives rise to changes in catalytic activity and/or selectivity

Consider a metal (or metal oxide) catalyst (c) supported by an O^{2-} conducting solid electrolyte (s), both in contact with a gas phase (g) containing oxygen. For oxygen species, the reaction scheme is shown in Figure 2-7 [93, 94].

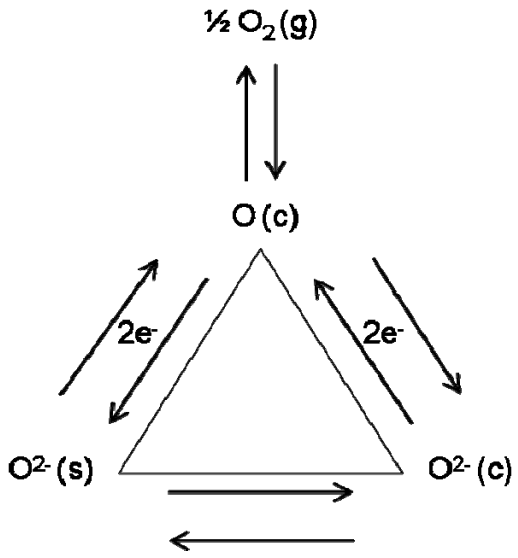

Figure 2-7 Reaction network for oxygen species associated with an electron conductor catalyst (c) on an oxygen-ion (O^{2-})-conducting solid-electrolyte support (s) in contact with an oxygen (O_2)-containing gas phase (g)

In the charge transfer reaction, O^{2-} is oxidized to O. The catalyst/solid electrolyte (c/s) interface is not accessible to O or O_2, therefore, direct charge transfer between O^{2-} (s) and O (c) may occur only at the three-phase boundaries (tpb). Considering the possibility of backspillover of O^{2-} from the tpb to the gas-exposed catalyst surface, however, charge transfer will no longer be restricted to the tpb but may take place through O^{2-} (c) species over the entire catalyst/gas (c/g) interface. Under open-circuit conditions, all reactions come to equilibrium:

$$\mu_{O^{2-}}(s) = \mu_{O^{2-}}(c) = 2\overline{\mu_{e^-}}(c) + \mu_O(c) = 2\overline{\mu_{e^-}}(c) + \frac{1}{2}\mu_{O_2}(g) \qquad \text{(Eq. 2-17)}$$

where μ_i is the chemical potential and $\bar{\mu}$ ($=\mu_i + z_i F \phi$) is the electrochemical potential of species i, z_i is its charge number, and ϕ is the inner (Galvani) potential.

Obviously, the driving force for O^{2-} backspillover from the solid electrolyte to the catalytically active surface (c/g) is given by $\bar{\mu}_{O2-}(s) - \bar{\mu}_{O2-}(c)$. This difference vanishes at equilibrium when an effective double layer is established at the c/g interface, by analogy to the case of an immersed electrode in aqueous electrochemistry [95].

A potential step is applied to the electrochemical cell in a typical electrochemical promotion experiment. In the ideal case, a reference electrode has an invariant potential. The induced change in the ohmic-drop-free potential between the catalyst (working electrode) and the reference electrode, U_{WR}, is equal to the change in the inner (Galvani) potential of the catalyst, ϕ:

$$\Delta U_{WR} = \Delta\phi \qquad \text{(Eq. 2-18)}$$

This difference is measurable. By changing the potential of the catalyst one modifies its Fermi level, E_F, or – in other terms – the electrochemical potential of the electrons in the catalyst ($\bar{\mu}_e = E_F$). This quantity, which is previously defined in section 2.1.4.1, is also defined as the difference between the zero-energy state of the electrons (taken in the ground state at infinite distance from the solid) and the energy of conduction electron in the bulk of the catalyst. It is common practice to count this energy difference in two conceptually different ways. One of them is common in electrochemistry, the other is common in surface science.

In electrochemistry, one considers the electrochemical potential of electrons as the sum of their chemical potential in the solid, μ_e, and the contribution due to the electrostatic (inner) potential:

$$\overline{\mu_e} = \mu_e + \left(-e\phi\right) \qquad \text{(Eq. 2-19)}$$

Under polarization, the chemical potential of electrons in the bulk solid remains invariant:

$$\Delta\overline{\mu_e} = -e\Delta\phi = \left(-e\Delta U_{WR}\right) \qquad \text{(Eq. 2-20)}$$

Hence, in the electrochemical approach formulated in terms of the bulk properties, $\bar{\mu}_e$, ϕ and μ_e, the change in electrochemical potential of the electrons can be related directly to the applied potential difference.

Looking back at the surface science approach - section 2.1.4.1, (Eq. 2-12) expresses electrochemical potential as a function of the work function, Φ, and outer (Volta) potential, Ψ. This, compared to (Eq. 2-19), has an advantage due to the fact that both terms are surface properties, which are measureable quantities.

Population of the surface with dipoles via O^{2-} backspillover, ie, the formation of an electric double layer, will increase the surface potential, and the concomitant increase in work function will affect the binding strength of chemisorbed reactants. It follows that the adsorption energy of electron acceptors (eg. atomic O) will be weakened while that of electron donors (eg, C_2H_4) will be strengthened. This results in a variation of adsorption equilibrium constants, as well as in coverage of the adsorbed species [59]. A corresponding change in catalytic reaction rate must then be expected.

The catalyst's work function is a quantity directly measureable, either by the Kelvin probe technique or by electron cut-off energy technique. It has been found experimentally [58] that for steady-state electrochemical promotion, the following relationship holds over a wide range of conditions (ie, as long as ion backspillover from the solid electrolyte forms a double layer at the metal/gas interface) [74]:

$$e\Delta U_{WR} = \Delta\Phi \qquad \text{(Eq. 2-21)}$$

It follows that solid-electrolyte cells may be used as work function probes. Comparing this experimental relationship with (Eq. 2-12) and (Eq. 2-20), one may conclude that the Volta potential difference at the catalyst surface remains invariant, provided the electric double layer has been built up at the catalyst/gas interface. Based on electrodynamic arguments, it has also been concluded [59] that in an overall neutral electrochemical cell, this invariant Volta potential difference is zero, since the double layer formed via ion backspillover is overall neutral.

The validity of (Eq. 2-21) has been demonstrated, both with the Kelvin probe technique and with the UPS technique [58] (use of electron cutoff energy in UPS experiments), for

work function measurements at gas-exposed electrode surfaces and for catalysts in contact with YSZ and β"-Al_2O_3 (a Na^+ conductor) [58] at temperatures of 200 to 550 °C. Although changes in catalyst work function with catalyst potential have been widely studied and understood, (Eq. 2-21) has still been the subject of vivid controversy and discussions [69, 71].

2.2.3 Electrochemical cell types

Electrochemical cell can be assembled in numerous manners, often by varying the shape of the solid electrolyte or arrangement of the electrodes. For instance, solid electrolyte can be in form of thin (1 to 2 mm) disk, hollow tubular, fuel-cell like or monolithic-reactor like [59]. In a laboratory studies, thin disk of solid electrolyte is typically used for preliminary experiments because it is simple and quick to assemble an electrochemical cell in this configuration compared to other types. There are different configurations within the thin disk electrochemical cell types, which will be discussed in the next section.

2.2.3.1 Different configurations in disk type electrochemical cell

2.2.3.1.1 Conventional cell configuration

Conventional cell configuration means using a well dispersed thin metal film as working electrode, and inert material, such as bulk gold as reference and counter electrodes. The working electrode is deposited on one side of the solid electrolyte, while the other two electrodes are deposited on the other side.

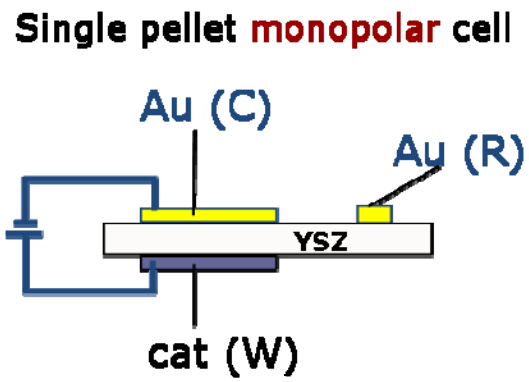

Figure 2-8 Conventional cell configuration. The catalyst functions as working electrode [96].

In the later section the thesis, electrochemical promotion of platinum catalyst film is shown using such a classical cell.

2.2.3.1.2 Bipolar cell configuration

It has been recently found that direct electrical contact, via a metal wire to the catalyst-electrode is not necessary to induce the effect of electrochemical promotion [85-90]. It is found that it suffices to apply the potential, or current, between two terminal electrodes which may, or may not, be catalytically active. The concept appears to be very similar with that of the "bipolar" design used now routinely in aqueous electrochemistry. The implication of this discovery for electrochemical promotion are quite significant since it shows that, at least in principle, the design of an electrochemically promoted reactor can become much simpler than that of a fuel cell.

The first bipolar or "wireless" EPOC study has been done by Marwood and Vayenas et al in 1998 [85]. In their experiment, YSZ disc with two terminal Au electrodes

and one Pt catalyst film deposited on one side and a reference Au electrode on the other side is placed in a single-chamber reactor to examine ethylene oxidation on the Pt catalyst film. They applied potential between the two terminal Au electrodes, inducing EPOC on the Pt film which is not connected to any metal wire but simply in contact with the YSZ solid electrolyte. Since then, numerous designs for bipolar cell have been studied, as shown in Figure 2-9.

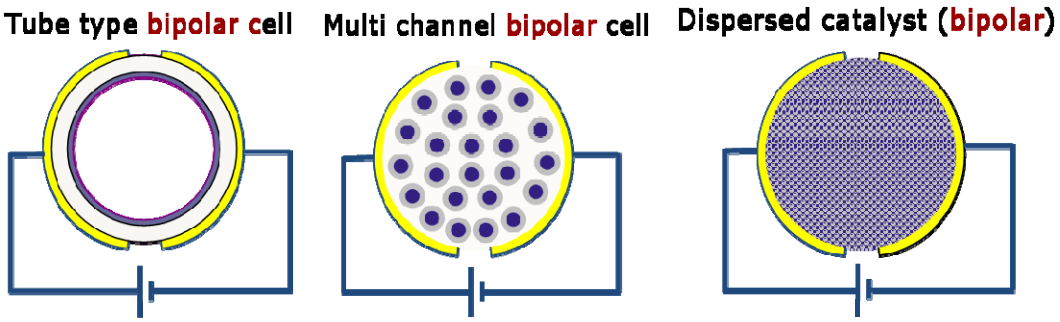

Figure 2-9 Examples of single-disk type bipolar configuration [96]

The observed rate enhancement is roughly half of that obtained in the same setup when the Pt catalyst is connected to a wire and potential is applied between it and one of the Au terminal electrodes [85].

More recently, bipolar configuration of EPOC cell has been enhanced by using nanoparticles as catalysts. For example, CO oxidation of induced bipolar Pt nanoparticles supported on YSZ has been done by Xia and Comninellis et al [89, 90]. They showed in-plane polarization of Pt particles resulted in a bipolar system which led to the formation of a large number of galvanic cells partially or completely polarized. Although the catalytic

activity of the bipolar configuration is lower than the conventional configuration [86], the fact that the bipolar configurations do not need electrical connection to the catalyst and can be adapted more easily to commercial exhaust units make this field of EPOC unique and worth researching. A research by Wodiunig has estimated the current bypass of the bipolar electrochemical cell and has shown that the nonuniform distribution of the work function led to a smaller increase in EPOC effect [88].

For the first time, catalytic activity of induced bipolar Au particles supported on YSZ is conducted and detailed results will be shown in the later section of the thesis.

2.2.4 Solid Electrolyte

Solid electrolytes should have high ionic conductivity and low electronic conductivity. Known electrolyte materials mainly differ in the nature of conductivity - either having pure ionic conductivity or mixed ionic-electronic conductivity. The preparation, properties, and some applications of solid electrolyte have been discussed elsewhere [72, 85, 97-101]. Solid electrolytes play an increasingly important role in heterogeneous catalysis, both as nanodispersed catalyst carriers and as supports of thick or thin, electrochemically promoted films [59]. The lowest acceptable ionic conductivity of a solid electrolyte in practical fuel cell applications is 0.1 to 1 $ohm^{-1}\,cm^{-1}$. This places severe restrictions on the choice of materials and operating temperatures. On the other hand, catalytic (promotional) and sensor applications require much lower conductivities (10^{-4} $ohm^{-1}\,cm^{-1}$). This implies that more varieties of solid electrolytes, such as YSZ, NASICON, Nafion, CaF_2, TiO_2 and CeO_2 [59], can be used over wide temperature range. All the

experiments conducted by the author were done with YSZ, which is suitable for oxidation reactions.

2.2.4.1 YSZ

The majority of defects in pure ZrO_2 are oxygen vacancies and electrons, both at very low concentration. Lower-valent oxides such as Y_2O_3 or CaO when added to ZrO_2 raise its oxygen vacancy concentration, and thus lead to a much higher ionic conductivity. The conductivity of ZrO_2 doped with Y_2O_3 is plotted schematically as a function of oxygen partial pressure in Figure 2-10.

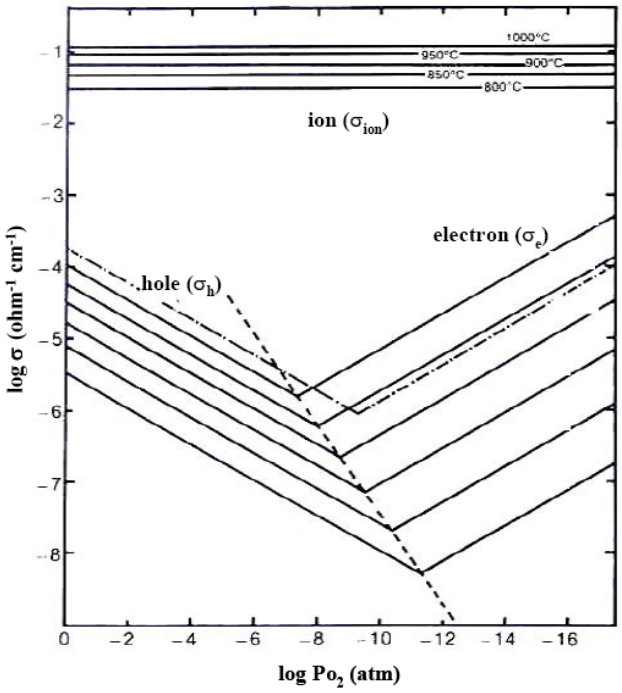

Figure 2-10 Electron, hole, and ion conductivities in yttria-stabilized zirconia

The range of partial pressure over which a compound is an ionic conductor is relatively wide for the stabilized zirconia, covering about 20 to 30 orders of magnitude around the minimum of electronic conductivity.

The cubic fluorite structure is one of the most important crystal structures in the field of ionically conducting oxides. In the face-centered cubic structure, the anions occupy the tetrahedral sites of the zirconia lattice, which is a fluorite type. Each metal cation is surrounded by eight oxygen anions and each oxygen anion is tetrahedrally coordinated with four metal cations. This is rather open arrangement, with a large number of octahedral interstitial voids and it is suitable for fast oxygen ion diffusion at high temperature. Doping of zirconia with divalent or trivalent ions stabilizes the cubic structure down to ambient temperature and creates oxygen vacancies by charge compensation.

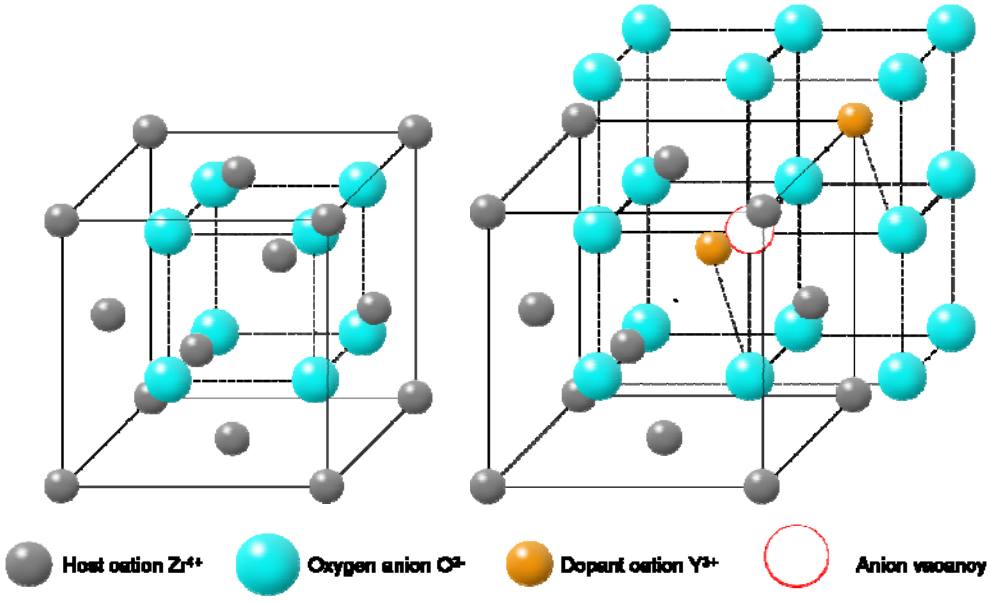

Figure 2-11 The face centered cubic structure of the zirconia lattice

In the lattice, the oxygen vacancies may be surrounded by two Y^{3+} and two Zr^{4+} ions (neutral vacancy), or by three Zr^{4+} and one Y^{3+} (single-charged vacancy), or by four Zr^{4+} ions (double-charged vacancy) [102, 103]. For these reasons, YSZ makes an interesting type of support for nanoparticles to research. Some properties of ZrO_2 + 8% Y_2O_3 are given in Table 2-1.

Table 2-1 Properties of YSZ

Property	Value
Melting point [℃]	2680
Density [g cm^{-3}]	5.9
Conductivity (1000℃) [ohm^{-1} m^{-1}]	12
Thermal conductivity [W cm^{-1} K^{-1}]	0.02
Standard enthalpy (25℃) [kJ mol^{-1}]	1097.5
Standard entropy (25℃) [kJ mol^{-1} K^{-1}]	50.4

2.3 Complete Oxidation of Ethylene

The detoxification of hydrocarbon pollutants is one of the global environmental challenges. The complete catalytic oxidation of hydrocarbons to carbon dioxide and water has received much attention in order to reduce their emission from motor vehicles and processing plants [104, 105]. The promoting effect of gold nanoparticles in catalysts used for the complete oxidation of various unsaturated hydrocarbons has already been reported [15]. Gold deposited on Co_3O_4 exhibits highest catalytic activity amongst supported metal catalysts for the complete oxidation of hydrocarbons [15].

Volatile organic compounds (VOCs), present in buildings or cars, are wide-ranging classes of chemicals and currently over 300 compounds are considered as VOCs by the US Environmental Protection Agency (EPA). Their release has widespread environmental implications, and has been linked to the increase in photochemical smog, the depletion of atmospheric ozone and the production of ground-level ozone. EPA has validated that indoor air pollution is one of the top human health risks. The studies on indoor air quality (IAQ) have been transited gradually to indoor volatile organic compounds. The removal of formaldehyde is vital for improving IAQ and human health due to a carcinogenic risk. In addition, ethylene is unwanted for other reasons. For instance, in fruit storage areas such as refrigerated warehouse, ethylene is released from fruit, which accelerates the maturing of the fruits and enhances their softening [106, 107]. In order to maintain freshness in this kind of controlled air quality system, the removal of ethylene is necessary.

In the field of classical heterogeneous catalysis (open circuit) of gold nanoparticles, YSZ has not been used extensively as support to gold nanoparticles due to its inferior catalytic performance compared to other metal oxides [105, 108]. However, the versatility of YSZ as both open and closed circuit support makes the material an interest support to conduct experiments.

2.3.1 Mechanism of complete oxidation of ethylene in open circuit condition

The detailed mechanism of complete ethylene oxidation is still a matter for debate. The reported values of the activation energy vary from 63 to 143 kJ/mol for complete ethylene combustion. Large discrepancies also exist in the reported values for the reaction

order. Apparent orders from -0.3 to 2 are found with respect to oxygen and from 0 to 1 with respect to ethylene.

Generally, the reaction proceeds between both reactants in an adsorbed state and a Langmuir-Hinshelwood model can describe the reaction kinetics. Generation of CO_2 shows a bell-shaped dependence on the concentration of pre-adsorbed oxygen.

Another mechanism, called Eley-Rideal, has also been proposed for complete oxidation of ethylene at temperature above 280 ^{0}C on Pt films deposited on doped zirconia [59]. It has been found that the open-circuit catalytic kinetics can also be described quantitatively by the rate expression

$$r_o = \frac{k k_{ad} P_{C_2H_4} P_{O_2}}{k P_{C_2H_4} + k_{ad} P_{O_2}} \qquad \text{(Eq. 2-22)}$$

On the fuel-lean side ($k_{ad} P_{O_2} >> k P_{C_2H_4}$) the oxygen coverage is near unity and the ethylene reaction step is the rate limiting step. Thus equation (Eq. 2-22) reduces to:

$$r_o = k P_{C_2H_4} \qquad \text{(Eq. 2-23)}$$

On the fuel-rich side ($k_{ad} P_{O_2} << k P_{C_2H_4}$) the oxygen adsorption is the rate limiting step and equation (Eq. 2-22) reduces to:

$$r_o = k_{ad} P_{O_2} \qquad \text{(Eq. 2-24)}$$

2.3.2 Mechanism of complete oxidation of ethylene using O^{2-} conductors in closed circuit condition

It turns out [59] that varying U_{WR} and Φ cause dramatic (up to sixty fold) increases in k but have practically no effect on k_{ad}. Thus EPOC is much more pronounced on the fuel-lean side, i.e. when equation (Eq. 2-23) is valid.

It is found that the kinetic constant k depends on Φ according to:

$$\ln\left(\frac{k}{k_O}\right) = \alpha \frac{\left(\Phi - \Phi_O\right)}{k_b T} \qquad \text{(Eq. 2-25)}$$

and that the rate expression equation (Eq. 2-22) remains valid under EPOC conditions as well with k given from equation (Eq. 2-25). Therefore EPOC does not induce a change in reaction mechanism, but only a pronounced increase in the rate constant k. For high $\Delta\Phi$ values when k has become sufficiently large, then EPOC causes a change in the rate limiting step, i.e. EPOC causes oxygen adsorption to become rate limiting even under fuel-lean conditions.

2.4 Research objectives

The aim of the present research is:

(i) To synthesize gold nanoparticles supported on yttria-stabilized zirconia (8% Y_2O_3-stabilized ZrO_2), since this support has never been studied before. YSZ is an attractive support for heterogeneous catalysis because it possesses ionic conductivity at high temperatures, and thus, can be used as solid electrolyte.

(ii) To study the catalytic activity of the synthesized gold nanoparticles for the complete oxidation of ethylene and carbon monoxide in the temperature range of 25 ^{0}C to 350 ^{0}C and 25 ^{0}C to 250 ^{0}C, respectively.

(iii) To study the feasibility of electrochemical promotion of Au/YSZ-p in order to increase its catalytic activity for ethylene oxidation. Complete oxidation of ethylene is the model reaction studied in the thesis because of its simplicity and well established reaction mechanism. Also, ethylene is present in polluted air as volatile organic compounds, which can be harmful to environment as well as human; therefore, removal of ethylene through catalytic reaction is one of the applications of interest.

2.5 **References**

[1] G. Ertl, *Handbook of Hetergeneous Catalysis* vol. 1: Wiley, 2008.

[2] N. Lopez*, et al.*, "On the origin of the catalytic activity of gold nanoparticles for low-temperature CO oxidation," *Journal of Catalysis,* vol. 223, pp. 232-235, 2004.

[3] M. S. Chen and D. W. Goodman, "The structure of catalytically active gold on titania," *Science,* vol. 306, pp. 252-255, 2004.

[4] Y. D. Kim*, et al.*, "Characterization of various oxygen species on an oxide surface: RuO2(110)," *Journal of Physical Chemistry B,* vol. 105, pp. 3752-3758, 2001.

[5] D. W. Goodman*, et al.*, "CO oxidation on ruthenium: The nature of the active catalytic surface," *Surface Science,* vol. 601, pp. L124-L126, 2007.

[6] B. K. Min*, et al.*, "Efficient CO oxidation at low temperature on Au(111)," *Journal of Physical Chemistry B,* vol. 110, pp. 19833-19838, 2006.

[7] X. Deng*, et al.*, "Partial oxidation of propene on oxygen-covered Au(111)," *Journal of Physical Chemistry B,* vol. 110, pp. 15982-15987, 2006.

[8] W. Hermann, *Synthetic Method of Organimetallic and Inorganic Chemistry* vol. 9. Stuttgart: Thieme, 2000.

[9] P. N. Rylander, *Organic Chemistry* vol. 28. New York: Academic Press, 1973.

[10] M. Haruta*, et al.*, "Gold catalysts prepared by coprecipitation for low-temperature oxidation of hydrogen and of carbon monoxide," *Journal of Catalysis,* vol. 115, pp. 301-309, 1989.

[11] S. Tsubota*, et al.*, "CO oxidation over gold supported on TiO2," vol. 77, ed, 1993, pp. 325-328.

[12] M. Haruta*, et al.*, "Low-Temperature Oxidation of CO over Gold Supported on TiO2, α-Fe2O3, and Co3O4," *Journal of Catalysis,* vol. 144, pp. 175-192, 1993.

[13] M. Haruta*, et al.*, "Mechanistic Studies of CO Oxidation on Highly Dispersed Gold Catalysts for Use in Room-Temperature Air Purification," vol. 75, ed, 1993, pp. 2657-2660.

[14] M. Haruta*, et al.*, "Synergism in the catalysis of supported gold," vol. 77, ed, 1993, pp. 45-52.

[15] M. Haruta, "Size- and support-dependency in the catalysis of gold," *Catalysis Today,* vol. 36, pp. 153-166, 1997.

[16] G. J. Hutchings and M. Haruta, "A golden age of catalysis: A perspective," *Applied Catalysis A: General,* vol. 291, pp. 2-5, 2005.

[17] M. A. P. Dekkers*, et al.*, "CO adsorption and oxidation on Au/TiO2," *Catalysis Letters,* vol. 56, pp. 195-197, 1998.

[18] A. Wolf and F. Schüth, "A systematic study of the synthesis conditions for the preparation of highly active gold catalysts," *Applied Catalysis A: General,* vol. 226, pp. 1-13, 2002.

[19] R. J. H. Grisel*, et al.*, "Influence of the preparation of Au/Al2O3 on CH4 oxidation activity," *Journal of Catalysis,* vol. 191, pp. 430-437, 2000.

[20] A. C. Gluhoi, *et al.*, "Comparative studies of the N2O/H2, N2O/CO, H2/O2 and CO/O2 reactions on supported gold catalysts: Effect of the addition of various oxides," *Journal of Catalysis,* vol. 219, pp. 197-205, 2003.
[21] Y. Iizuka, *et al.*, "Adsorption of CO on gold supported on TiO2," *Catalysis Today,* vol. 36, pp. 115-123, 1997.
[22] Y. Iizuka, *et al.*, "A kinetic and adsorption study of CO oxidation over unsupported fine gold powder and over gold supported on titanium dioxide," *Journal of Catalysis,* vol. 187, pp. 50-58, 1999.
[23] J. R. Mellor, *et al.*, "The application of supported gold catalysts to automotive pollution abatement," *Catalysis Today,* vol. 72, pp. 145-156, 2002.
[24] H. H. Kung, *et al.*, "Supported Au catalysts for low temperature CO oxidation," *Journal of Catalysis,* vol. 216, pp. 425-432, 2003.
[25] S. J. Lee, *et al.*, "Effect of drying conditions of AU-Mn co-precipitates for low-temperature CO oxidation," *Journal of Catalysis,* vol. 200, pp. 298-308, 2001.
[26] F. Boccuzzi, *et al.*, "Au/TiO2 nanosized samples: A catalytic, TEM, and FTIR study of the effect of calcination temperature on the CO oxidation," *Journal of Catalysis,* vol. 202, pp. 256-267, 2001.
[27] N. A. Hodge, *et al.*, "Microstructural comparison of calcined and uncalcined gold/iron-oxide catalysts for low-temperature CO oxidation," *Catalysis Today,* vol. 72, pp. 133-144, 2002.
[28] F. Moreau, *et al.*, "Gold on titania catalysts for the oxidation of carbon monoxide: Control of pH during preparation with various gold contents," *Journal of Catalysis,* vol. 231, pp. 105-114, 2005.
[29] T. Hayashi, *et al.*, "Formation of propylene oxide by the gas-phase reaction of propane and propene mixture with oxygen," *Industrial and Engineering Chemistry Research,* vol. 34, pp. 2298-2304, 1995.
[30] G. Mul, *et al.*, "Stability and selectivity of Au/TiO2 and Au/TiO2/SiO2 catalysts in propene epoxidation: An in situ FT-IR study," *Journal of Catalysis,* vol. 201, pp. 128-137, 2001.
[31] E. J. A. X. Van De Sandt, *et al.*, "Catalyst development for the selective hydrogenolysis of CCl2F2 (CFC-12) into CH2F2 (HFC-32)," *Catalysis Today,* vol. 35, pp. 163-170, 1997.
[32] A. Wiersma, *et al.*, "Comparison of the performance of activated carbon-supported noble metal catalysts in the hydrogenolysis of CCl2F2," *Journal of Catalysis,* vol. 177, pp. 29-39, 1998.
[33] S. Ordóñeza, *et al.*, "Performance of activated carbon-supported noble metal catalysts in the hydrogenolysis of CCl3F," *Applied Catalysis B: Environmental,* vol. 29, pp. 13-22, 2001.
[34] M. Makkee, *et al.*, "Development of a palladium on activated carbon for a conceptual process in the selective hydrogenolysis of CCl2F2 (CFC-12) into CH2F2 (HFC-32)," *Catalysis Today,* vol. 55, pp. 125-137, 2000.
[35] C. W. Corti, *et al.*, "Commercial aspects of gold catalysis," *Applied Catalysis A: General,* vol. 291, pp. 253-261, 2005.

[36] Q. Xu, *et al.*, "The preparation of highly dispersed Au/Al2O3 by aqueous impregnation," *Catalysis Letters,* vol. 85, pp. 229-235, 2003.
[37] G. Pattrick, *et al.*, "The potential for use of gold in automotive pollution control technologies: A short review," *Topics in Catalysis,* vol. 30-31, pp. 273-280, 2004.
[38] J. A. Rodriguez, *et al.*, "Activation of gold on titania: Adsorption and reaction of SO2 on Au/TiO2(110)," *Journal of the American Chemical Society,* vol. 124, pp. 5242-5250, 2002.
[39] K. Ruth, *et al.*, "The effects of SO2 on the oxidation of CO and propane on supported Pt and Au catalysts," *Applied Catalysis B: Environmental,* vol. 24, pp. L133-L138, 2000.
[40] V. Patil, *et al.*, "Role of particle size in individual and competitive diffusion of carboxylic acid derivatized colloidal gold particles in thermally evaporated fatty amine films," *Langmuir,* vol. 15, pp. 8197-8206, 1999.
[41] D. G. Duff, *et al.*, "A new hydrosol of gold clusters. 2. A comparison of some different measurement techniques," *Langmuir,* vol. 9, pp. 2310-2317, 1993.
[42] H. Tsunoyama, *et al.*, "Colloidal gold nanoparticles as catalyst for carbon-carbon bond formation: Application to aerobic homocoupling of phenylboronic acid in water," *Langmuir,* vol. 20, pp. 11293-11296, 2004.
[43] D. V. Leff, *et al.*, "Thermodynamic control of gold nanocrystal size: Experiment and theory," *Journal of Physical Chemistry,* vol. 99, pp. 7036-7041, 1995.
[44] H. Hirai, "FORMATION AND CATALYTIC FUNCTIONALITY OF SYNTHETIC POLYMER-NOBLE METAL COLLOID," *Journal of macromolecular science.Chemistry,* vol. A13, pp. 633-649, 1979.
[45] T. Ashida, *et al.*, "Synthesis and characterization of Rh(PVP) nanoparticles studied by XPS and NEXAFS," *ECOSS-24, Proceedings of the 24th European Conference on Surface Science,* vol. 601, pp. 3898-3901, 2007.
[46] Y. Leng, *et al.*, "Iron nanoparticles dispersible in both ethanol and water for direct silica coating," *Powder Technology,* vol. 196, pp. 80-84, 2009.
[47] C. Li, *et al.*, "Mass synthesis of large, single-crystal Au nanosheets based on a polyol process," *Advanced Functional Materials,* vol. 16, pp. 83-90, 2006.
[48] G. C. Bond and D. T. Thompson, "Gold-catalysed oxidation of carbon monoxide," *Gold Bulletin,* vol. 33, pp. 41-50, 2000.
[49] G. C. Bond and D. T. Thompson, "Catalysis by Gold," *Catalysis Reviews - Science and Engineering,* vol. 41, pp. 319-388, 1999.
[50] G. Riahi, *et al.*, "Preparation, characterization and catalytic activity of gold-based nanoparticles on HY zeolites," *Catalysis Today,* vol. 72, pp. 115-121, 2002.
[51] L. Prati and G. Martra, "New gold catalysts for liquid phase oxidation," *Gold Bulletin,* vol. 32, pp. 96-101, 1999.
[52] E. R. S. A. Wieckowski, C.G. Vayenas, *Catalysis and Electrocatalysis at Nanoparticle Surfaces*. New York: Marcel Dekker, Inc, 2003.
[53] G. M. Schwab, *Advances in Catalysis* vol. 27. Orlando: Academic Press, 1978.
[54] F. Solymosi and K. Fónagy, "Effect of cadmium oxide and cadmium perchlorate on the decomposition and ignition of ammonium perchlorate," *Symposium (International) on Combustion,* vol. 11, pp. 429-437, 1967.

[55] S. Trassatti, *Comprehensive Treatise of Electrochemistry* vol. 1. New York: Plenum Press, 1980.
[56] N. D. M. N.W. Ashcroft, *Solid State Physics*. New York: Holt, Rinehart and Winston, 1976.
[57] M. Stoukides and C. G. Vayenas, "ELECTROCATALYTIC RATE ENHANCEMENT OF PROPYLENE EPOXIDATION ON POROUS SILVER ELECTRODES USING A ZIRCONIA OXYGEN PUMP," vol. 131, pp. 839-845 jesoan, 1984.
[58] C. G. Vayenas*, et al.*, "Dependence of catalytic rates on catalyst work function," *Nature,* vol. 343, pp. 625-627, 1990.
[59] C. G. Vayenas, S. Bebelis, C. Pilangos, S. Brosda, D. Tsiplakides, *Electrochemical Activation of Catalysis - Promotion, Electrochemical Promotion, and Metal-Support Interactions* vol. 1. New York, Boston, Dordrecht, London, Moscow: Kluwer Academic Publishers, 2002.
[60] M. Stoukides and C. G. Vayenas, "Solid-electrolyte-aided study of the ethylene oxidation on polycrystalline silver," *Journal of Catalysis,* vol. 69, pp. 18-31, 1981.
[61] M. Stoukides and C. G. Vayenas, "The effect of electrochemical oxygen pumping on the rate and selectivity of ethylene oxidation on polycrystalline silver," *Journal of Catalysis,* vol. 70, pp. 137-146, 1981.
[62] C. G. Vayenas*, et al.*, "Non-faradaic electrochemical modification of catalytic activity," *Journal of Physical Chemistry,* vol. 92, pp. 5083-5085, 1988.
[63] K. Jüttner*, et al.*, "Electrochemical approaches to environmental problems in the process industry," *Electrochimica Acta,* vol. 45, pp. 2575-2594, 2000.
[64] D. Tsiplakides*, et al.*, "Electrochemical promotion of catalysis: Mechanistic investigations and monolithic electropromoted reactors," *Catalysis Today,* vol. 100, pp. 133-144, 2005.
[65] C. G. Vayenas*, et al.*, "The double-layer approach to promotion, electrocatalysis, electrochemical promotion, and metal-support interactions," *Journal of Catalysis,* vol. 216, pp. 487-504, 2003.
[66] C. G. Vayenas, M. M. Jaksic, S. I. Bebelis, S. G. Neophytides, *Modern aspects of Electrochemistry*. New York: Plenum Press, 1996.
[67] C. Koutsodontis*, et al.*, "Electrochemical promotion of NO reduction by C2H4 in excess O2 using a monolithic electropromoted reactor and Pt-Rh sputtered electrodes," *Topics in Catalysis,* vol. 50, pp. 192-199, 2008.
[68] N. A. Anastasijevic, "NEMCA-From discovery to technology," *Catalysis Today,* vol. 146, pp. 308-311, 2009.
[69] R. Imbihl, "Electrochemical promotion of catalytic reactions," *Progress in Surface Science,* vol. 85, pp. 241-278, 2010.
[70] E. Mutoro*, et al.*, "Electrochemical promotion of Pt(111)/YSZ(111) and Pt-FeOx/YSZ(111) thin catalyst films: Electrocatalytic, catalytic and morphological studies," *Applied Catalysis B: Environmental,* vol. 100, pp. 328-337, 2010.
[71] A. Toghan*, et al.*, "Origin of non-Faradayicity in electrochemical promotion of catalytic ethylene oxidation," *Physical Chemistry Chemical Physics,* vol. 12, pp. 9811-9815, 2010.

[72] J. Nicole and C. Comninellis, "Electrochemical promotion of oxide catalyst for the gas phase combustion of ethylene," *Solid State Ionics,* vol. 136-137, pp. 687-692, 2000.
[73] A. de Lucas-Consuegra, *et al.*, "Pt/K-βAl2O3 solid electrolyte cell as a "smart electrochemical catalyst" for the effective removal of NOx under wet reaction conditions," *Catalysis Today,* vol. 146, pp. 330-335, 2009.
[74] D. Tsiplakides and C. G. Vayenas, "Electrode Work Function and Absolute Potential Scale in Solid-State Electrochemistry," *Journal of the Electrochemical Society,* vol. 148, pp. E189-E202, 2001.
[75] D. Kek, *et al.*, "A note on the impedance response of Li/LiCl/solid electrode system," *Solid State Ionics,* vol. 91, pp. 101-108, 1996.
[76] D. Kek, *et al.*, "A Study of Metal (Ni, Pt, Au)/Yttria-Stabilized Zirconia Interface in Hydrogen Atmosphere at Elevated Temperature," *Journal of the Electrochemical Society,* vol. 148, pp. A878-A886, 2001.
[77] R. M. Lambert, *et al.*, "Electrochemical promotion in emission control catalysis," *Ionics,* vol. 1, pp. 29-31, 1995.
[78] T. Arakawa, *et al.*, "Surface study of a Ag electrode on a solid electrolyte used as oxygen sensor," *Applications of Surface Science,* vol. 16, pp. 365-372, 1983.
[79] S. G. Neophytides, *et al.*, "Temperature-programmed desorption of oxygen from Pt films interfaced with Y2O3-Doped ZrO2," *Journal of Catalysis,* vol. 178, pp. 414-428, 1998.
[80] D. Tsiplakides and C. G. Vayenas, "Temperature programmed desorption of oxygen from Ag films interfaced with Y2O3-Doped ZrO2," *Journal of Catalysis,* vol. 185, pp. 237-251, 1999.
[81] S. Balomenou, *et al.*, "Novel monolithic electrochemically promoted catalytic reactor for environmentally important reactions," *Applied Catalysis B: Environmental,* vol. 52, pp. 181-196, 2004.
[82] J. Poppe, *et al.*, "Electrochemically Induced Surface Changes on Microstructured Pt Films on a Solid YSZ Electrolyte," *Berichte der Bunsengesellschaft/Physical Chemistry Chemical Physics,* vol. 102, pp. 1019-1022, 1998.
[83] J. Poppe, *et al.*, "Electrochemical promotion of catalytic CO oxidation on Pt/YSZ catalysts under low pressure conditions," *Physical Chemistry Chemical Physics,* vol. 1, pp. 5241-5249, 1999.
[84] A. Toghan, *et al.*, "The electrochemical promotion of ethylene oxidation at a pt/YSZ catalyst," *ChemPhysChem,* vol. 11, pp. 1452-1459, 2010.
[85] M. Marwood, *et al.*, "Electrochemical promotion of electronically isolated and dispersed Pt catalysts," *Ionics,* vol. 4, pp. 207-214, 1998.
[86] C. Pliangos, *et al.*, "Electrochemical promotion of conventional and bipolar reactor configurations for NO reduction," *Ionics,* vol. 8, pp. 372-382, 2002.
[87] D. Tsiplakides and S. Balomenou, "Milestones and perspectives in electrochemically promoted catalysis," *Catalysis Today,* vol. 146, pp. 312-318, 2009.
[88] S. Wodiunig, *et al.*, "Electrochemical promotion of bipolar electrodes: An estimation of the current bypass," *Electrochimica Acta,* vol. 46, pp. 357-363, 2000.

[89] C. Xia, *et al.*, "Electrochemical promotion of CO combustion over non-percolated Pt particles supported on YSZ using a novel bipolar configuration," *Electrochemistry Communications,* vol. 13, pp. 99-101, 2011.
[90] C. Xia, *et al.*, "Quantifying electrochemical promotion of induced bipolar Pt particles supported on YSZ," *Electrochemistry Communications,* vol. 12, pp. 1551-1554, 2010.
[91] D. Poulidi and I. S. Metcalfe, "Electrochemical promotion of a metal catalyst supported on a mixed-ionic conductor," *Solid State Ionics,* vol. 177, pp. 2211-2215, 2006.
[92] S. Ladas, *et al.*, "Work function measurements on catalyst films subject to in situ electrochemical promotion," *Surface Science,* vol. 251-252, pp. 1062-1068, 1991.
[93] I. S. Metcalfe, "Electrochemical Promotion of Catalysis: II: The Role of a Stable Spillover Species and Prediction of Reaction Rate Modification," *Journal of Catalysis,* vol. 199, pp. 259-272, 2001.
[94] I. S. Metcalfe, "Electrochemical Promotion of Catalysis: I: Thermodynamic Considerations," *Journal of Catalysis,* vol. 199, pp. 247-258, 2001.
[95] S. Trasatti, "Physical electrochemistry of ceramic oxides," *Electrochimica Acta,* vol. 36, pp. 225-241, 1991.
[96] G. F. E.A. Baranova, Ch. Comninellis, "Reactor development for practical utilization of electrochemical promotion of catalysis," in *International Conference on Solid State Ionics*, Baden-Baden, Germany, July 17-22, 2005.
[97] E. Varkaraki, *et al.*, "Electrochemical promotion of IrO2 catalyst for the gas phase combustion of ethylene," *Journal of Applied Electrochemistry,* vol. 25, pp. 978-981, 1995.
[98] M. Marwood and C. G. Vayenas, "Electrochemical promotion of a dispersed platinum catalyst," *Journal of Catalysis,* vol. 178, pp. 429-440, 1998.
[99] J. Nicole and C. Comninellis, "Electrochemical promotion of IrO2 catalyst activity for the gas phase combustion of ethylene," *Journal of Applied Electrochemistry,* vol. 28, pp. 223-226, 1998.
[100] S. Wodiunig, *et al.*, "Electrochemical promotion of RuO2 catalyst dispersed on an yttria-stabilized zirconia monolith," *Electrochemical and Solid-State Letters,* vol. 2, pp. 281-283, 1999.
[101] S. Balomenou, *et al.*, "Electrochemical promotion of Pd, Fe and distributed Pt catalyst-electrodes," *Solid State Ionics,* vol. 136-137, pp. 857-862, 2000.
[102] C. B. Azzoni, *et al.*, "Defect model for the optical and EPR activity of the T-center in yttrium-stabilized zirconia," *Radiation Effects and Defects in Solids,* vol. 134, pp. 485-488, 1995.
[103] C. B. Azzoni, *et al.*, "About some features of the T center EPR signal in YSZ," *Journal of Magnetism and Magnetic Materials,* vol. 140-144, pp. 175-176, 1995.
[104] D. Andreeva, *et al.*, "Nanosize gold catalysts promoted by vanadium oxide supported on titania and zirconia for complete benzene oxidation," *Applied Catalysis A: General,* vol. 209, pp. 291-300, 2001.
[105] A. Naydenov, *et al.*, "Ozone decomposition on gold supported catalysts," *Oxidation Communications,* vol. 26, pp. 492-495, 2003.

[106] M. Chun Yan, *et al.*, "Mesoporous co3o4 and AU/CO3o4 catalysts for low-temperature oxidation of trace ethylene," *Journal of the American Chemical Society,* vol. 132, pp. 2608-2613, 2010.
[107] J. Li, *et al.*, "Efficient elimination of trace ethylene over nano-gold catalyst under ambient conditions," *Environmental Science and Technology,* vol. 42, pp. 8947-8951, 2008.
[108] K. Arve, *et al.*, "Selective catalytic reduction of NOx over nano-sized gold catalysts supported on alumina and titania and over bimetallic gold-silver catalysts supported on alumina," *Topics in Catalysis,* vol. 52, pp. 1762-1765, 2009.

Chapter 3 Experimental

3.1 Introduction

In this chapter, the experimental procedure for gold nanoparticle preparation, their physiochemical characterizations, as well as an experimental setup for catalytic activity measurements of gold nanoparticles in complete oxidation of carbon monoxide and ethylene are described.

3.2 Synthesis of Gold Nanocatalyst

Refluxing precursor salt with ethanol yields the following reaction [1]:

$$2HAuCl_4 + 3CH_3CH_2OH \rightarrow 2Au_{(0)} + 3CH_3CHO + 8HCl \qquad \text{(Eq. 3-1)}$$

3.2.1 Synthesis Method

Au nanoparticles (Au) deposited on YSZ powder (Au/YSZ-p) are synthesized using chemical reduction method. A previously developed synthesis method for colloidal platinum nanoparticles [2] is adopted to make the supported gold nanoparticles. Gold (III) chloride (Aldrich, 99.999%) precursor salt is dissolved in mixture of nanopure water (18 MΩ cm) and ethanol (99%, Fisher) with the ratio of H_2O:C_2H_5OH of 1:1, in the presence of PVP (10,000 average molecular weight, Sigma) and YSZ powder (YSZ-p 8% Y_2O_3-ZrO_2, with average crystallite size of 25 nm, 0.6 μm particle size, bulk density of 1.3 g cm^{-3} and

specific surface area of 13 $m^2 g^{-1}$, TOSOH). The molar ratio of PVP to gold is varied from 3:1 to 20:1. The appropriate amount of YSZ-p is added to the solution to attain the gold loading of 1 wt. % on YSZ-p. The obtained mixture is stirred for 30 min at room temperature then refluxed at 100 °C for 2 h, following by extensive washing with nanopure water and drying in the air at 70 °C. The initial color of the opaque mixture appears yellow. After about 30 minutes, the mixture color turns pink or purple, depending on the concentration of PVP. Upon drying, the synthesized 1 wt. % Au nanoparticles on YSZ powder has pink to purple color depending on the particle size of Au. The schematic of the synthesis method is shown in Figure 3-1 and the synthesis details of Au/YSZ-p catalysts are summarized in Table 3-1.

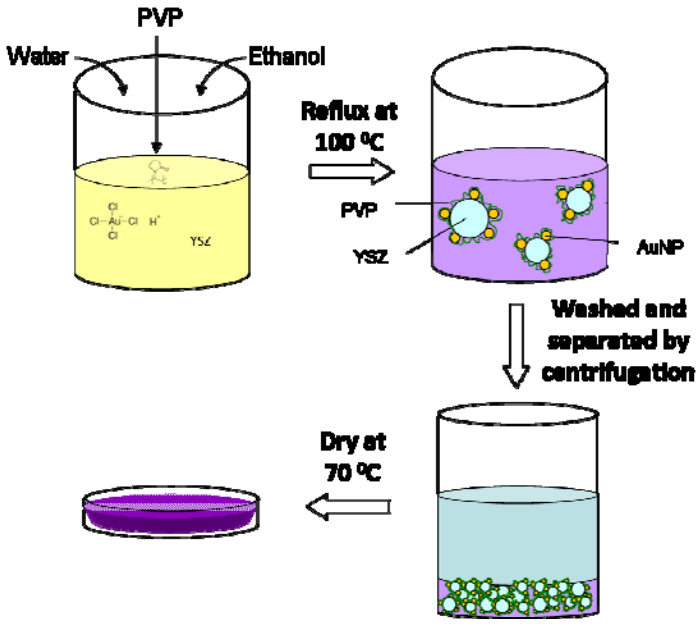

Figure 3-1 Schematics of the synthesis method of Au nanoparticles supported on YSZ-p

Table 3-1 Properties of synthesized Au/YSZ-p catalysts

Name	PvP:Au	Wt of Au on YSZ	Color	
	[mol:mol]	[%]	Before calcination	After calcination
Au1/YSZ-p	3:1	0.99	Dark pink	Bright purple
Au2/YSZ-p	6:1	1.00	Pink	Purple
Au3/YSZ-p	10:1	1.00	Bright pink	Dark purple
Au4/YSZ-p	20:1	1.00	Brightest pink	Brightest purple

It is expected that increasing the molar ratio of PVP to Au will result in the formation of smaller gold nanoparticles, due to the excess of PVP protective agents [3, 4].

3.2.2 Removal of PVP

As previously described in section 2.1.3.2, the polymer protective agents contribute to synthesizing smaller nanoparticles [3-6]. However, these polymers have negative effect on the catalytic performance of the nanoparticles [2, 3] as they block catalytically active sites. Therefore, the PVP is removed from the synthesized Au/YSZ-p catalyst by two different treatments - calcination at 600 °C for 2 h in air and oxygen plasma etching at radio frequency of 113 for 10 minutes (Anatech Plasma Asher Etcher SP-100 Chamber 6'').

3.3 Characterizations of Gold Nanoparticles

Several methods are used to characterize the resulting Au/YSZ-p catalysts, among them are scanning electron microscopy (SEM), transmission electron microscopy (TEM), X-ray diffraction (XRD), X-ray photoelectron spectroscopy (XPS), and thermogravimetric

analysis (TGA). Both quantitative and qualitative analyses of the catalysts are carried out using above mentioned characterization methods.

3.3.1 Scanning Electron Microscopy (SEM)

The measurements were carried out with a scanning electron microscope (JEOM JSM 7500F). The type of signal used to image the gold nanoparticles samples is back-scattered electrons (BSE), which allows easier detection of gold nanoparticles on YSZ support than the typical transmission imaging signal. Because the intensity of the BSE signal is strongly related to the atomic number (Z) of the specimen, BSE images can provide information about the distribution of gold among YSZ support. For SEM measurements, the Au/YSZ-p is dispersed in ethanol, deposited on a carbon-meshed copper grid (Carbon Film 300 Mesh, EMS) and then dried in the air for 5 min. The samples are analyzed qualitatively as well as quantitatively by measuring and computing the average size of nanoparticles using measuring software called MeasureIT.

3.3.2 Transmission Electron Microscopy (TEM)

High-resolution transmission electron microscopy (HRTEM) images are taken for the Au/YSZ-p catalysts tested (High-Resolution Transmission Electronic Microscopy, JEOL 2010 LaB6) in order to obtain a higher resolution so that the morphology and size of Au particles may be better investigated. An extraction replica technique is used for sample preparation [7]. The catalyst is dispersed in ethanol, deposited on a mica film and covered with a carbon layer. The YSZ support and film of mica are then dissolved in hydrogen

fluoride solution for 24 hours resulting in Au particles being fixed on the carbon film. These particles are directly observed by HRTEM. A conventional technique has also been used to observe gold nanoparticles supported on YSZ-p by simply depositing the dispersed catalyst in ethanol directly onto the copper grid. The use of MeasureIT software allowed for the determination of Au particle size distribution.

3.3.3 X-ray Diffraction (XRD)

The specific instrument used for XRD measurements is Bruker AXS D8 Advance system (θ-θ power diffractometer) with Cu Kα source between 25^0 and 65^0. The crystallographic structure, crystal size, and preferred orientation of catalyst powders are characterized. By comparing diffraction data with other journals [8-11], the substance of the sample is determined. In addition, Scherrer formula [12] is applied to estimate the size of the nanoparticle

$$\tau = \frac{K\lambda}{\beta \cos\theta} \qquad \text{(Eq. 3-2)}$$

where τ is the crystallite size, K is the Scherrer constant, λ is the x-ray wavelength, β is the full width at half maximum (FWHM), and θ is the Bragg angle. The values of β and θ are obtained from analyzing the raw data. K and λ are constant values.

3.3.4 X-ray Photoelectron Spectroscopy (XPS)

The measurements are carried out using KRATOS Axis Ultra, X-Ray source with an aluminum anode at 150 W, monochromated. Deconvolution of the XPS spectra and

element quantification are performed using the CasaXPS program. The carbon peak from the run is used as an internal standard to correct for any shift in binding energies that could occur mainly due to surface charging during the XPS measurements. Obtained raw data are adjusted according to binding energy of carbon (284.4 eV) from the *XPS handbook of The Elements and Native Oxide*, by XPS International, INC [13].

3.3.5 Thermogravimetric Analysis (TGA)

Since PVP is used to synthesize gold nanoparticles on YSZ powder (Au/YSZ-p), a method to remove the PVP after synthesis is required. The chosen method is to calcine the sample at high temperature. The temperature range should be high enough to decompose the carbons and other volatile compounds in the PVP polymer, but also, the temperature should be low enough that sintering and formation of agglomerates of Au nanoparticles are minimized. In order to determine the proper calcination temperature, TGA is run to establish the temperature range at which carbon decomposes. The model of the TGA instrument used is 2960 SDT V3.0F. Heating ramp is done at 1.2 ^{0}C min^{-1} from room temperature to 580 ^{0}C

3.4 Catalytic Measurement Units

The schematic diagram for the catalytic measurement experiment is described in Figure 3-2. For all catalytic experiments, three trials are done and the average of them are calculated.

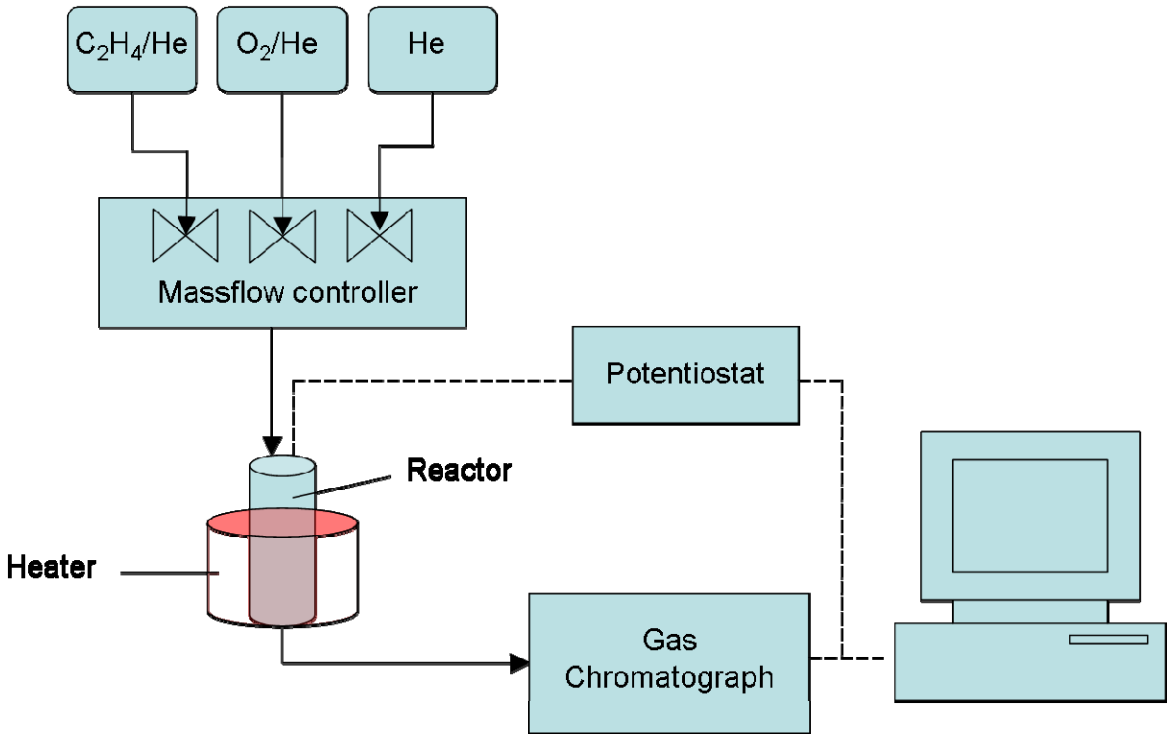

Figure 3-2 Flow diagram of the experimental setup

Reactants of diluted ethylene, oxygen and pure helium are fed into the reactor through mass flow controller. Two types of mass flow controllers are used: Omega (Gas Proportioning Rotameter, FL-1GP Series) rotameter and MKS electronic mass flow controller are used to control the mass flow of the inlet gases. The reaction gases are mixtures of 5% C_2H_4 (Grade 5, 99.999%, Linde Canada) balances in He (Grade 5, 99.999%, Linde Canada) and 20% O_2 (Grade 4.5, 99.995%, Linde Canada) balanced in He (Grade 5, 99.999%, Linde Canada) and a pure He (Grade 5, 99.999% Linde Canada) as a carrier gas. The temperature of the reactor is controlled by an external controller (Fuzypro, HCS). The products exiting the reactor are analyzed by online-gas chromatograph (Gowmac 350).

Electrochemical promotion experiments are performed under potentiostatic control using the potentiostat/galvanostat (Princeton Applied Research, PARstat 2263). The outlet gases are exposed to atmospheric pressure.

The catalytic measurements are carried out using two reactor types. One reactor is used for heterogeneous catalytic measurements under open circuit conditions. The reactor consists of a tubular, atmospheric pressure, plug flow reactor (PFR) type of quartz (V = 25 cm^3, Figure 3-3 (A)) reactor. Gold nanoparticles supported on YSZ-p (Au/YSZ-p) are placed on the 5 mm of fritted glass membrane (Figure 3-3 (A)) with outer diameter of 20 mm. Typical amount of Au/YSZ-p per experiment is 50 mg.

For electrochemical promotion experiments under open and closed circuit, the electrochemical cell (Figure 3-4) is placed in a continuously stirred tank reactor (CSTR) type of quartz (V = 100 cm^3) (Figure 3-3 (B)) reactor. The schematic illustrations of both reactors are shown in Figure 3-3.

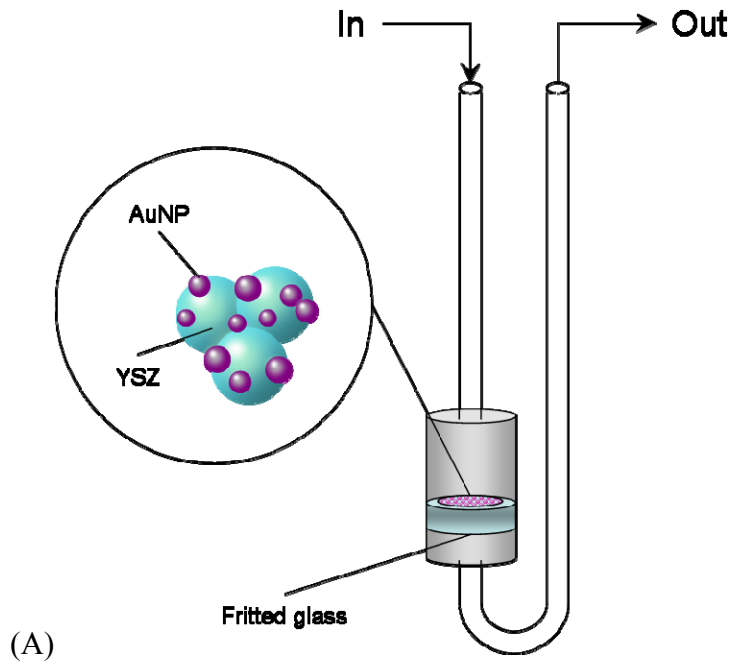

(A)

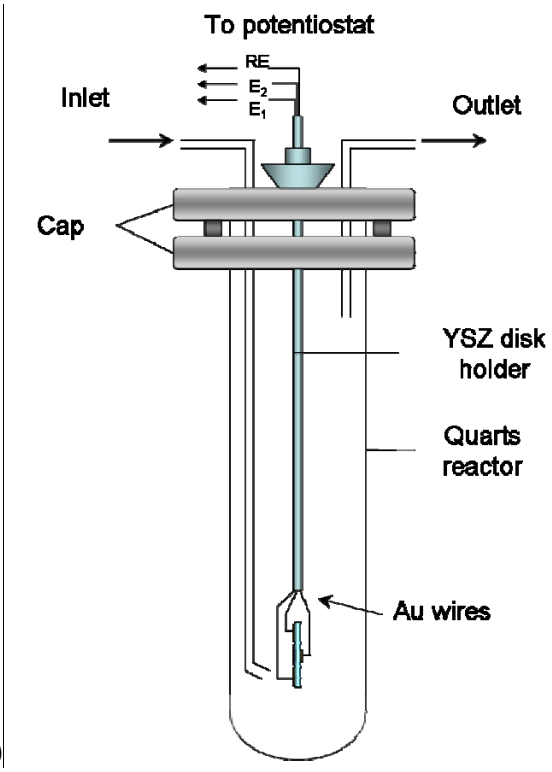

(B)

Figure 3-3 plug flow reactor (A) for heterogeneous catalysis measurements and continuously stirred tank reactor (B) for electrochemical promotion measurements.

3.5 **Electrochemical cells**

All electrochemical cells used in the following experiments are single-disk type with the disk dimension of 10 mm radius and 1 mm thickness. These disks are preliminarily sandblasted for 20 seconds and sonicated in deionized water for 10 minutes in order to increase the roughness of the surface, which is important in order to increase the contact area between catalyst and support.

As mentioned in section 2.2.3.1, there are different configurations within the specific electrochemical cell type [14-16]. Bipolar configuration is used for the electrochemical promotion of gold nanoparticles since the nanoparticles cannot be dispersed with continuous electronic conductivity on YSZ solid electrolyte to function as working electrode. Therefore, electronically isolated gold nanoparticles will be polarized by two auxiliary electrodes. The bipolar configuration with gold nanoparticles dispersed on YSZ has never been reported previously.

3.5.1 Bipolar cell configuration of gold nanoparticles

The bipolar configuration is presented in Figure 3-4. First, three gold film electrodes are deposited onto both sides of the YSZ disk by applying gold paste (C20904284, Gwent). Two inert gold films (E1 and E2, Figure 3-4) are used as feeder electrodes in order to apply a constant polarization across the YSZ. On the other side of the disk, the gold pseudo reference electrode is applied. The three electrodes are let dry in air for 10 min, followed by calcination at 600 ^{0}C for 3 hours. Finally, 18 mg of the synthesized

gold nanoparticles supported on YSZ powder (Au/YSZ-p) catalyst are deposited on the YSZ disk by placing 18 µL of the dispersed catalyst in ethanol (0.666g of catalyst per ml of ethanol) using micro pipette.

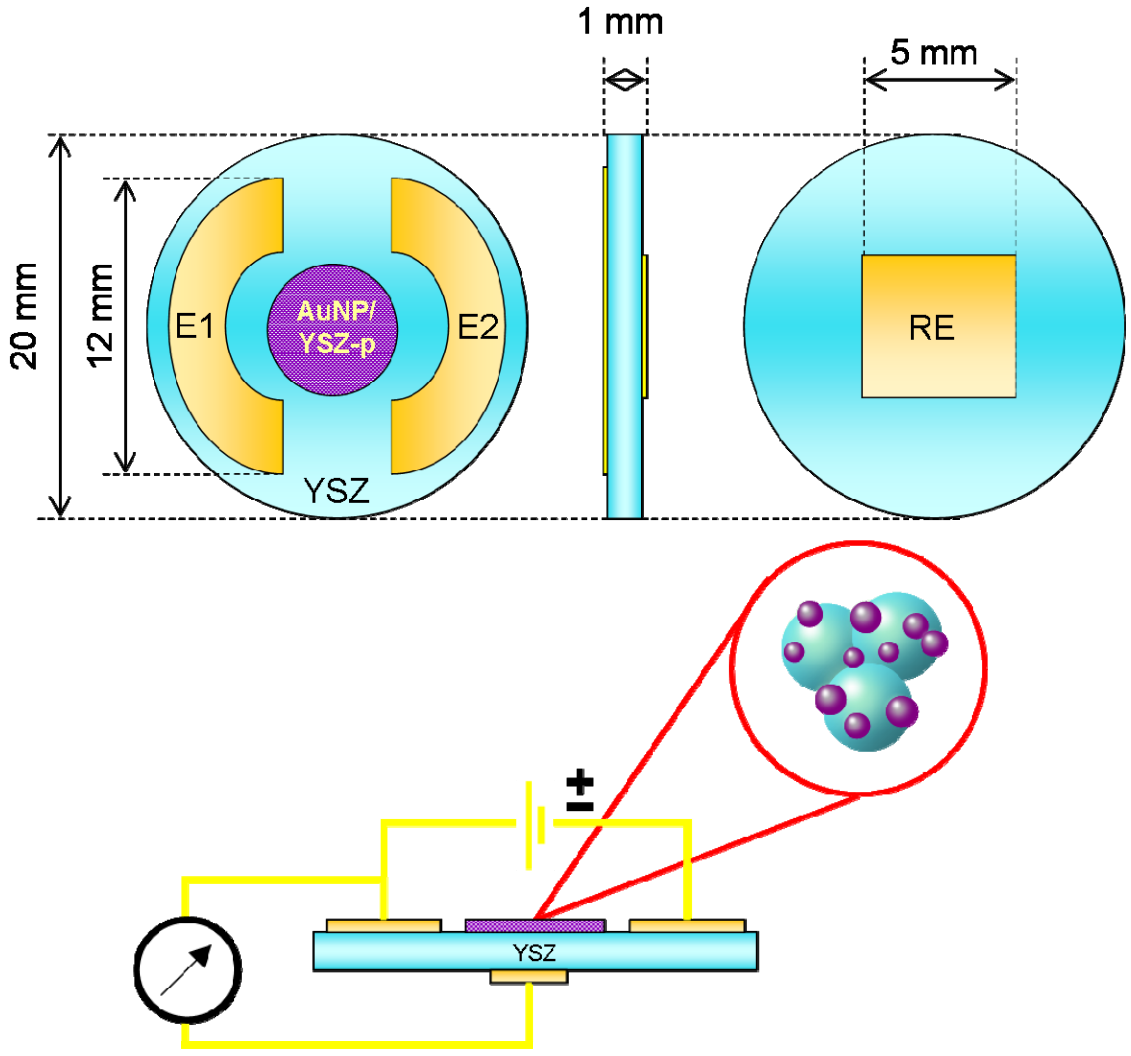

Figure 3-4 Dimension of the single-disk type bipolar electrochemical cell configuration. A) top view, b) bottom view, c) and d) side view

The resulting electrochemical cell is used to carry out catalytic measurements of ethylene oxidation under open and closed circuit conditions which is discussed in further detail in the later section of the thesis.

3.6 **References**

[1] W. Hermann, *Synthetic Method of Organimetallic and Inorganic Chemistry* vol. 9. Stuttgart: Thieme, 2000.

[2] S. R. Wang and W. J. Tseng, "Aggregate structure and crystallite size of platinum nanoparticles synthesized by ethanol reduction," *Journal of Nanoparticle Research,* vol. 11, pp. 947-953, 2009.

[3] C. Li, *et al.*, "Mass synthesis of large, single-crystal Au nanosheets based on a polyol process," *Advanced Functional Materials,* vol. 16, pp. 83-90, 2006.

[4] P. Y. Silvert and K. Tekaia-Elhsissen, "Synthesis of monodisperse submicronic gold particles by the polyol process," *Solid State Ionics,* vol. 82, pp. 53-60, 1995.

[5] Y. Leng, *et al.*, "Iron nanoparticles dispersible in both ethanol and water for direct silica coating," *Powder Technology,* vol. 196, pp. 80-84, 2009.

[6] B. Zhao and Y. W. Chen, "The effect of poly-N-vinylpyrrolidone modification on NiCoB catalysts for hydrogenation of p-chloronitrobenzene," *Materials Chemistry and Physics,* vol. 125, pp. 763-768, 2011.

[7] L. B. J. Ayache, J. Boumendil, G. Ehret, and D. Laub, "Sample Preparation Handbook for Transmission Electron Microscopy," in *Chapter 5*, ed: Springer, 2010, pp. 229-256.

[8] J. H. Liu, *et al.*, "Synergistic effect in an Au-Ag alloy nanocatalyst: CO oxidation," *Journal of Physical Chemistry B,* vol. 109, pp. 40-43, 2005.

[9] V. Deepak, *et al.*, "Synthesis of gold and silver nanoparticles using purified URAK," *Colloids and Surfaces B: Biointerfaces,* vol. 86, pp. 353-358, 2011.

[10] M. Ousmane, *et al.*, "Supported Au catalysts for propene total oxidation: Study of support morphology and gold particle size effects," *Catalysis Today,* 2011.

[11] E. Mutoro, *et al.*, "Electrochemical promotion of Pt(111)/YSZ(111) and Pt-FeOx/YSZ(111) thin catalyst films: Electrocatalytic, catalytic and morphological studies," *Applied Catalysis B: Environmental,* vol. 100, pp. 328-337, 2010.

[12] A. R. West, *Solid State Chemistry and Its Applications*. New York: Wiley, 1984.

[13] V. Crist, "Demo Version (87 pages) PDF Handbooks of Monochromatic XPS Spectra," in *Handbook of The Elements and Native Oxides*, ed, 1999.

[14] M. Marwood, *et al.*, "Electrochemical promotion of electronically isolated and dispersed Pt catalysts," *Ionics,* vol. 4, pp. 207-214, 1998.

[15] S. Wodiunig, *et al.*, "Electrochemical promotion of RuO2 catalyst dispersed on an yttria-stabilized zirconia monolith," *Electrochemical and Solid-State Letters,* vol. 2, pp. 281-283, 1999.

[16] C. Xia, *et al.*, "Electrochemical promotion of CO combustion over non-percolated Pt particles supported on YSZ using a novel bipolar configuration," *Electrochemistry Communications,* vol. 13, pp. 99-101, 2011.

Chapter 4 Physiochemical Characterizations of Gold Nanoparticle Catalysts

4.1 Introduction

Advancements in the understanding of nanoparticles have been arriving from the developments of numerous nanoparticle synthesis methods as well as their accurate characterizations. This can eventually lead us to efficiently applying nanoparticles to various catalytic processes, using size-dependent properties of small nanoparticles [1-5]. In this chapter, a new synthesis method for gold nanoparticles, supported on yttria-stabilized zirconia (YSZ), is shown. YSZ is an interesting support for catalyst because it possesses ionic conductivity at high temperatures, and thus, can be used as solid electrolyte. Physiochemical characterizations of the synthesized supported nanoparticles are also presented.

4.2 Characterizations of Au/YSZ-p

4.2.1 TGA

Thermogravimetric analysis is carried out to determine an optimum temperature range at which the synthesized Au/YSZ-p samples are to be calcined in order to completely remove PVP stabilizing agent. The temperature range should be high enough to decompose the carbons and other volatile compounds in the PVP polymer, but also, the temperature

should be low enough that sintering and formation of agglomerates of Au nanoparticles are minimized. TGA on Au1/YSZ-p has been done (Figure 4-1).

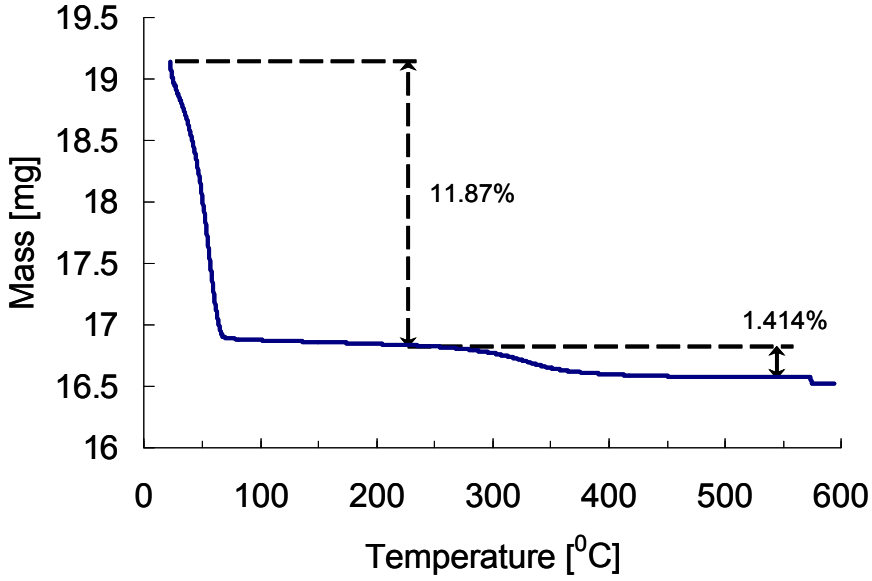

Figure 4-1 TGA of 1 wt. % Au1/YSZ-p prepared at Au:PVP ratio of 3:1

The first loss in mass of 11.87 % is related to water evaporation and the second loss of 1.414 % is related to polymer decomposition. There is a slight loss of mass just below 600 ^{0}C, likely being a partial removal of oxygen from YSZ. In order to account for all losses detected from TGA, 600 ^{0}C is selected to be the suitable temperature for calcination. To give enough time for all PVP to decompose, 2 hours are chosen for the calcination time. However, optimization of the calcination temperature is necessary to obtain a catalyst with smaller nanoparticles.

4.2.2 SEM

The morphology and surface properties of the Au/YSZ-p is studied by scanning electron microscopy (SEM). Backscattered (BS) electron detector is used to detect gold nanoparticles. Without the BS detector, the thick YSZ support does not allow enough transmission of electrons to display clear image, but only shows black clouds of support. BSE detector allows heavy elements (high atomic number) to backscatter electrons more strongly than light elements (low atomic number), resulting in heavier elements to appear brighter in the image. Therefore, with the BSE detector, 1 weight percent of gold nanoparticles appeared as brighter dots amongst YSZ supports, which appeared in less bright color.

As previously mentioned in 3.2, three different Au/YSZ-p samples are synthesized, varying by their initial PVP contents. The Au/YSZ-p samples then undergoes calcination treatment to remove the PVP. The figures below show SEM images of Au1/YSZ-p sample before and after the treatment.

Untreated

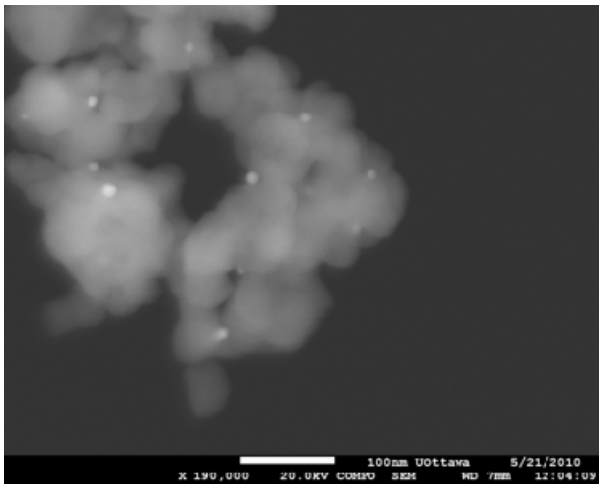

(A)

Calcinated

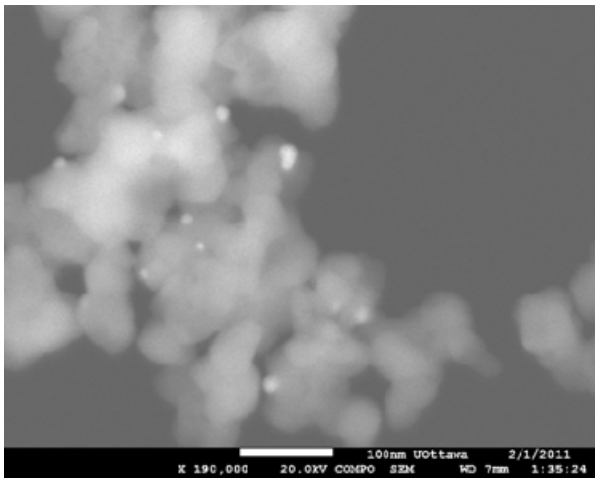

(B)

Figure 4-2 SEM (BS detector) micrographs of Au1/YSZ-p sample before treatment (A) and after 600 ^{0}C calcination treatment (B)

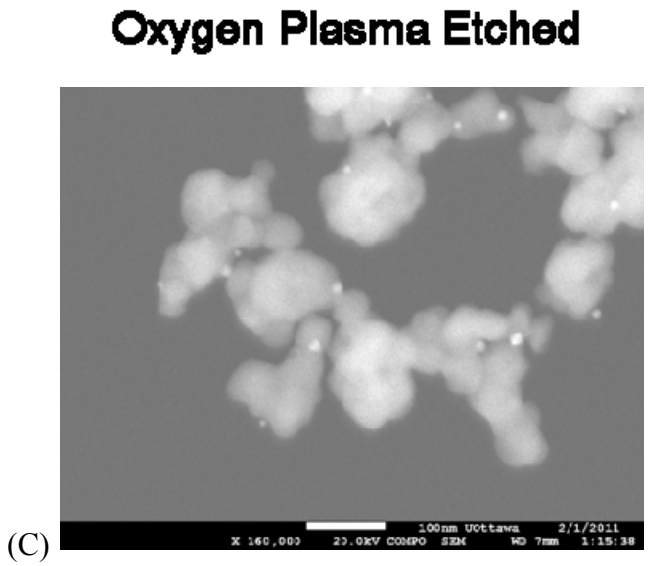

(C)

Figure 4-3 (Continued) SEM (BS detector) micrographs of Au1/YSZ-p sample after oxygen plasma etching at 112 RF for 10 minutes (C)

The image shows that the gold nanoparticles are stable after calcination or oxygen plasma etching treatment, showing no significant change in the appearance of the samples. Calcination treatment is chosen as the default treatment to all catalysts. Figure 4-4 summarizes the SEM images of calcined Au1/YSZ-p, Au2/YSZ-p, Au3/YSZ-p and Au4/YSZ-p catalysts and their particle size distribution.

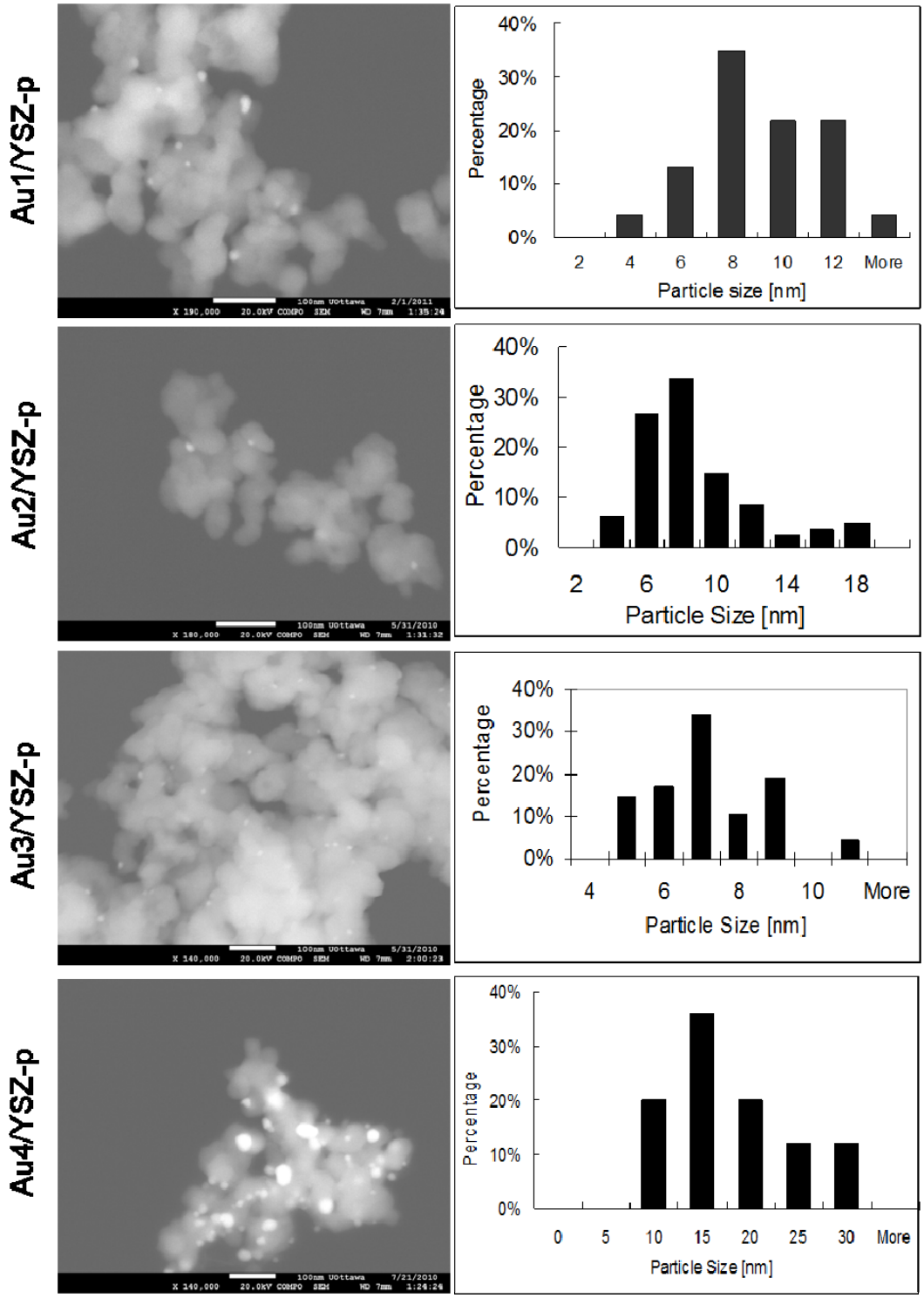

Figure 4-4 SEM (BS detector) micrographs of different calcined Au/YSZ-p samples (left) and their particle size distributions (right)

Small bright white dots indicate qualitatively that the gold nanoparticles are well dispersed throughout YSZ powder. Due to the low resolution of SEM images, it is difficult to distinguish their exact size, shape and possible presence of agglomerates from the SEM. Therefore, TEM, which has significantly higher resolution than SEM was used to identify the shape and size of the nanoparticles (section 4.2.3).

Histograms of Au nanoparticles reveal that the mean of particle size has decreased as PVP concentration increased. However, great excess amount of PVP actually hinders the reaction and thorough mixing of the solution that the particle sizes start to increase, as shown in the case of Au4/YSZ-p. Also, very small particles (< 3nm) are not easily detectable in SEM. Overall, SEM is only used in the preliminary stage to confirm that there are nanoparticles present in the sample and that they are well dispersed on YSZ-p support.

4.2.3 TEM

TEM is used in order to obtain the higher resolution micrographs of Au/YSZ-p samples. Two different methods are used to look at the Au/YSZ-p samples. First, the sample is analyzed as it is, i.e., gold nanoparticles supported on YSZ. This is done to observe how gold nanoparticles are interacting with the support. The second TEM method used is called replica technique. Replica technique can extract gold nanoparticles from YSZ, thus, this technique is useful to examine surface features, size and the shape of the nanoparticles.

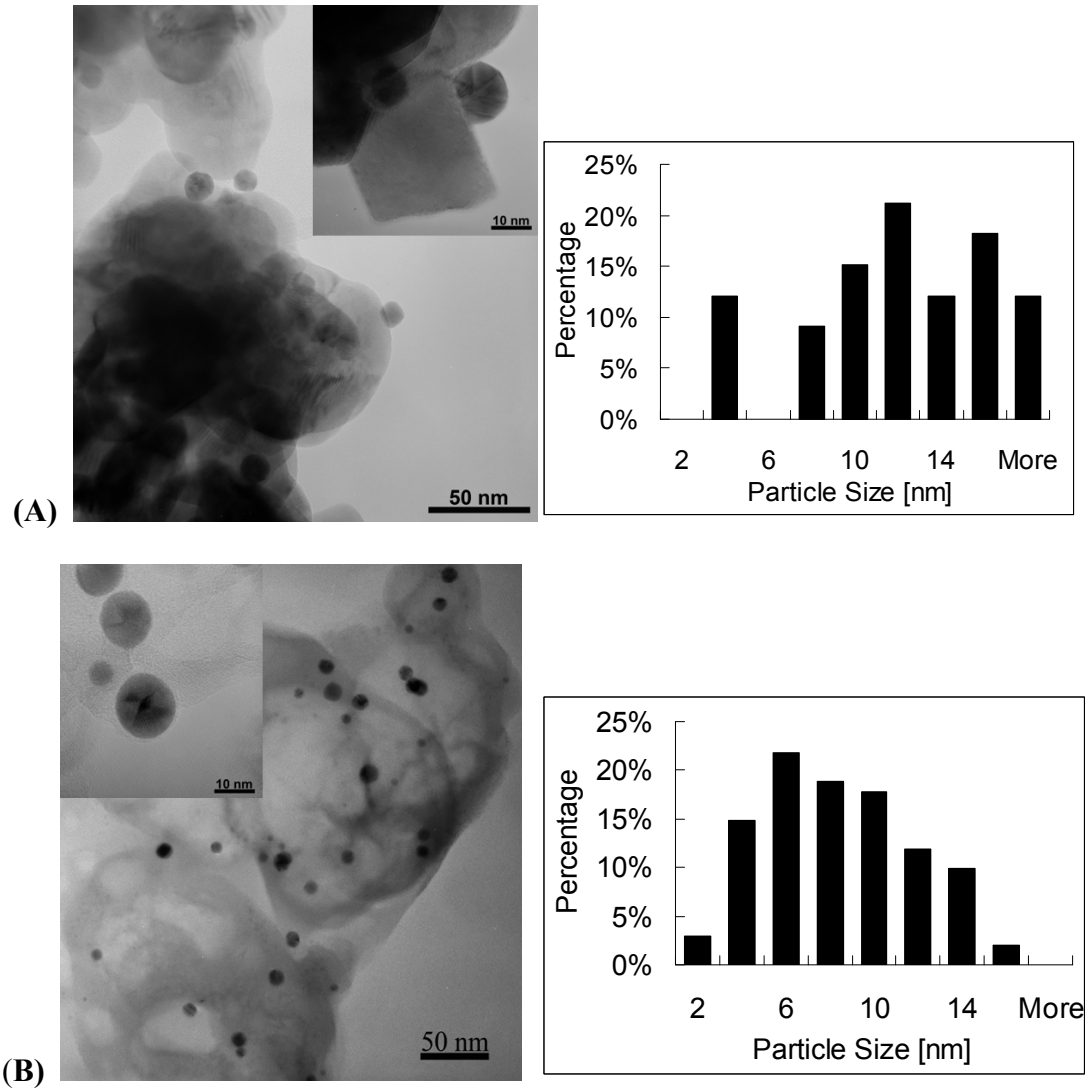

Figure 4-5 TEM of calcined Au1/YSZ-p, (A) and Au after support removal using replica technique, (B) (left) and corresponding histograms (right) Molar ratio of Au:PVP = 1:3.

Figure 4-5 (A) shows TEM images of Au sample supported on YSZ. It appears that the gold nanoparticles are spherical and well dispersed on YSZ support. Interestingly, TEM using the replica technique, shown in Figure 4-5 (B), reveals that smaller nanoparticles are also present, either inside of the YSZ or underneath the YSZ that would not have been

visible from the images using the conventional TEM technique. In agreement to TEM of supported Au/YSZ-p, the particles appear to be spherical in shape.

4.2.4 XRD

Using X-Ray Diffraction one can determine the crystallographic structure, crystal size and preferred crystallographic orientation of gold nanoparticles.

First, a broad $2\theta^0$ scan is carried out between 25 and 65 $2\theta^0$ to examine the content of the samples, as well as their crystallographic structure. The full scan of calcined Au1/YSZ-p sample is shown in Figure 4-7.

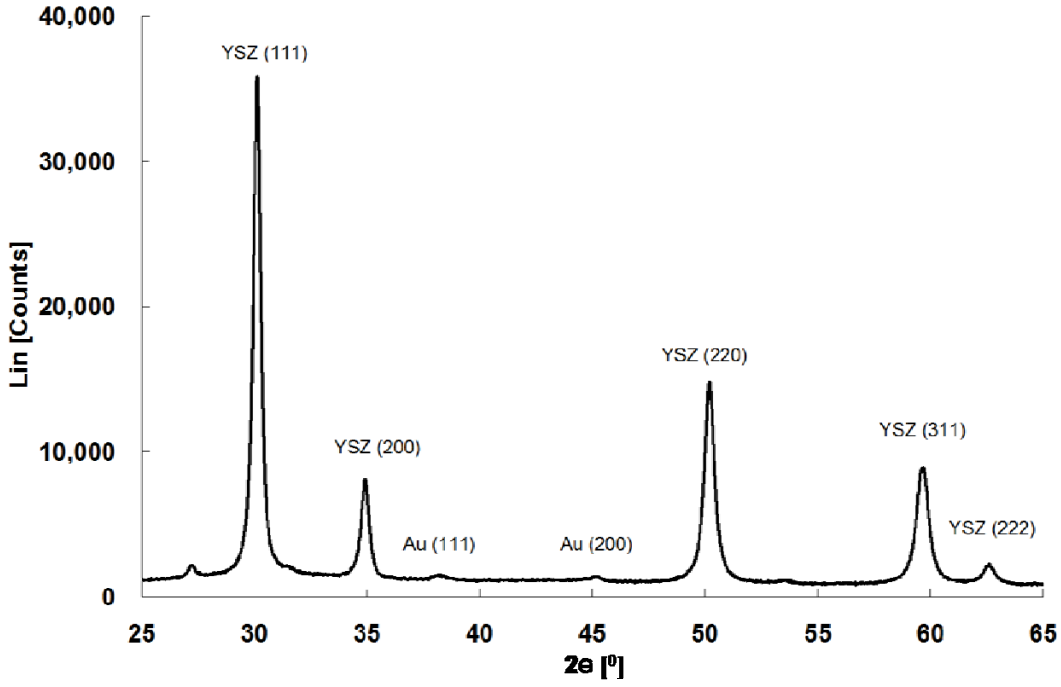

Figure 4-6 XRD patterns in the broad range from 28 to 65 ^{0}2θ

The results indicate that there are YSZ and gold present in the sample. The appearance of YSZ peaks in order of (111), (200), (220), (311) and (222) indicates that YSZ are face-centered cubic (fcc) structure [6]. Similarly Au peaks appear in order of (111) and (200) at 38 and 45 $^{0}2\theta$, which indicates that Au nanoparticles have fcc structure [7]. Similar results are obtained for all Au/YSZ-p samples.

In order to find a crystallite size of Au nanoparticles, Scherrer equation (Chapter 3, (Eq. 3-2)) is applied. Full widths at half maximum (FWHM) of the (111) peak evaluated between 37 and 39.5 $^{0}2\theta$ is calculated using interpolation (Figure 4-7). The background counts are set at 65 $^{0}2\theta$ for all samples.

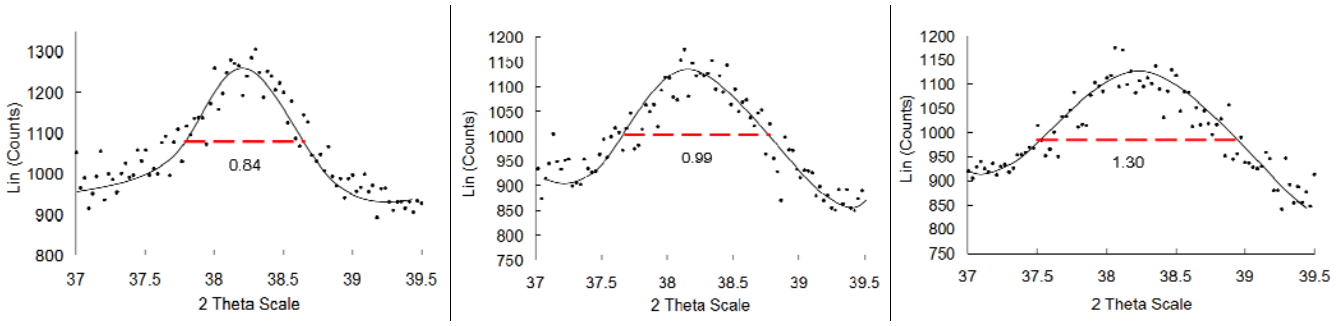

Figure 4-7 X-ray diffraction patterns of calcined Au1/YSZ-p (a), Au2/YSZ-p (b) and Au3/YSZ-p (c) around Au (111) peak. The numbers indicate the values of the calculated FWHM.

The crystallite sizes calculated using Scherrer equation for four calcined Au/YSZ-p catalysts is summarized in Table 4-1.

Table 4-1 FWHM, average particle size and dispersion of Au/YSZ-p catalysts from XRD

Nanoparticles	Au:PVP ratio [%]	FWHM [$2\theta^0$]	Average Particle Size [nm]	Dispersion [%]
Au1/YSZ-p	1:3	0.84	9.7	4.6
Au2/YSZ-p	1:6	0.99	8.3	5.4
Au3/YSZ-p	1:10	1.30	6.3	7.1
Au4/YSZ-p	1:20	0.78	10.3	4.3

The trend in particle size obtained from XRD is similar to that of SEM measurements, which suggests that in general, increasing in the amount of PVP leads to decreasing the size of gold nanoparticles. However, having an extreme amount of PVP can actually increase the particle size because the solution becomes very viscous and disallows homogeneous mixing.

Dispersion calculation is performed for all Au/YSZ-p catalysts using the average crystallite diameter from the XRD measurements and the following equation,

$$dispersion\ (\%) = \frac{MW_{Au} \times 600}{\rho_{Au} d_{avg} a_{Au} N_a} \qquad \text{(Eq. 4-1)}$$

Where MW_{Au} is the molecular weight of Au (196.97 g mol^{-1}), ρ_{Au} is the density of Au (19.43 g cm^{-3}), d_{avg} is the average particle size, a_{Au} is the surface area of one Au atom (2.29 x 10^{-17} cm^2 $atom^{-1}$), and N_a is Avogadro's number (6.022 x 10^{23} atom mol^{-1}). The dispersion of metal in catalyst sample allows determining the turn over frequency (TOF):

$$TOF = \frac{r}{n_{tot} \times dispersion} \qquad \text{(Eq. 4-2)}$$

Where r = reaction rate and n_{tot} = total number of Au moles in the catalytic reactor.

4.2.5 XPS

Using X-ray photoelectron spectroscopy one can quantify the atomic composition of surfaces. Particular interest is paid to the oxidation state of Au and to the amounts of oxygen present at the surface due to either gold oxide formation and/or oxygen adsorption.

Prior to quantification of the atomic composition, survey spectra are recorded. A representative XPS spectrum is shown in Figure 4-8 for calcined Au1/YSZ-p sample. This is a spectrum recorded with a wide binding energy window. Similar surveys are obtained for Au3/YSZ-p as well.

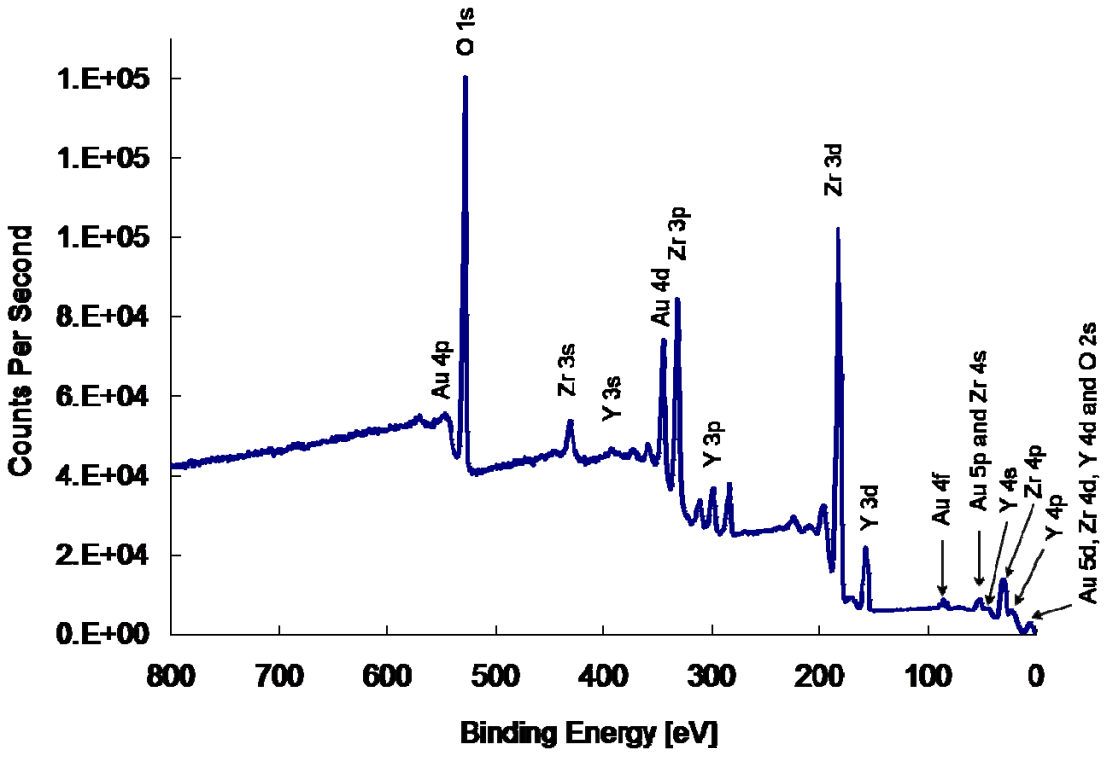

Figure 4-8 Representative XPS survey spectrum for Au1/YSZ-p catalyst

The elements expected on the surface of the sample and adsorbed species from surrounding are the following:

- Gold
- Oxygen from gold oxide, YSZ or oxygen adsorbed on the surface from the air
- Carbon, as a result of CO_2 adsorption from air or PVP remains
- Zirconium and yttrium from the YSZ

All Au samples display similar results from the XPS. This confirms that all samples have gold nanoparticles on the surface of the YSZ.

After recording the survey spectra, further analysis are performed within the narrow binding energy range of the gold atoms. This binding energy range yields important information as to whether the gold atom is bonded to oxygen atoms. This indicates different oxidation state of the gold in the sample. The carbon peak is used as an internal standard to correct for any shift in binding energies that could occur mainly due to surface charging during the XPS measurements.

Figure 4-9 (A-1) and Figure 4-10 (A-2) compare high resolution XPS spectra for two different treatments of Au1/YSZ-p (calcined vs. oxygen plasma etched) and Figure 4-10 (B) shows XPS result of calcined Au3/YSZ-p around the binding energy of gold. For each of the spectra, the atomic abundance at the catalyst surface is determined by peak deconvolution. The XPS spectrum of Au 4f region for Au1/YSZ-p and Au3/YSZ-p are compared. For the control samples of Au nanoparticles, Au $4f_{7/2}$ and Au $4f_{5/2}$ levels give rise to peaks positioned at 83.8 and 87.5 respectively, consistent with the value of pure metallic Au [8]. The deconvolution of the Au 4f spectrum of both calcined and oxygen

plasma etched Au1/YSZ-p is shown in Figure 4-9 (A-1) and Figure 4-10 (A-2), respectively, which indicate only one Au $4f_{7/2}$ components at BE = 83.8 that can be attributed to Au^0 [9]. It appears that different post treatments after synthesizing gold nanoparticles have no effect in the oxidation states of gold nanoparticles. The Au 4f spectrum of Au3/YSZ-p catalyst is shown in Figure 4-10 (B), which consists of two Au $4f_{7/2}$ components located at BE = 83.8 and 85.8 that can be attributed to Au^0 and Au^{3+}, respectively [9].

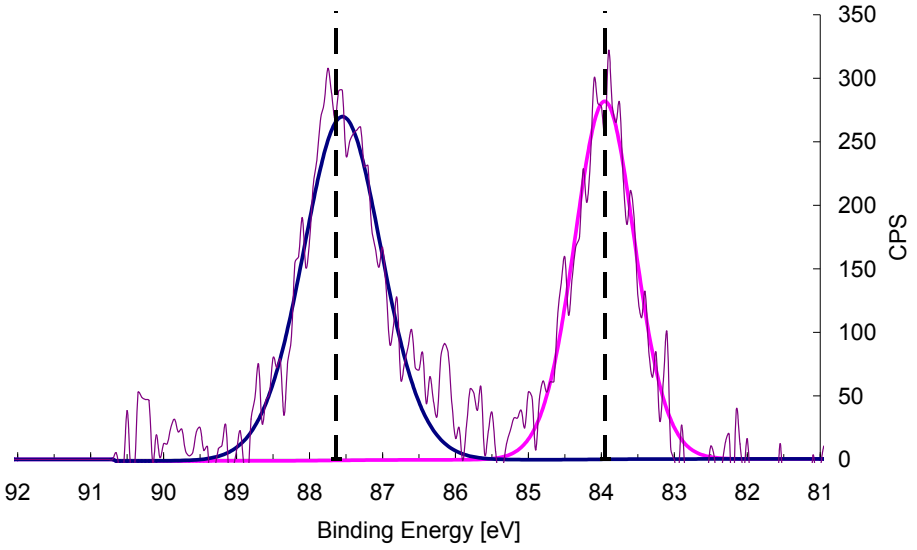

(A-1)

Figure 4-9 XPS spectra at the gold core level electrons 4f for calcined Au1/YSZ-p (A-1). Thin purple lines correspond to the experimental spectra and other lines correspond to the deconvoluted spectra.

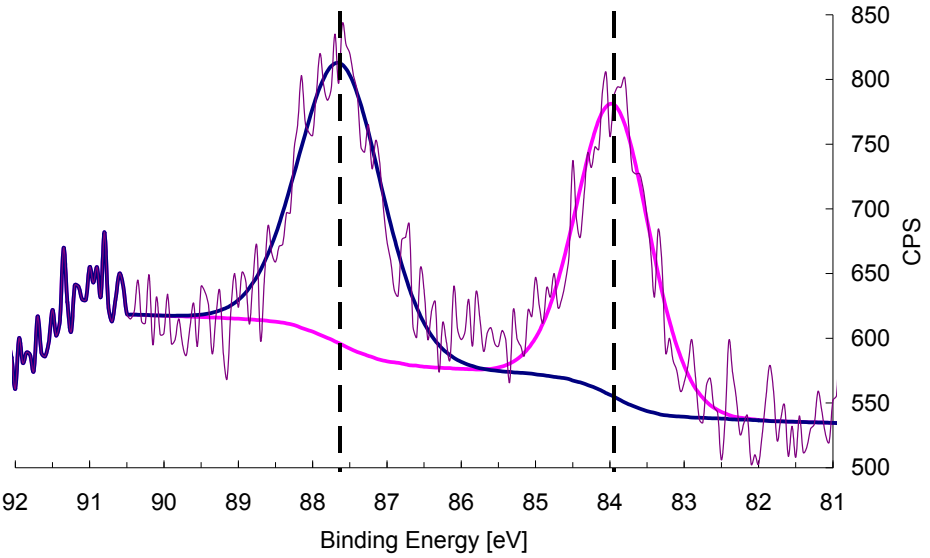

(A-2)

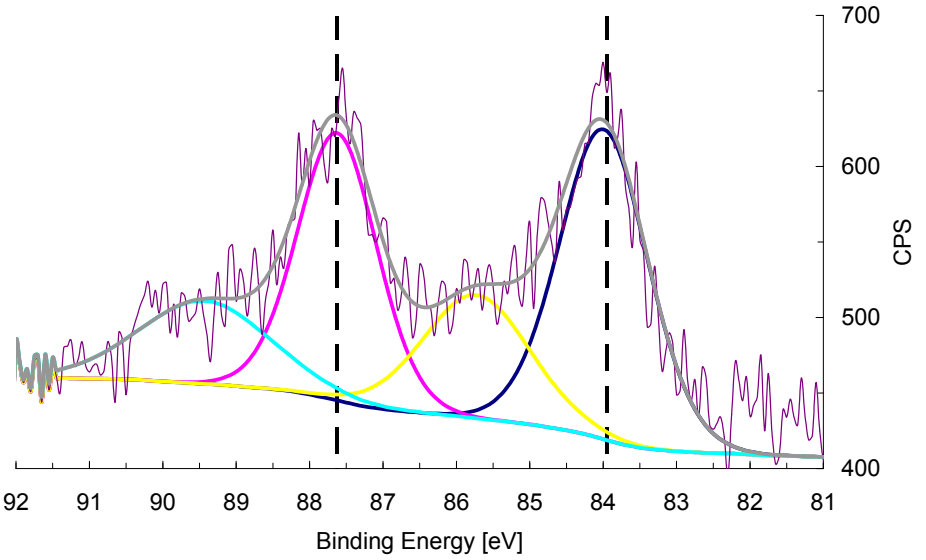

(B)

Figure 4-10 (Continued) XPS spectra at the gold core level electrons 4f for oxygen plasma etched Au1/YSZ-p (A-2) and calcined Au3/YSZ-p (B). Thin purple lines correspond to the experimental spectra and other lines correspond to the deconvoluted spectra.

Interestingly, Au3/YSZ-p catalyst contains 67% metallic gold and 33% gold oxide. Since the synthesis methods for Au1/YSZ-p and Au3/YSZ-p are identical except for the

amount of PVP added, it is presumed that the gold nanoparticles are oxidized during the calcination treatment. Perhaps, small gold nanoparticles may have higher tendency to get oxidized. Further investigation is necessary to determine the exact cause of the difference in the oxidation states of two samples. The difference in the oxidation state of gold for the two samples may contribute to difference in their catalytic performances.

4.3 **Conclusion**

Gold nanoparticles supported on YSZ have been investigated using SEM, TEM, XRD and XPS techniques. The SEM and TEM analyses show that spherical gold nanoparticles are well dispersed on YSZ powder support. SEM confirmed that Au nanoparticles of different average sizes are formed. Au4/YSZ-p shows the largest average particle size, whereas Au3/YSZ-p shows the smallest average size. It appears that the amount of PVP added to the reaction has an effect on the resulting particle size, until a point where excess of PVP hinders the reduction reaction.

According to XRD analysis, the structures of Au nanoparticles are found to be face centered cubic. This is evident from the order at which the crystalline planes of the gold nanoparticles appeared, i.e. (111) and (200) planes at 38^0 and 45^0, respectively. Scherrer equation is applied to estimate crystallite size of the gold nanoparticles. In agreement with SEM measurements, Au3/YSZ-p sample shows the smallest particle size. The summary of the particle size calculations are shown in the Table 4-2.

Table 4-2 Average particle sizes and dispersions of Au/ YSZ-p samples from SEM, TEM and XRD analysis

Catalyst name	Ratio of Au to PVP [mol %]	Particle Size from SEM [nm]	Particle Size from TEM [nm]	Particle size from XRD [nm]	Dispersion from TEM [%]	Dispersion from XRD [%]
Au1/YSZ-p	1:3	8.3	11.1	9.7	4.0	4.6
Au2/YSZ-p	1:6	7.9	N/A	8.3	N/A	5.4
Au3/YSZ-p	1:10	7.1	7.42	6.3	6.0	7.1
Au4/YSZ-p	1 :20	15.1	N/A	10.3	N/A	4.3

From the XPS analysis, the oxidation states of the Au nanoparticles are determined. Au1/YSZ-p contained gold atoms with oxidation state of Au^0 only while Au3/YSZ-p contained gold atoms with oxidation state of Au^0 and Au^{3+}. As mentioned in section 2.1.2.2.2, not much information is currently available on how the oxidation states of gold catalysts affect their reactivity. While the effects of pre-oxidation on the catalytic activity of metal surfaces are the subject of extensive studies, much less is known about such phenomena on supported nanoparticles. Au1/YSZ-p and Au3/YSZ-p are not only different in their average particle size, but also their oxidation states. Both factors might affect the performance of the catalysts.

4.4 **References**

[1] B. Zhao and Y. W. Chen, "The effect of poly-N-vinylpyrrolidone modification on NiCoB catalysts for hydrogenation of p-chloronitrobenzene," *Materials Chemistry and Physics,* vol. 125, pp. 763-768, 2011.

[2] V. Deepak, *et al.*, "Synthesis of gold and silver nanoparticles using purified URAK," *Colloids and Surfaces B: Biointerfaces,* vol. 86, pp. 353-358, 2011.

[3] Y. Zhang, *et al.*, "Gold catalysts supported on the mesoporous nanoparticles composited of zirconia and silicate for oxidation of formaldehyde," *Journal of Molecular Catalysis A: Chemical,* vol. 316, pp. 100-105, 2010.

[4] C. Sealy, "Nanoporous Au shows promise as 'green' catalyst," *Nano Today,* vol. 5, p. 82, 2010.

[5] B. R. Cuenya, "Synthesis and catalytic properties of metal nanoparticles: Size, shape, support, composition, and oxidation state effects," *Thin Solid Films,* vol. 518, pp. 3127-3150, 2010.

[6] E. Mutoro, *et al.*, "Electrochemical promotion of Pt(111)/YSZ(111) and Pt-FeOx/YSZ(111) thin catalyst films: Electrocatalytic, catalytic and morphological studies," *Applied Catalysis B: Environmental,* vol. 100, pp. 328-337, 2010.

[7] J. H. Liu, *et al.*, "Synergistic effect in an Au-Ag alloy nanocatalyst: CO oxidation," *Journal of Physical Chemistry B,* vol. 109, pp. 40-43, 2005.

[8] W. M. R. C.D. Wagner, L.E. Davis, J.F. Moulder, G.E. Muilenberg, *Handbook of X-ray Photoelectron Spectroscopy*. Minneapolis, MN: Perkin-Elmer, 1978.

[9] A. M. Venezia, *et al.*, "Relationship between structure and CO oxidation activity of ceria-supported gold catalysts," *Journal of Physical Chemistry B,* vol. 109, pp. 2821-2827, 2005.

Chapter 5 CO Oxidation Reaction on Gold Nanoparticle Catalysts

5.1 Introduction

In gold nanoparticle (AuNP) catalyzed CO oxidation by O_2 that can occur down to 200 K [1-6] , the oxide support (Fe_2O_3 , TiO_2 or Co_3O_4) is indispensable, a seminal discovery by Haruta in 1988 that has been due to his recognition of the crucial requirement for the small size of the AuNPs [1] . This surprising discovery, given the long believed chemical inertia of gold, has completely changed the way chemists look at this metal. The finding of below-room-temperature catalysis of CO oxidation is also of great interest, because the Pt/Pd catalysts that are used in catalytic converter in cars for CO oxidation work only at temperatures above 200 K. Thus, CO pollution essentially occurs during the first five minutes after starting the engines. The low-temperature supported AuNP catalyzed CO oxidation obviously could solve this problem. Also, gold nanocatalysts are being considered as alternative catalyst in indoor air quality improvement by completely oxidizing volatile organic compound.

The exact mechanism of CO oxidation on gold nanoparticles is still unknown. A recent publication by Cies et al proposes that the presence of gold dramatically increases the amount of CO, which is strongly chemisorbed on gold supported on ceria-zirconia [7]. CO molecules get initially adsorbed on the gold nanoparticles then further transfers to the support by means of a spillover process. Cies et al. further states that it is the small gold

particles (< 3nm) that represent the major sources of spillover of CO from gold to the support.

The oxidation of CO to CO_2 on gold-based catalysts has been extensively investigated in the instance of Au dispersed on different supports [2, 8], such as ceria, titania and cobalt oxide. It has been demonstrated that the catalytic performance of the gold nanoparticle depends on many parameters discussed in section 2.1.2.2. In general, small (< 6 nm) gold nanoparticles supported on ceria [9] or titania [10] have higher catalytic activity than other supports. In this section, catalytic activity between commercial gold nanoparticles supported on g-alumina (γ-Al_2O_3) and the synthesized gold nanoparticles supported on YSZ are compared. YSZ is considered as an "active" support because it is known to be an O^{2-} conductor due to the presence of oxygen vacancies inside its crystallographic structure. In addition, gold nanoparticles supported on YSZ can be used in EPOC since YSZ is a type of solid electrolyte. This is the first report of CO oxidation over Au nanoparticles supported on YSZ.

5.2 **Experimental**

The quartz PFR reactor described in section 3.4 (Figure 3-3 (A)) is used for the CO oxidation experiments. 50 mg of the Au/YSZ-p catalysts is placed inside of the quartz reactor. The total gas flowrate is 4.3 L/h with reactant compositions of 730-780 ppm of CO, 4.4-4.5% of O_2 and the balance of He. The initial temperature is at room temperature and the heating ramp is 3 ^{0}C min^{-1} until the temperature reached 250 ^{0}C. The temperature is

held constant at 250 ^{0}C for 5 min and then decreases to room temperature. For each catalyst, three heating cycles are performed to observe the stability of the catalyst. The catalytic performance of the two catalysts, Au1/YSZ-p and Au3/YSZ-p, are compared to commercial gold nanoparticles supported on alumina.

5.3 **Results and Discussion**

5.3.1 Treatment comparison

CO oxidation catalytic performances of Au1/YSZ-p sample with calcination and oxygen plasma etching are compared. It is observed that the catalytic activity of the Au1/YSZ-p improved upon either treatment. Calcination treatment significantly improves the CO conversion while oxygen plasma etching gives slight improvement to the catalyst performance, as shown in Figure 5-1.

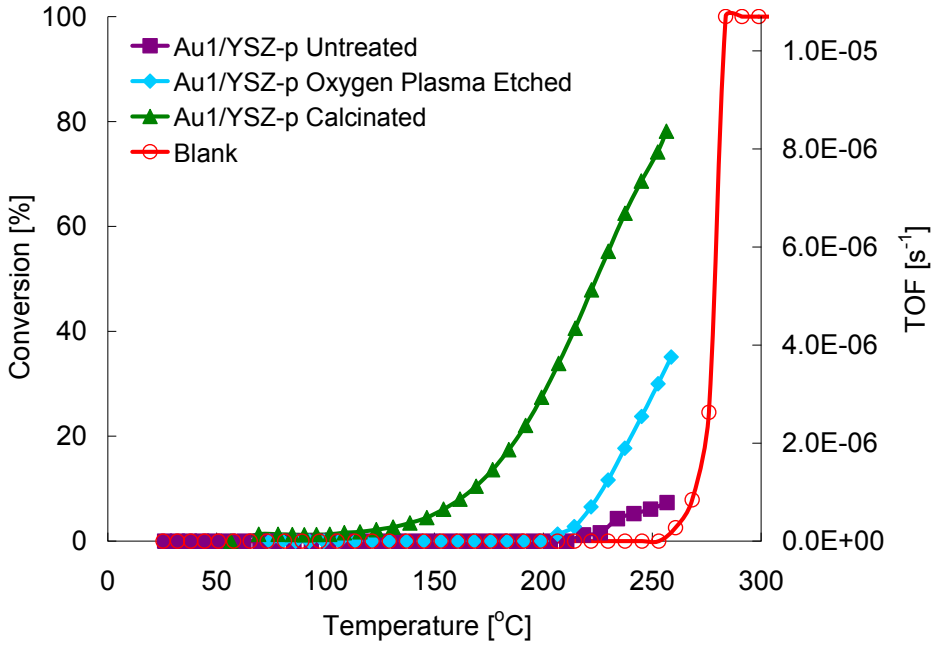

Figure 5-1 CO oxidation on Au1/YSZ-p (3:1 molar ratio of PVP to Au) after different catalyst treatments.

There are several explanations to such results. First, the experiment has shown that the PVP does block the active sites of gold nanoparticles as previously discussed by Lu and Zhao [11, 12]. Regarding the different results attained from different treatments of PVP, oxygen plasma etching may not have completely removed all the PVP in the sample, but only what is on the surface. Therefore, optimization of the procedure is required. For instance, plasma etching the sample powder multiple times, while stirring or mixing the sample powders each time is recommended.

5.3.2 Particle size and stability comparison

As shown from Figure 5-2 and Figure 5-3, the catalyst exhibits stable performance after the first cycle where the activity is observed from around 65 ^{0}C. It is observed that the first cycle shows lower catalytic activity compared to the successive cycles. This may have caused from remaining PVP and other organic compounds present in the first cycle, thus blocking the active site initially. Similar multi-cycle performance has been observed by other research groups [13-15]; however, the opposite performance has also been observed [16, 17] due to the nanoparticle sintering and agglomeration at high temperature.

For Au3/YSZ-p, CO conversion increases at around 120 ^{0}C, while for Au1/YSZ-p and Au4/YSZ-p this happens much later at 150 and 200 ^{0}C, respectively. The results demonstrate that the best performance is achieved by the smallest nanoparticles (~ 6 nm average size), due to the higher amount of the surface active sites per mass of catalyst. The smaller the size of the nanoparticle, the earlier the 100% conversion of CO is achieved (Figure 5-2 and Figure 5-3). However, different compositions of gold and gold oxide of Au1/YSZ-p and Au3/YSZ-p, shown from the XPS analysis may contribute to the difference in their catalytic activity as well.

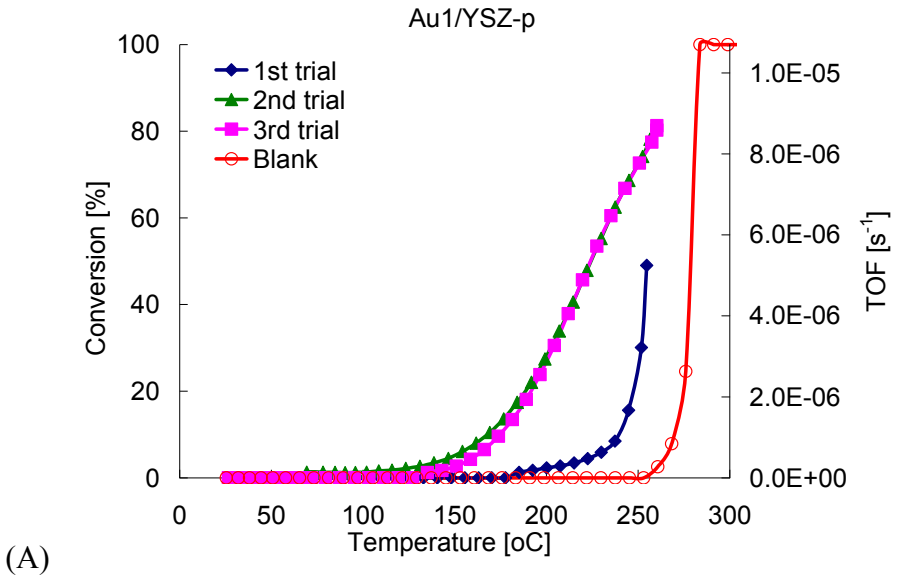

(A)

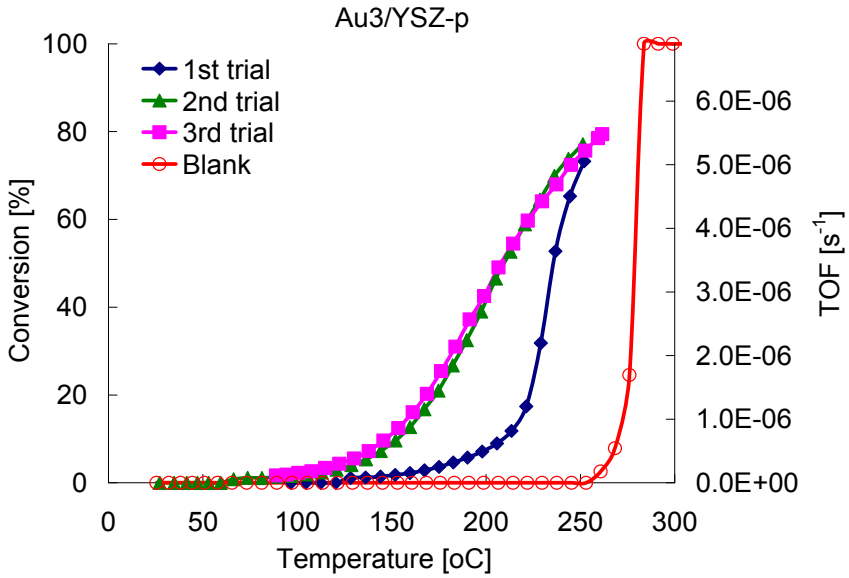

(B)

Figure 5-2 Catalytic performance for CO oxidation of Au1/YSZ-p (A, 3:1 molar ratio of PVP to Au) and Au3/YSZ-p (B, 10:1 molar ratio of PVP to Au).

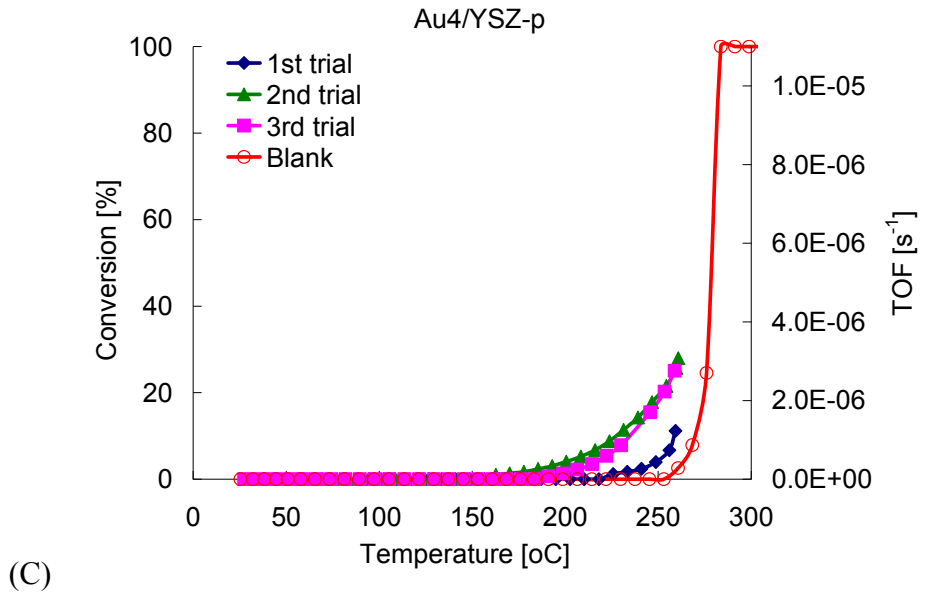

(C)

Figure 5-3 (Continued) Catalytic performance for CO oxidation of Au4/YSZ-p (C, 20:1 molar ratio of PVP to Au).

Previous research by Cies et al. [7] reported that small nanoparticles are mainly responsible for the complete CO oxidation on the gold surface. This trend is also present in the case of our experiments. Since the average particle size of Au3/YSZ-p is smaller, it would have more catalytically active sites, leading to the higher CO conversion. At the same time, the turnover frequency (TOF) value is higher for Au1/YSZ-p than Au3/YSZ-p. TOF indicates the number of oxygen atoms reacting per surface site per second. The results may suggest that although Au3/YSZ-p has smaller nanoparticle size and higher dispersion (i.e. number of active sites) the observed increase in CO conversion has only a geometric effect and not changes in the intrinsic properties of AuNPs.

The catalytic properties of small gold nanoparticles are expected to differ significantly from those of bulk metals, due to an increase in the surface bonds and/or change in the electronic structure due to quantum size effects with a decrease in the particle size [18]. Therefore, among the synthesized gold nanoparticles, Au3/YSZ-p (average particle size ~ 6 nm), has the best performance for CO oxidation. Conversely, all the Au samples are not as catalytically active as the commercial gold nanoparticles supported on γ-Al_2O_3 (AUROlite^{TM}, 79-0160, ~2-3 nm), as shown in Figure 5-4. However, direct size comparison of the synthesized catalysts and the commercial catalyst is not applicable because there are many differences in their parameters - the type of supports are different (YSZ versus alumina) and the compositions of the catalyst's oxidation states may also be different (Au versus Au^{3+}).

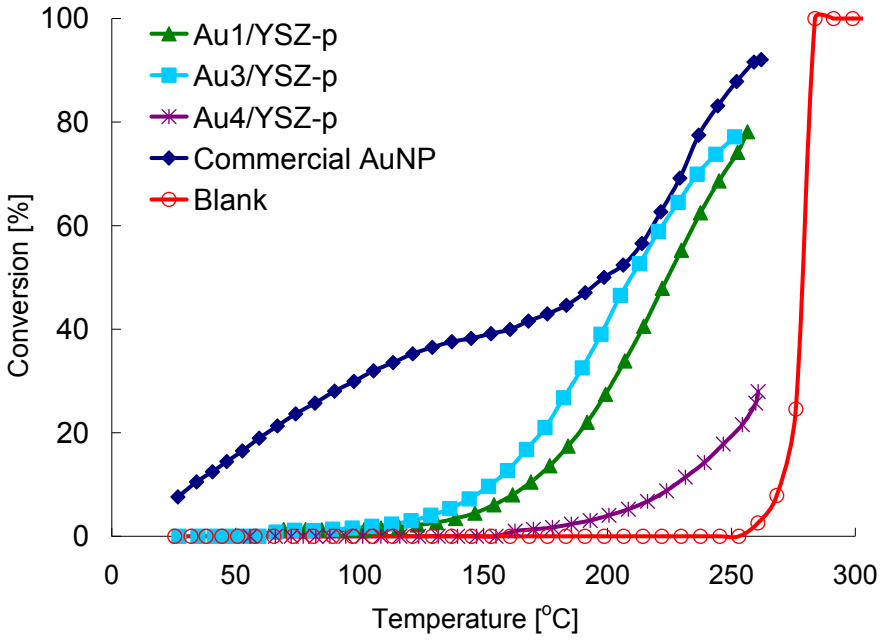

Figure 5-4 Comparison of catalytic performance for CO oxidation of Au1/YSZ-p, Au3/YSZ-p and Au4/YSZ-p to commecial gold nanocatalyst (Au/γ-Al_2O_3). The second run is compared.

The behaviour of the commercial and the synthesized AuNPs from Figure 5-4 are significantly different. The commercial AuNP has a plateau region around 100 ^{0}C, whereas the synthesized AuNPs do not. The presence of plateau may be explained by the difference in the particle size as well as from the point of view of the metal-support interactions (MSI) between Au-YSZ and Au-γ-Al_2O_3. MSI is responsible for modifications in electronic structure of a metal through changes in the density of states at the Fermi level, and a shift of the Fermi level due to the different work functions of metal and support [19, 20]. The metal-semiconductor boundary-layer theory states that, at thermodynamic equilibrium, the Fermi energy levels of electrons in the two solids in contact are equal. Upon contact of two solids having different Fermi levels (work functions), charge must be transported from one material to the other until the Fermi levels at the interface are equilibrated. For the same metal, the strength of MSI would depend on the support as well as on the particle size. One would expect stronger MSI for the smaller catalyst particles.

Therefore, MSI may play a role in the chemical properties of Au. The hemispherical particles indicate strong interaction between the gold particles and the oxide supports. Haruta et al. [18, 21, 22] have proposed that small Au particles supported on γ-Al_2O_3 become electron deficient by donating electrons to the supports and the catalytic properties of the electron deficient Au particles then resemble somewhat those of Pt, which is the element left to Au in the Periodic table.

It appears that the activity to CO at low temperature is dependent on the particle size and possibly the type of metal oxide support as well. On YSZ, the gold catalysts do not exhibit high catalytic activity than alumina.

5.4 **Conclusion**

Oxidation reactions of CO on supported gold nanoparticles have been examined. The study has shown that Au3/YSZ-p, which has the smallest average particle size showed superior catalytic activity toward oxidation of CO if compared to larger nanoparticles. It can be concluded that the particle size plays crucial role in determination of catalytic activity of gold nanoparticles. When the synthesized AuNPs supported on YSZ were compared the commercial AuNP catalyst supported on gamma-alumina, the catalytic activity of the synthesized catalysts did not perform as well. However, no clear conclusions could be drawn from the comparison because there were too many differences in terms of their parameters.

Regardless, YSZ brings an advantage of utilization of electrochemical promotion phenomenon due to its ionic conductivity. YSZ support can serve as both supports to the gold nanoparticles as well as solid electrolyte in an electrochemical cell.

5.5 **References**

[1] T. Kobayashi, *et al.*, "A selective CO sensor using Ti-doped α-Fe2O3 with coprecipitated ultrafine particles of gold," *Sensors and Actuators,* vol. 13, pp. 339-349, 1988.

[2] M. Haruta, *et al.*, "Low-Temperature Oxidation of CO over Gold Supported on TiO2, α-Fe2O3, and Co3O4," *Journal of Catalysis,* vol. 144, pp. 175-192, 1993.

[3] M. Haruta, *et al.*, "Mechanistic Studies of CO Oxidation on Highly Dispersed Gold Catalysts for Use in Room-Temperature Air Purification," vol. 75, ed, 1993, pp. 2657-2660.

[4] M. Haruta, *et al.*, "Synergism in the catalysis of supported gold," vol. 77, ed, 1993, pp. 45-52.

[5] S. Tsubota, *et al.*, "CO oxidation over gold supported on TiO2," vol. 77, ed, 1993, pp. 325-328.

[6] P. Diao, *et al.*, "Electrocatalytic activity of supported gold nanoparticles toward CO oxidation: The perimeter effect of gold-support interface," *Electrochemistry Communications,* vol. 12, pp. 1622-1625, 2010.

[7] J. M. Cíes, *et al.*, "Contributions of electron microscopy to understanding CO adsorption on powder Au/ceria-zirconia catalysts," *Chemistry - A European Journal,* vol. 16, pp. 9536-9543, 2010.

[8] K. Arve, *et al.*, "Selective catalytic reduction of NOx over nano-sized gold catalysts supported on alumina and titania and over bimetallic gold-silver catalysts supported on alumina," *Topics in Catalysis,* vol. 52, pp. 1762-1765, 2009.

[9] G. Glaspell, *et al.*, "Nanocatalysis on supported oxides for CO oxidation," *Topics in Catalysis,* vol. 47, pp. 22-31, 2008.

[10] M. Jia, *et al.*, "Preparation of Au/CeO2 catalyst and its catalytic performance for HCHO oxidation," *Journal of Rare Earths,* vol. 26, pp. 528-531, 2008.

[11] Y. Lu, *et al.*, "Silver nanorods for oxygen reduction: Strong effects of protecting ligand on the electrocatalytic activity," *Journal of Power Sources,* vol. 196, pp. 3033-3038, 2011.

[12] B. Zhao and Y. W. Chen, "The effect of poly-N-vinylpyrrolidone modification on NiCoB catalysts for hydrogenation of p-chloronitrobenzene," *Materials Chemistry and Physics,* vol. 125, pp. 763-768, 2011.

[13] S. Arrii, *et al.*, "Oxidation of CO on Gold Supported Catalysts Prepared by Laser Vaporization: Direct Evidence of Support Contribution," *Journal of the American Chemical Society,* vol. 126, pp. 1199-1205, 2004.

[14] W. C. Li, *et al.*, "Highly reproducible syntheses of active Au/TiO2 catalysts for CO oxidation by deposition-precipitation or impregnation," *Journal of Catalysis,* vol. 237, pp. 190-196, 2006.

[15] E. Quinet, *et al.*, "H2-induced promotion of CO oxidation over unsupported gold," *Catalysis Today,* vol. 138, pp. 43-49, 2008.

[16] R. J. H. Grisel and B. E. Nieuwenhuys, "Selective Oxidation of CO, over Supported Au Catalysts," *Journal of Catalysis,* vol. 199, pp. 48-59, 2001.
[17] M. Lamallem, *et al.*, "Effect of the preparation method on Au/Ce-Ti-O catalysts activity for VOCs oxidation," *Catalysis Today,* vol. 137, pp. 367-372, 2008.
[18] M. Haruta, "Size- and support-dependency in the catalysis of gold," *Catalysis Today,* vol. 36, pp. 153-166, 1997.
[19] S. J. Tauster, *et al.*, "Strong metal-support interactions. Group 8 noble metals supported on TiO2," *Journal of the American Chemical Society,* vol. 100, pp. 170-175, 1978.
[20] S. J. Tauster and S. C. Fung, "Strong metal-support interactions: Occurrence among the binary oxides of groups IIA-VB," *Journal of Catalysis,* vol. 55, pp. 29-35, 1978.
[21] K. Ruth, *et al.*, "The effects of SO2 on the oxidation of CO and propane on supported Pt and Au catalysts," *Applied Catalysis B: Environmental,* vol. 24, pp. L133-L138, 2000.
[22] Y. Iizuka, *et al.*, "A kinetic and adsorption study of CO oxidation over unsupported fine gold powder and over gold supported on titanium dioxide," *Journal of Catalysis,* vol. 187, pp. 50-58, 1999.

Chapter 6 Ethylene Oxidation on Gold Nanoparticle Catalyst

6.1 Introduction

Gold at the nanoscale manifests extraordinary catalytic activity which increases with a decrease in the cluster size down to 1-5 nm [1-8]. The origin of such size-dependent catalytic activity of gold remains highly debated and yet to be fully understood. The adsorption of small hydrocarbons like ethylene on transition metal surfaces is of considerable scientific interest due to their involvement in several elementary catalytic reactions [9]. However, most studies of the gold nanocatalysts have mainly focused on the investigation of adsorption and reaction of O_2 and CO [3, 8, 10-19]; the study of catalytic oxidation of ethylene on gold clusters has been relatively unexplored despite the tremendous importance of this process in practical applications, such as removal of ethylene in fruit warehouses for preventing fast-ripening [6, 20] and control of volatile organic compounds in air for air quality improvement.

In this section, catalytic activity of synthesized gold nanoparticles supported on YSZ towards ethylene oxidation is examined at various external parameters. Such parameters are average size of gold nanoparticles, partial pressure of C_2H_4 and O_2, reaction temperature and overall gas flowrate. The optimum parameters are will be determined and their effect on the reaction of C_2H_4 oxidation will be discussed.

6.2 Experimental

6.2.1 PFR Reaction

Two reactors, described in section 3.4, are used for the C_2H_4 oxidation experiment. For preliminary screening of the catalysts, the quartz PFR reactor is first used. To this end, 50 mg of the Au/YSZ-p catalyst is placed inside of the quartz reactor. PFR reactor allows fast screening of catalytic activity at different operating conditions since the synthesized catalyst powder is placed directly into the reactor. The reaction is studied at different temperatures: 25, 200, 250, 275, 300, and 350 ^{o}C, at constant oxygen partial pressure of 3 kPa. The partial pressure of ethylene is varied from 0.1 to 1.5 kPa, and the conversion is plotted against the ratio of reactants $P_{C_2H_4} / P_{O_2}$. The volumetric flow rate is 200 ml min^{-1}, reported at normal conditions. The experimental parameters are shown in Table 6-1.

Table 6-1 Varying parameters for ethylene oxdiation experiment with plug flow reactor. Mass of catalyst = 50 mg.

	Unit	Au1/YSZ-p	Au3/YSZ-p
Reactor Type		PFR	PFR
Flowrate	**ml/min**	200	200
Temperature	**C**	25-350	25-350
$P_{C_2H_4} / P_{O_2}$	**kPa/kPa**	0.1:3 0.2:3 0.3:3 0.5:3 1:3 1.5:3	0.1:3 0.2:3 0.3:3 0.5:3 1:3 1.5:3

6.2.2 CSTR Reaction

After the preliminary experiments using the PFR reactor, single disk type, wireless configuration of electrochemical cell with the Au/YSZ-p catalysts are installed in the CSTR reactor. The schematic diagram of the electrochemical cell is described in section 3.4 (Figure 3-3 (B)). Studying catalytic activity in this type of setting allows application of electrical current or potential to the catalyst, therefore performing catalytic testing under electrochemical promotion of catalysts (EPOC) conditions. Results of the EPOC experiments are shown in the next chapter (Chapter 7). To deposition Au catalyst on the YSZ disk, 18 μL of synthesized 1 wt.% Au/YSZ-p dispersed in ethanol with concentration of 0.666 g (Au + YSZ-p) mL^{-1}, is placed in the center of the YSZ disk and dried in air at room temperature. Two inert gold films are used as feeder electrodes, which are only used in closed circuit EPOC experiments (Chapter 7). It has been confirmed that film gold electrodes are catalytically inert towards C_2H_4 oxidation at given conditions. The electrochemical cell is suspended in the reactor through gold wires.

The reaction is studied at six temperatures: 25, 200, 250, 275, 300, and 350 ^oC, at constant oxygen partial pressure of 3 kPa. The partial pressure of ethylene is varied from 0.1 to 1.5 kPa, and the conversion is plotted against the ratio of reactants $P_{C_2H_4} / P_{O_2}$. The volumetric flow rate is 200 ml min^{-1}, reported at normal conditions. The experimental parameters are summarized in Table 6-2.

Table 6-2 Varying parameters for ethylene oxdiation experiment with the CSTR reactor. Mass of catalyst = 12 mg.

	Unit	Au1/YSZ-p		Au3/YSZ-p
Reactor Type		CSTR		CSTR
Flowrate	**ml/min**	80	200	80
Temperature	**C**	300-400	25-400	300-400
$P_{C_2H_4} / P_{O_2}$	**kPa/kPa**	0.3:3 0.3:0.45 0.3:0.6 0.3:0.9 0.3:1.2 0.3:1.8 0.3:2.4	0.1:3 0.2:3 0.3:3 0.4:3 0.5:3 1:3	0.3:3 0.3:0.45 0.3:0.6 0.3:0.9 0.3:1.2 0.3:1.8 0.3:2.4

The activity of the catalyst is very stable upon changing the gas concentrations at fixed temperature. The new steady-state is attained in approximately 15 minutes. The reproducibility of the measurements is confirmed by conducting three experimental runs for each operating conditions. The measurement at increasing and decreasing partial pressure give the same rate of CO_2 formation, therefore partial pressure ratio of ethylene and oxygen is used to provide the partial pressure condition.

6.3 Results and Discussion

6.3.1 Preliminary PFR Reaction

The dependence of the steady-state ethylene conversion and turnover frequency on the partial pressure ratio of ethylene to oxygen for Au1/YSZ-p and Au3/YSZ-p catalysts in PFR reactor is shown in Figure 6-1 and Figure 6-2.

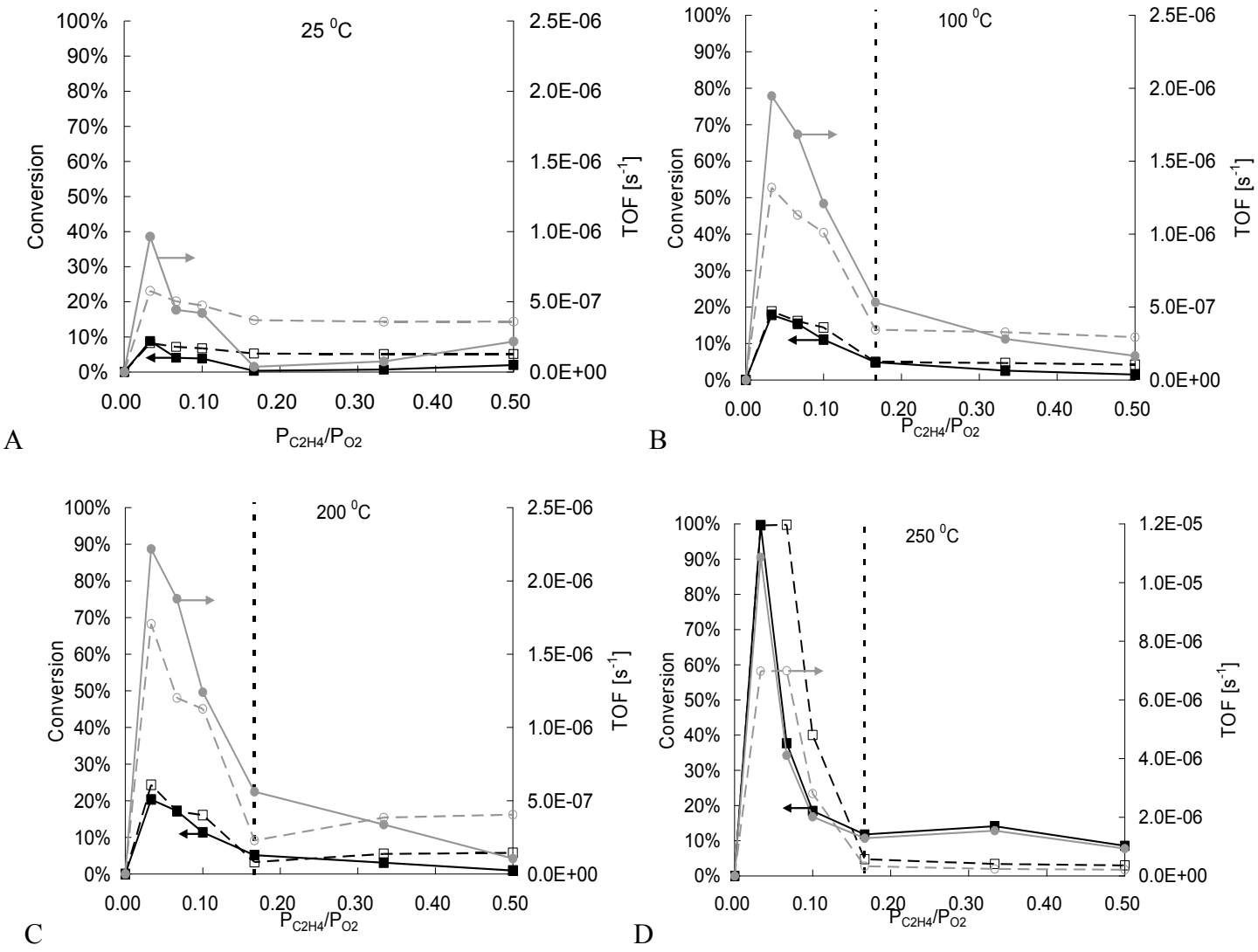

Figure 6-1 Open circuit ethylene conversion (black lines) and TOF (grey lines) of Au1/YSZ-p (solid lines) and Au3/YSZ-p (dotted lines) as a function of the partial pressure ratio of ethylene to oxygen at various reaction temperature (A = 25 ^{0}C, B = 100 ^{0}C, C = 200 ^{0}C, D = 250 ^{0}C). Vertical dashed lines indiate critical partial pressure ratio where ethylene conversion changes significantly. Flow rate = 200 ml min^{-1}.

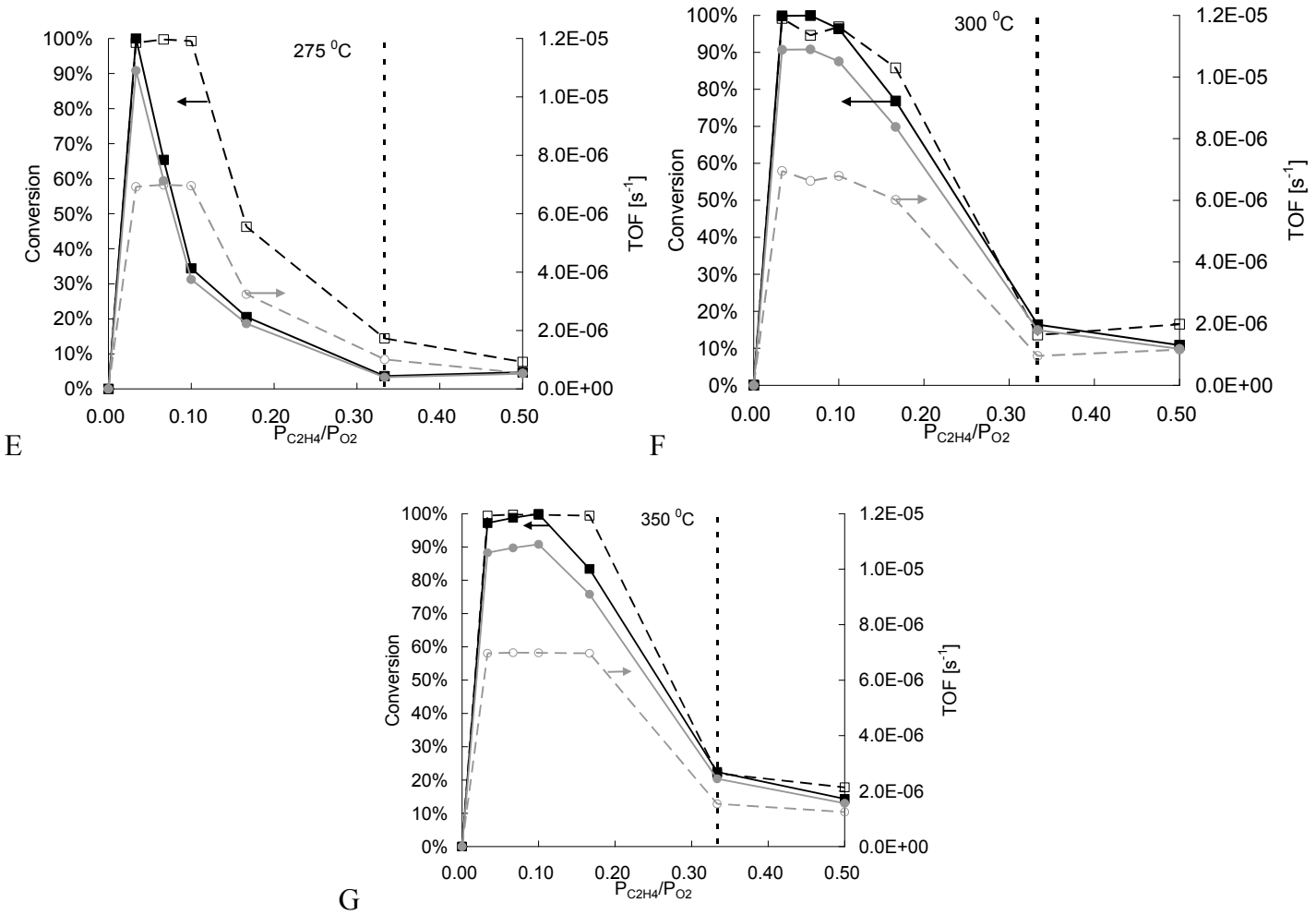

Figure 6-2 (Continued) Open circuit ethylene conversion (black lines) and TOF (grey lines) of Au1/YSZ-p (solid lines) and Au3/YSZ-p (dotted lines) as a function of the partial pressure ratio of ethylene to oxygen at various reaction temperature (E = 275 ^{0}C, F = 300, G = 350 ^{0}C). Vertical dashed lines indiate critical partial pressure ratio where ethylene conversion changes significantly. Flow rate = 200 ml min^{-1}.

As can be seen, Au nanoparticles are active towards ethylene oxidation even at room temperature in excess of oxygen. As temperature increases, the ethylene conversions increase as well. The range of highly reactive partial pressure ratio of ethylene to oxygen is indicated by the dashed vertical line. Conversion of ethylene reaches 100% for the

temperature above 250 ^{0}C. Comparison of Au1/YSZ-p and Au3/YSZ-p catalysts show that Au3/YSZ-p catalyst has wider partial pressure windows with higher ethylene conversion than Au1/YSZ-p, indicating that smaller gold nanoparticles are more active for ethylene oxidation similar to CO oxidation experiment, shown in the previous section. However, different compositions of gold and gold oxide of Au1/YSZ-p and Au3/YSZ-p, shown from the XPS analysis may contribute to the difference in their catalytic activity as well.

Regardless, a maximum conversion is observed when the reactants are present at fuel-lean condition. For the ethylene reaction, the gas phase stoichiometric ratio lies at $P_{C_2H_4} / P_{O_2}$ = 0.333. For the ratio of partial pressure less than 0.333, i.e. in the excess of oxygen, the highest conversion is achieved. The region at which ethylene conversions are observed in Figure 6-1 and Figure 6-2 lies below the gas phase stoichiometric ratio and shifts towards higher value of stoichiometric ratio with increase in temperature. At temperature 275 ^{o}C, the reactive partial pressure ratio reaches up to the stoichiometric ratio.

The value of TOF is proportional to the number of active site present on the Au surface. Hence, Au1/YSZ-p catalyst may have higher value of TOF. For instance, when 100% conversion is achieved for both Au1/YSZ-p and Au3/YSZ-p catalysts, Au1/YSZ-p has higher TOF value, because its dispersion is lower. This indicates that increase in the conversion for Au3/YSZ-p catalyst is mainly due to the geometric effect (decreasing of the particle size) and not change in the nanoparticle properties. It is worth to note that according to XPS, Au3/YSZ-p catalyst has some gold oxides on the surface. This along with the smaller particle size may result in the high activity of Au3/YSZ-p towards C_2H_4 oxidation. Activation energies of the process at different partial pressure ratios with

Au1/YSZ-p catalyst have also been determined from the slope after plotting ln of reaction rate versus T^{-1}, which arrived from the modified Arrhenius equation and are shown in Table 6-3:

$$\ln r = \frac{-E_a}{RT} + \ln k \qquad \text{(Eq. 6-1)}$$

where r is the reaction rate (mol s^{-1}), Ea is the activation energy (J mol^{-1}), R is the gas constant (J K^{-1} mol^{-1}), T is temperature (Kelvin) and k is the reaction constant (s^{-1}).

Table 6-3 Calculated activation energy at different reactant partial pressures

$P_{C_2H_4} : P_{O_2}$ [-]	**Activation Energy [kJ/mol]**
0.1:3	13.65
0.2:3	13.26
0.3:3	12.31
0.5:3	23.84
1:3	13.89
1.5:3	8.22

In the temperature and partial pressure range studied, the average activation energy of E_{av} = 14.2 kJ mol^{-1}. Although there are few differences in the value of activation energies, it appears that activation energy is independent of reactant partial pressure ratios. Generally, since both reactants are in the adsorbed state, the rate maximum probably corresponds to the surface optimum ratio of ethylene and oxygen. The optimum ratio of the reactants surface concentration is not necessarily equal to the stoichiometric ratio for complete ethylene oxidation. The catalytic reaction may proceed through a side reaction

that involves O_2 formation from adsorbed oxygen species without reacting with adsorbed C_2H_4 species, the CO_2 formation may actually requires more than 3 O_2 molecules.

Since the optimum conditions of CO_2 conversion occurs in excess of oxygen (i.e. fuel-lean condition), more experiments are conducted with CSTR reaction within the fuel-lean conditions.

6.3.2 CSTR Reaction

Ethylene oxidation is performed in CSTR at various temperature and gas composition. Catalyst with the smaller average particle size, Au3/YSZ-p, shows higher conversion if compared to Au1/YSZ-p. However, 100% conversion is not achieved even at high temperature (350 ^{0}C). This may be due to the lower amount of catalyst (12 mg vs 50 mg of Au/YSZ-p for CSTR and PFR, respectively) that is used in the CSTR. Having the Au/YSZ-p deposited on the surface of the YSZ disk compared to depositing the catalyst on the quartz fibre might also reduce active surface area of the catalyst. Moreover, a different flow pattern of CSTR versus PFR also significantly affects the conversion of ethylene. However this setup is necessary for the electrochemical promotion experiment.

Figure 6-3 shows the effect of temperature on the steady-state open circuit conversion of ethylene for Au1/YSZ-p and Au3/YSZ-p catalyst in the CSTR reactor. The mass flowrate is kept constant at 80 ml min^{-1}. Ethylene conversion is measured at various partial pressures of ethylene and oxygen.

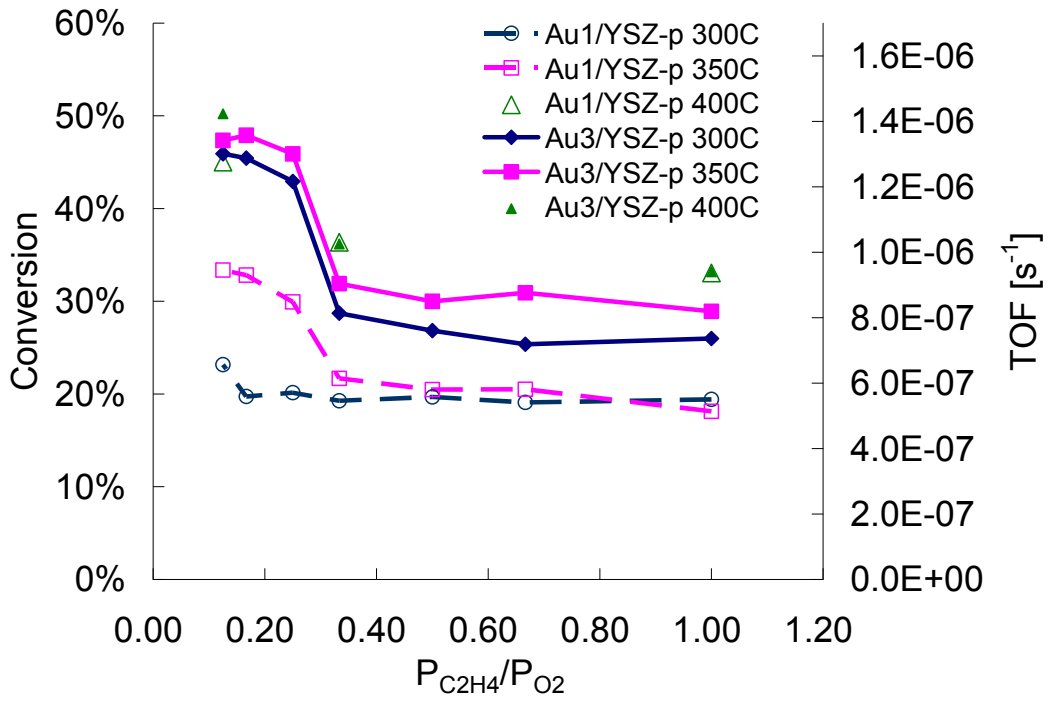

Figure 6-3 Open circuit ethylene conversion of Au1/YSZ-p and Au3/YSZ-p as a function of the partial pressure of ethylene to oxygen. T = 300, 350 and 400 ^{0}C. Flowrate = 80 ml min^{-1}.

At all operating conditions Au3/YSZ-p shows higher catalytic activity if compared to Au1/YSZ-p. The critical ratio of partial pressure, where the ethylene conversion changes dramatically, of $P_{C_2H_4} / P_{O_2}$ = 0.333 is also observable with CSTR experiment, similar to the experiment with the PFR. A conclusion can be drawn that smaller gold nanoparticles are more catalytically active towards complete oxidation of ethylene at fuel-lean condition.

Au1/YSZ-p catalyst is chosen for further investigations in the catalytic performance of ethylene oxidation. More experiments near the fuel-lean conditions are examined since higher ethylene conversions are obtained at these conditions. Figure 6-4

shows ethylene conversion and turnover frequency on Au1/YSZ-p catalyst at different temperatures and gas compositions.

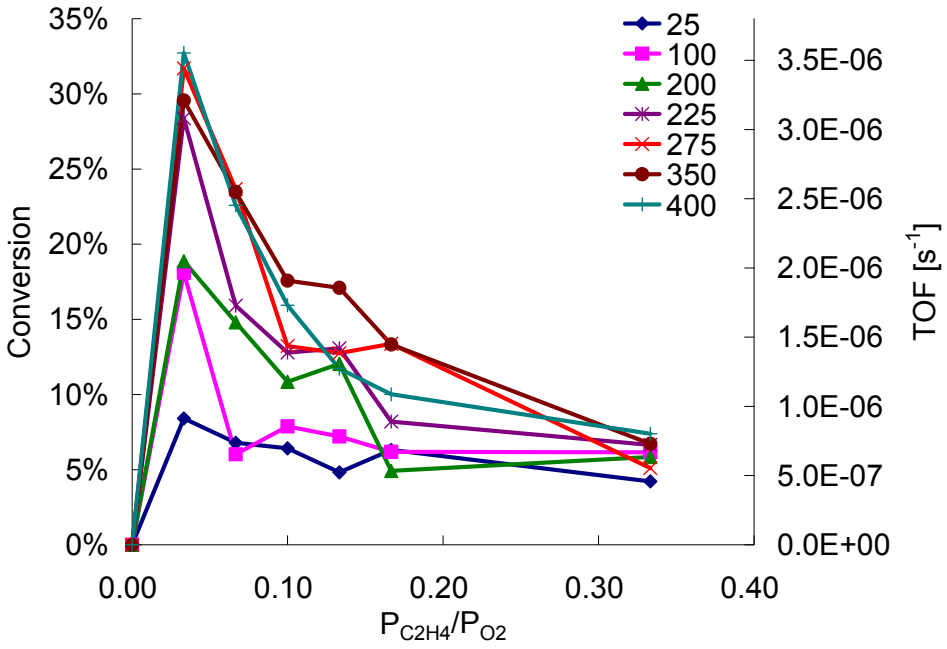

Figure 6-4 Open circuit ethylene conversion and turnover frequency of Au1/YSZ-p as a function of the partial pressure ratio of ethylene to oxygen at various temperatures. Flowrate = 200 ml/min.

Figure 6-4 indicates that optimum ratio of reactants is achieved in fuel-lean condition ($P_{C_2H_4} / P_{O_2} << 0.333$). It can be seen that ethylene is much strongly adsorbed on Au surface than gold. Ethylene adsorption seems to be favoured with respect to oxygen adsorption and oxygen adsorption is hindered with increasing partial pressure of ethylene since active surface sites become blocked by the adsorbed ethylene. At higher temperature, this competition for oxygen adsorption is less competitive with reduced activation energy.

In summary, for all investigated temperatures, increase in $P_{C_2H_4} / P_{O_2}$ ratio leads to the decrease in C_2H_4 conversion over Au/YSZ-p catalyst. Increase in $P_{C_2H_4}$ leads to C_2H_4 conversion decrease due to the saturation of the surface active sites by adsorbed ethylene. There is a critical partial pressure ratio at stoichiometric ratio, which is close to the stoichiometric ratio, where the reaction condition changes from fuel-lean side ($P_{O_2} >> P_{C_2H_4}$) to fuel-rich side ($P_{C_2H_4} >> P_{O_2}$). On the fuel-lean side, the oxygen coverage is near unity and thus, the rate limiting step is the ethylene adsorption step. On the other hand, on the fuel-rich side, the rate limiting step is the adsorption of oxygen because the oxygen coverage is scarce [21]. The higher ethylene conversion is observed at the fuel-lean side if compared to the fuel-rich side. This indicates that the adsorption of ethylene is stronger than the adsorption of oxygen. The drastic decrease in ethylene conversion at stoichiometric ratio indicates that ethylene is more strongly adsorbed on the gold surface and blocks the reaction active sites. The fact that gold nanoparticles are catalytic more active at fuel-lean condition enables utilization of gold nanoparticles in removal of VOC in air.

6.4 **Conclusion**

Since the average particle size of Au3/YSZ-p is smaller, it would have more small gold particles that are below 6 nm than Au1/YSZ-p, which leads to Au3/YSZ-p having higher catalytic activity for C_2H_4 oxidation. It appears that two different conditions, fuel-

rich and fuel-lean conditions exist for the reaction and they demonstrate different kinetics towards ethylene oxidation reaction.

In the range of the present operating conditions, several processes affect the C_2H_4 conversion. The reaction order with respect to ethylene and oxygen significantly depends on the reaction conditions. In order to understand the overall behaviour of the catalyst, the interaction of each reactant and product with the catalyst surface should be considered. In particular, the adsorption-desorption characteristics of ethylene and oxygen must be studied at constant coverage to determine the k_{ads}, E_{ads} and ΔH_{ads} values. The dependence of the adsorption characteristics on surface coverage is also important.

As discussed previously, having YSZ as support can utilize the phenomenon of electrochemical promotion due to its ionic conductivity. In the next chapter, catalytic activity of ethylene oxidation is determined in EPOC condition, i.e. under constant potential application.

6.5 **References**

[1] M. Haruta, "Size- and support-dependency in the catalysis of gold," *Catalysis Today,* vol. 36, pp. 153-166, 1997.

[2] G. C. Bond and D. T. Thompson, "Catalysis by Gold," *Catalysis Reviews - Science and Engineering,* vol. 41, pp. 319-388, 1999.

[3] Y. Iizuka, *et al.*, "A kinetic and adsorption study of CO oxidation over unsupported fine gold powder and over gold supported on titanium dioxide," *Journal of Catalysis,* vol. 187, pp. 50-58, 1999.

[4] M. Haruta, "When gold is not noble: Catalysis by nanoparticles," *Chemical Record,* vol. 3, pp. 75-87, 2003.

[5] G. J. Hutchings and M. Haruta, "A golden age of catalysis: A perspective," *Applied Catalysis A: General,* vol. 291, pp. 2-5, 2005.

[6] J. Li, *et al.*, "Efficient elimination of trace ethylene over nano-gold catalyst under ambient conditions," *Environmental Science and Technology,* vol. 42, pp. 8947-8951, 2008.

[7] C. Sealy, "Nanoporous Au shows promise as 'green' catalyst," *Nano Today,* vol. 5, p. 82, 2010.

[8] X. Zhou, *et al.*, "Size-dependent catalytic activity and dynamics of gold nanoparticles at the single-molecule level," *Journal of the American Chemical Society,* vol. 132, pp. 138-146, 2010.

[9] A. Lyalin and T. Taketsugu, "Adsorption of ethylene on neutral, anionic, and cationic gold clusters," *Journal of Physical Chemistry C,* vol. 114, pp. 2484-2493, 2010.

[10] S. Tsubota, *et al.*, "CO oxidation over gold supported on TiO2," vol. 77, ed, 1993, pp. 325-328.

[11] Y. Iizuka, *et al.*, "Adsorption of CO on gold supported on TiO2," *Catalysis Today,* vol. 36, pp. 115-123, 1997.

[12] M. M. Schubert, *et al.*, "CO oxidation over supported gold catalysts -"Inert" and "active" support materials and their role for the oxygen supply during reaction," *Journal of Catalysis,* vol. 197, pp. 113-122, 2001.

[13] M. Haruta, "Nanoparticulate gold catalysts for low-temperature CO oxidation," *Journal of New Materials for Electrochemical Systems,* vol. 7, pp. 163-172, 2004.

[14] N. Lopez, *et al.*, "On the origin of the catalytic activity of gold nanoparticles for low-temperature CO oxidation," *Journal of Catalysis,* vol. 223, pp. 232-235, 2004.

[15] G. Glaspell, *et al.*, "Nanocatalysis on supported oxides for CO oxidation," *Topics in Catalysis,* vol. 47, pp. 22-31, 2008.

[16] E. Quinet, *et al.*, "H2-induced promotion of CO oxidation over unsupported gold," *Catalysis Today,* vol. 138, pp. 43-49, 2008.

[17] M. Chun Yan, *et al.*, "Mesoporous co3o4 and AU/CO3o4 catalysts for low-temperature oxidation of trace ethylene," *Journal of the American Chemical Society,* vol. 132, pp. 2608-2613, 2010.
[18] J. M. Cíes, *et al.*, "Contributions of electron microscopy to understanding CO adsorption on powder Au/ceria-zirconia catalysts," *Chemistry - A European Journal,* vol. 16, pp. 9536-9543, 2010.
[19] P. Diao, *et al.*, "Electrocatalytic activity of supported gold nanoparticles toward CO oxidation: The perimeter effect of gold-support interface," *Electrochemistry Communications,* vol. 12, pp. 1622-1625, 2010.
[20] H. G. Ahn, *et al.*, "Complete oxidation of ethylene over supported gold nanoparticle catalysts," *Journal of Nanoscience and Nanotechnology,* vol. 6, pp. 3599-3603, 2006.
[21] C. G. Vayenas, *et al.*, "The role of PtOx in the isothermal rate oscillations of ethylene oxidation on platinum," *Journal of Catalysis,* vol. 67, pp. 348-361, 1981.

Chapter 7 Electrochemical Promotion of C_2H_4 Complete Oxidation with Gold Nanoparticle Catalyst

7.1 Introduction

Until recently, most of the electrochemical promotion studies have been done in catalyst-working electrode in the form of continues film, which is characterized by low dispersion. One of the factors that limits the commercial application of electrochemical promotion is the low degree of metal dispersion (typically 10^{-3} to 10^{-5}) found in the thick, porous film catalyst-electrode (typically 0.2 to 10 μm, most often produced by decomposition of a paste) [1]. However, thinner catalyst deposition methods, shown in the next paragraph, are continuously being developed to overcome this problem [2-6] .

In the early stage of electrochemical promotion experiments, most of the deposition has been done by Chemical Vapor Deposition (CVD) where a film is generated by reaction of appropriate precursors at the substrate surface [2, 7-11]. The deposition method has evolved over time and more recently it can be stimulated by supplying extra energy during the process, e.g. by means of plasma enhancement (PECVD) or laser stimulation (LCVD). A special form of this technique is Atomic Layer Deposition (ALD), which splits the CVD reaction process at the surface into two parts [12]. Also, precisely controlled physical vapor deposition has also been developed, such as magnetron sputtering [13, 14]. This is due to the use of a vacuum environment, high purity source materials as well as a great degree of control over morphology not found with the use of pastes.

Metal dispersion is defined by the percentage of metal catalyst or electrode exposed to the gaseous reactants. Dispersion is often calculated by using the following equation:

$$dispersion\ (\%) = \frac{MW_{Au} \times 600}{\rho_{Au} d_{avg} a_{Au} N_a} \qquad \text{(Eq. 7-1)}$$

Where MW_{Au} is the molecular weight of Au (196.97 g/mol), ρ_{Au} is the density of Au (19.43 g/cm^3), d_{avg} is the average particle size, a_{Au} is the surface area of one Au atom (2.29 x 10^{-19} m^2 $atom^{-1}$), and N_a is Avogadro's number (6.022 x 10^{23} atom mol^{-1}). The low degrees of dispersion typically found in prior EPOC studies may be acceptable for certain active catalyst phase materials but can be costly for many noble-metal applications [15]. Continuous improvements and researches are done to overcome this problem and a step forward to commercial application of EPOC has been achieved through wireless EPOC, which is described in section 2.2.3.1.2.

In this chapter, the catalytic activity of Au1/YSZ-p catalyst in complete ethylene oxidation reaction is studied under EPOC conditions in the developed wireless electrochemical cell. In this type of experiments the known value of electrical potential is applied in order to electrochemically promote the catalytic activity of Au/YSZ-p. Open circuit measurements shown in the previous chapter are compared to the closed circuit measurements at various reaction conditions. Electrochemical promotion of gold nanoparticles is quantified using the rate enhance ratio, ρ, which is the ratio of ethylene conversion at closed circuit to the conversion at open circuit.

$$\rho = \frac{r}{r_o} \qquad \text{(Eq. 7-2)}$$

and the Faradaic efficiency, Λ,:

$$\Lambda = \frac{r - r_o}{\left(\frac{I}{2F}\right)} = \frac{\Delta r}{r_F} \qquad \text{(Eq. 7-3)}$$

Electrochemical promotion of gold nanoparticles (AuNP) deposited on YSZ for the gas phase oxidation of ethylene is reported for the first time.

7.2 **Experimental**

The experimental setup and configuration are identical to the open circuit experiments, shown in 6.2.2. The only difference is that the auxiliary gold electrodes are now connected to a potentiostat for applying and measuring potential and current of the electrochemical cell.

In all cases, a series of blank experiments has been carried out to confirm that the catalytic activity of the Au auxiliary electrodes is negligible in comparison to that of the Au/YSZ-p catalyst. The choice of Au as a reference electrode, besides its low activity for C_2H_4 oxidation, is dictated by the fact that it acts as a good pseudo-reference electrode. Numerous parameters have been varied one at a time to examine the effect of these parameters in EPOC conditions. The experimental parameters are summarized in Table 7-1.

Table 7-1 EPOC Experimental summary

Flowrate	**mL min^{-1}**	80	200		200	300	400	600
Temperature	**^{o}C**	300-400	250-400		350	350	350	350
Applied Potential	**V**	0-1.2	0-2		0-2	0-2	0-2	0-2
$P_{C_2H_4} / P_{O_2}$	**kPa/kPa**	0.3:3	0.1:3	0.1:1	0.1:3	0.1:3	0.1:3	0.1:3
		0.3:0.45	0.2:3	0.1:2				
		0.3:0.6	0.3:3	0.1:3				
		0.3:0.9	0.4:3	0.1:4				
		0.3:1.2	0.5:3	0.1:5				
		0.3:1.8	1:3					
		0.3:2.4						

Effects of the flow rate, temperature, ratio of partial pressures of ethylene to oxygen are studied under application of different electrical potentials. The magnitude of EPOC is evaluated using the rate enhancement ratio, ρ.

7.3 Results and Discussion

7.3.1 Experiment at 200 ml min^{-1}

Ethylene oxidation under closed circuit conditions is carried out at different temperatures under fuel-lean conditions, which is determined to be the optimum condition from the last chapter. The total flow rate is kept at 200 ml min^{-1} and the partial pressure of ethylene and oxygen are kept at 0.1 kPa and 3 kPa, respectively. For the closed circuit experiments, potential of 0.3, 0.6, 1 and 2 V are applied. The variations of C_2H_4 conversion versus temperature are plotted in Figure 7-1 upon applying different amount of potential to the electrochemical cell. The experiment depicts the unpromoted, open circuit catalyst

performance, as well as the catalytic behaviour upon electrochemical promotion. Dashed lines indicate the open circuit catalyst performance, while solid lines correspond to electrochemically promoted catalytic behaviour. The figure shows a considerable effect of electrochemical promotion for ethylene oxidation reactions. Potential application of 0.3 V to 2 V between the two auxiliary electrodes causes enhancement of the conversion of C_2H_4 over the Au1/YSZ-p catalyst. The increase in C_2H_4 conversion due to potential application is reversible and after potential interruption conversion returns to its initial open circuit value.

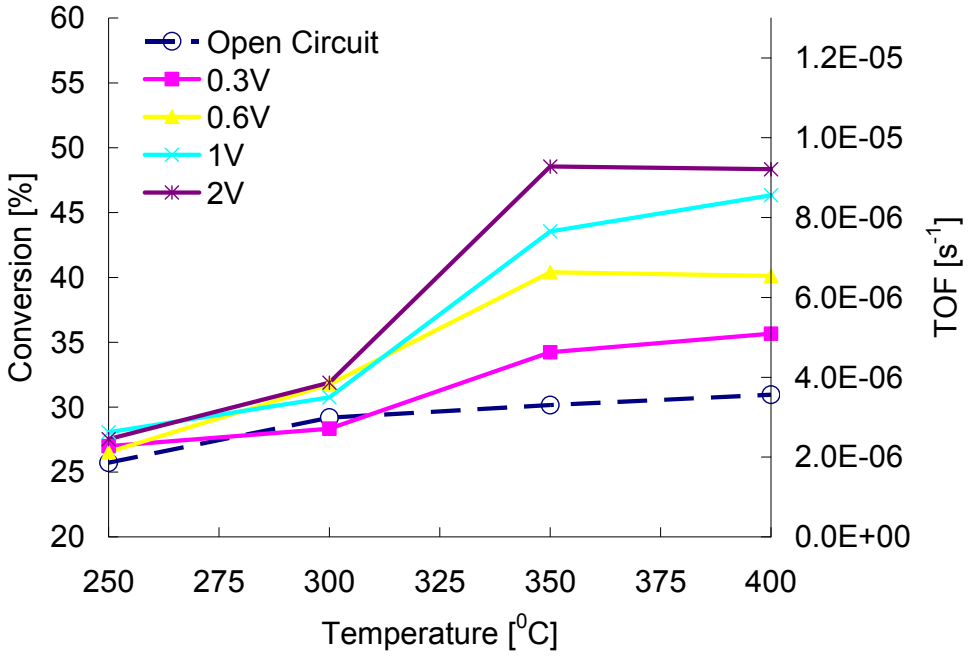

Figure 7-1 Effects of reaction temperature on ethylene conversion and turnover frequency at different potential applications. Gas composition: $P_{C_2H_4}$ = 0.1 kPa and P_{O_2} = 3 kPa. Flow rate: 200 ml min^{-1}.

The electrochemical promotion of ethylene oxidation is temperature dependent. Between 350 ^{0}C and 400 ^{0}C, rate enhancement ratio, shown in (Eq. 7-2), is more prominent. The value of the maximum rate enhancement ratio is 1.68 at 300 ^{0}C when 2 V is applied to the electrochemical cell. Another way to visualize the change in ethylene conversion upon application of potential is to plot rate enhancement ratio versus applied potential, as shown in Figure 7-2.

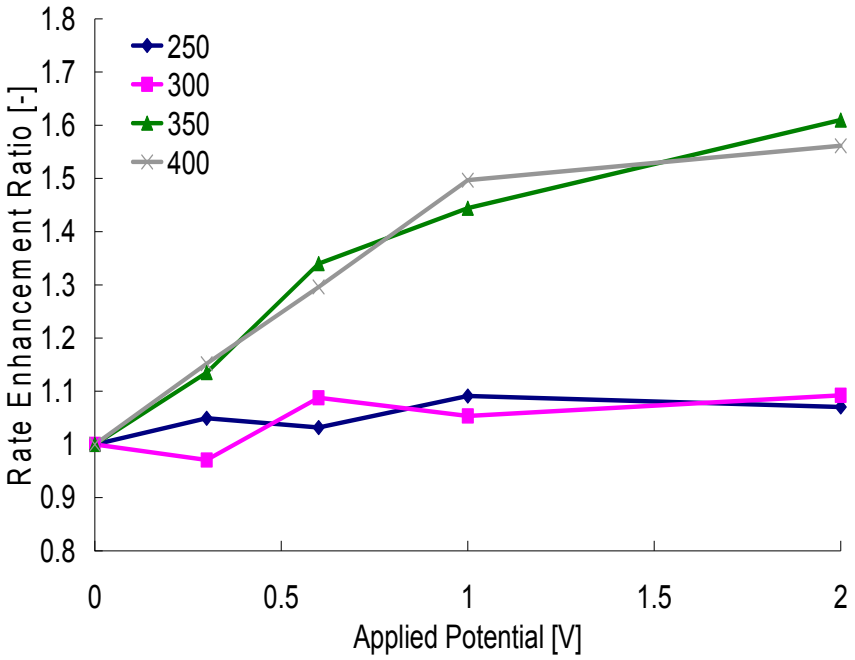

Figure 7-2 Rate enhancement ratio, ρ, as a function of the applied potential. Gas composition: $P_{C_2H_4}$ = 0.1 kPa and P_{O_2} = 3 kPa. Flow rate: 200 ml min^{-1}.

Temperature corresponds to that of O^{2-} ion conductivity. It is important that the reaction temperature above 350 ^{0}C is sufficient enough for the O^{2-} spillover-backspillover to occur. Increasing the operating temperature further to 400 ^{0}C does not increase the rate

enhancement ratio. In addition, it is observed that the application of higher potential polarizes more gold nanoparticles place in between the electrodes, making the ethylene oxidation with temperature much more abrupt.

This can also be explained by the current of the electrochemical cell when constant potential is applied, as shown in Figure 7-3. There are no difference in the current of the electrochemical cell up to 300 ^{0}C, indicating that the cell is not conductive enough at low temperatures to polarize the gold nanoparticles.

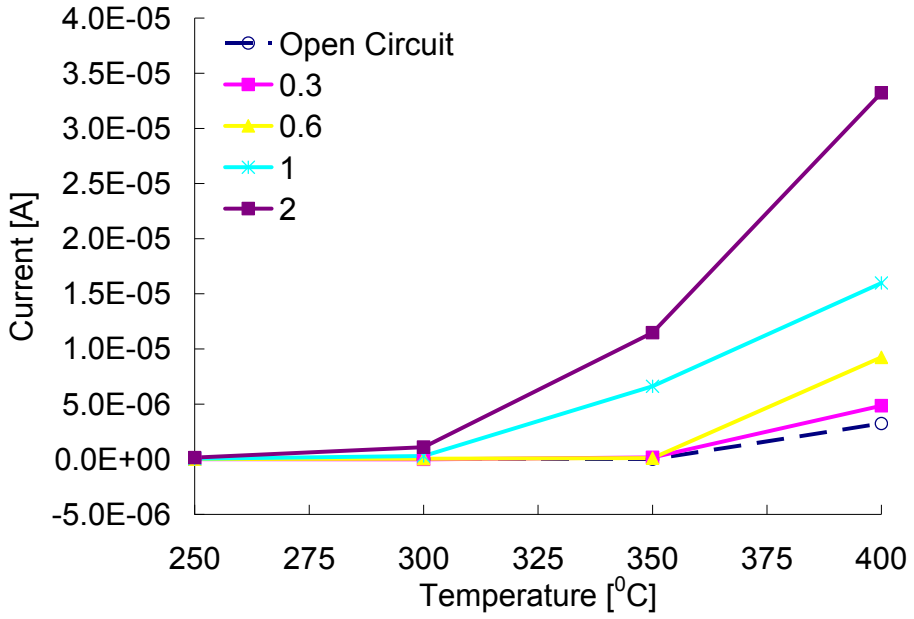

Figure 7-3 Response of current on different potential applications as a function of temperature. Gas compositions: $P_{C_2H_4}$ = 0.1 kPa and P_{O_2} = 3 kPa. Flow rate: 200 ml/min.

The results are in agreements with other studies dealing with electrochemical promotion of platinum nanoparticles in bipolar configuration using Pt nanoparticles [2, 14, 16-19]. These studies look into different aspects of bipolar configuration of electrochemical

promotion, including the current bypass. Wodiunig discusses the low rate enhancement ratio compared to the classical electrochemical promotion due to current bypass and a non-uniform distribution of the work function in past experiments [18]. The partly anodic and partly cathodic polarization of the electrodes leads to a non-uniform promotion effect on the nanoparticles. Therefore, in order to further characterize and analyze the electrochemical promotion effect, one needs to determine the amount of current that is bypassing and make improvements on the design of the cell to minimize the loss.

Figure 7-4 and Figure 7-5 show transient behaviour of electrochemical promotion experiment at three different fuel-lean conditions. The graph plots applied potential and conversion versus time. The partial pressures of ethylene are 0.1, 0.2 and 0.5 kPa, respectively while keeping oxygen pressure constant at 3 kPa. Operating temperature is chosen to be 350 ^{0}C.

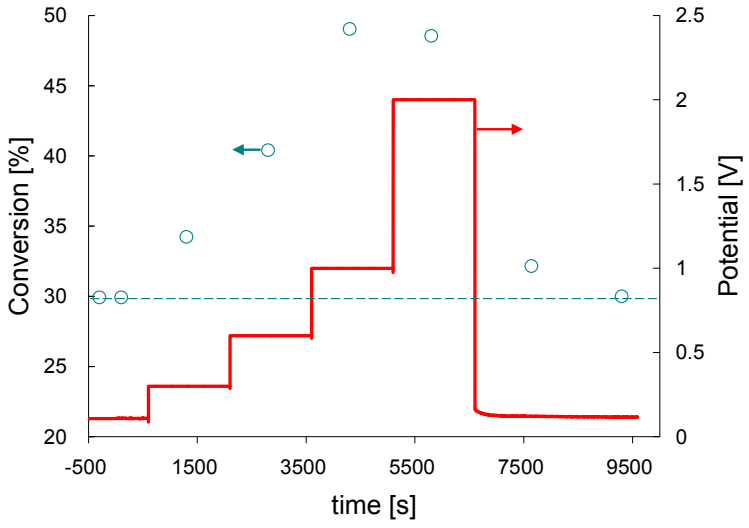

(A)

Figure 7-4 Transient effect of applied potential on the ethylene conversion (green points) and catalyst potential (red line) at ethylene partial pressure of 0.1 kPa (A). T = 350℃, P_{O_2} = 3 kPa, flow rate = 200 ml min^{-1}.

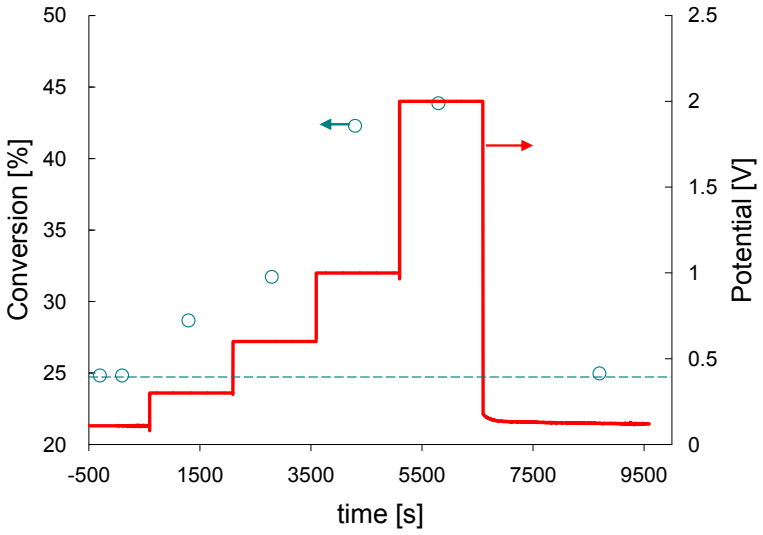

(B)

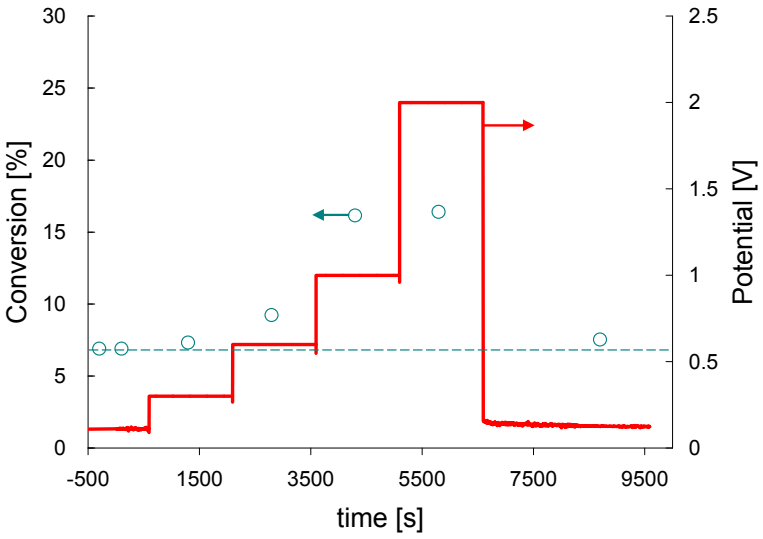

(C)

Figure 7-5 (Continued) Transient effect of applied potential on the ethylene conversion (green points) and catalyst potential (red line) at different partial pressure of ethylene (B = 0.2, C = 0.5 kPa). T = 350℃, P_{O_2} = 3 kPa, flow rate = 200 ml min^{-1}.

Potential interruption causes both ethylene conversion and open circuit potential to return to their initial values after approximately 30 minutes. This is useful for the application in the industry as one can control the electrochemical promotion when desired.

7.3.2 Experiment at 80 ml min^{-1}

Another set of experiments is carried out at flow rate of 80 ml min^{-1}. This time, the partial pressure ratio of C_2H_4 to O_2 covered wider ranges of conditions, from fuel-rich condition to fuel-lean condition.

7.3.2.1 Effect of temperature and reactant partial pressure

The effect of temperature from 300, 350 and 400 ^{0}C on the behaviour of ethylene conversion at fuel-lean ($P_{C_2H_4} / P_{O_2}$ = 0.125), stoichiometric ($P_{C_2H_4} / P_{O_2}$ = 0.333) and fuel-rich ($P_{C_2H_4} / P_{O_2}$ = 1) conditions are shown in Figure 7-6 and Figure 7-7. Maximum rate enhancement ratio of 1.79 is observed at 350 ^{0}C upon potential application of 2V at stoichiometric condition. Maximum Faradaic efficiency determined by (Eq. 7-3) is 6.5×10^5.

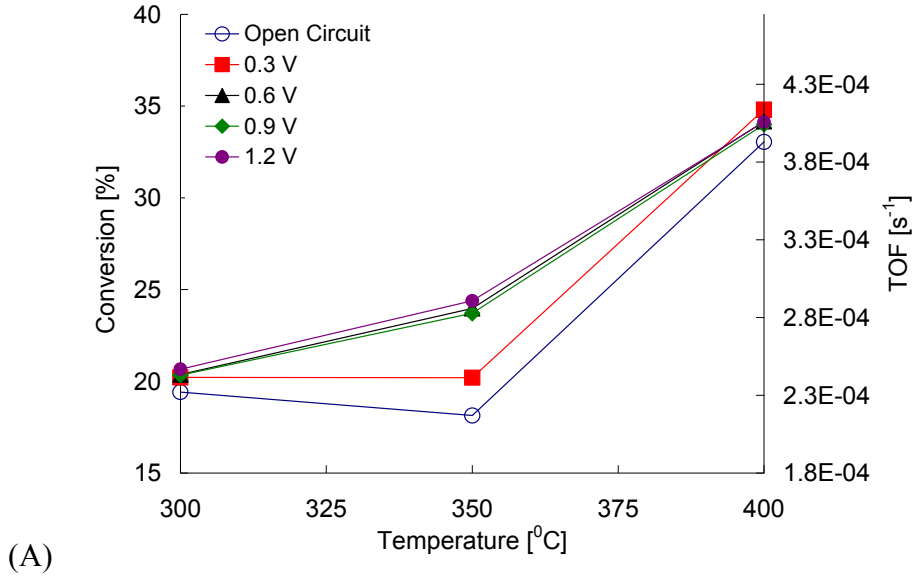

(A)

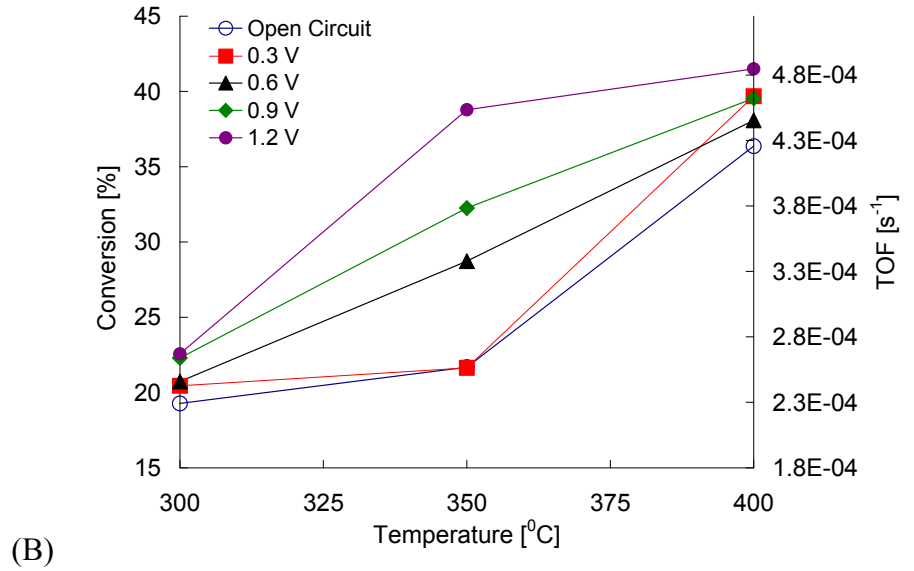

(B)

Figure 7-6 C_2H_4 conversion of Au1/YSZ-p as function of temperature under (A) fuel-rich and (B) stoichiometry condition. Flow rate = 80 ml min^{-1}. $P_{C_2H_4} / P_{O_2}$ = 1, 0.333 and 0.125, respectively.

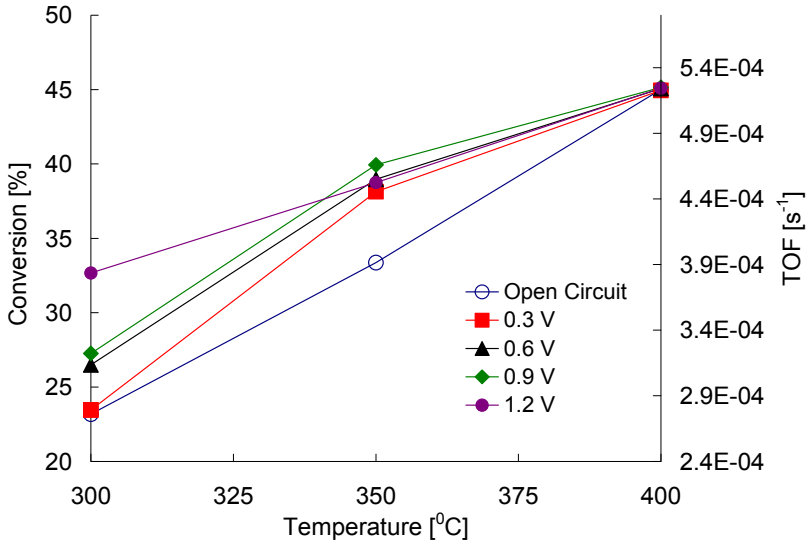

(C)

Figure 7-7 (Continued) C_2H_4 conversion of Au1/YSZ-p as function of temperature under fuel-lean condition (C). Flow rate = 80 ml min^{-1}. $P_{C_2H_4} / P_{O_2}$ = 1, 0.333 and 0.125, respectively.

Interestingly, electrochemical promotion effect is minimal at 400 ^{0}C as maximum conversion of about 45 percent is attained regardless of potential application. This suggests that at temperature above 400 ^{0}C, kinetics for the charge transfer reaction, shown in Figure 2-7, is slower than the kinetics for the gas-exposed catalyst surface ethylene oxidation reaction. Under such condition, the reactants covered on the gas exposed catalyst surface constantly react before the backspillover takes place for the electrochemical promotion effect to occur.

The increase in ethylene conversion during an application of potential depends on the ratio of partial pressures of ethylene to oxygen, as well as temperature. A maximum conversion at both open and closed circuit is observed at 400 ^{0}C at fuel-lean condition, but maximum increase in conversion (i.e. rate enhancement ratio) is observed at 350 ^{0}C at

stoichiometric condition. At lower temperature, the influence of the promotion is less important due to the low current passed through the cell since O^{2-} conductivity is low, whereas at higher temperature the conversion approaches a maximum value which leads to a decrease in promotion effect.

7.3.3 Effect of flow rates

Figure 7-8 shows the effect of flow rate on the steady-state TOF of ethylene over Au1/YSZ-p catalyst interfaced with YSZ disk. TOF is measured at constant P_{O_2} = 3 kPa and $P_{C_2H_4}$ = 0.1 kPa under an applied potential of 0.3, 0.6, 1 and 2 V.

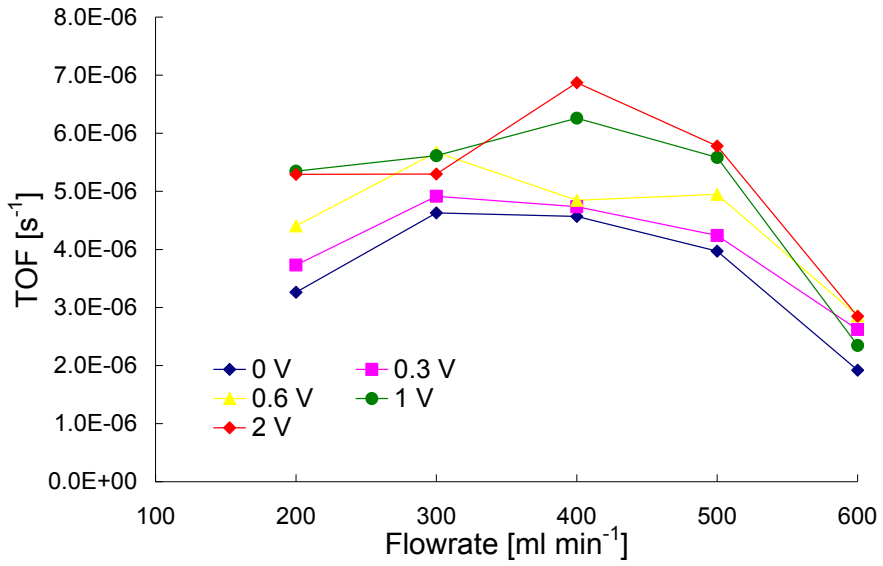

Figure 7-8 Turnover frequency as function of flow rates at different applied potentials. T = 350 ^{0}C. $P_{C_2H_4}$ = 0.1 kPa, P_{O_2} = 3 kPa.

At flow rates above 400 ml min^{-1}, either internal or external mass transfer limitations are present within the reaction temperature as turnover frequency starts to decrease. This indicates that the number of oxygen atoms reacting per surface site per second is decreasing, possibly from the decrease in residence time. As a result, electrochemical promotion effect also decreases. Under the conditions of external mass-transfer control, electrochemical promotion itself is not operative anymore since the catalytic rate is controlled by gaseous diffusion rather than by the surface kinetics. Vayenas et al. stated that in highly dispersed catalysis, the main problem is to overcome the current bypass and internal mass transfer limitations due to high catalytic activity of such fully dispersed catalyst systems [4, 15].

In order to enhance catalytic reaction rate by wireless EPOC, the process should not be subjected to external or internal mass transfer limitations [15] within the desired temperature range, which can obscure or even completely hide the electrochemical promotion effect. To avoid external mass transfer limitations, one needs to keep the reaction flowrate within the range at which the rate of consumption of reactants does not change with varying flow rate. To prevent the internal mass transfer limitations, operating temperature needs to be high enough to maintain ionic conductivity across the electrochemical cell. Also, proper setting of location and geometric shape of the auxiliary electrodes can modify ionic transfer gradient across the electrochemical cell, improving the mass transfer of ions.

Xia et al. have proposed a mechanism responsible for induced bipolar electrochemical promotion in CO oxidation reaction with platinum nanoparticles supported on YSZ. They state in-plane polarization of Pt particles result in a bipolar system and leads to the formation of a large number of galvanic cells partially or completely polarized [14, 19], which changes their work functions (Figure 7-9).

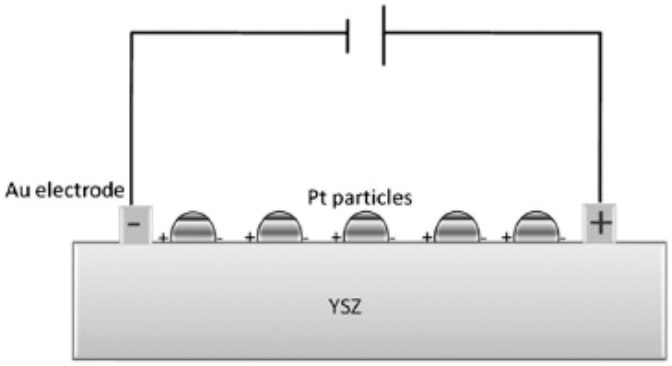

Figure 7-9 Proposed mechanism by Xia et al. In-plane polarization of Pt particles result in a bipolar system and leads to the formation of a large number of galvanic cells partially or completely polarized.

The average size of Pt nanoparticles they used is 40 nm, comparatively larger from the Au nanoparticles being used in present experiment (< 10 nm). In addition, the platinum particles are directly placed on YSZ solid electrolyte, whereas in the present case, gold nanoparticles already supported on YSZ powder (YSZ-p) are placed on YSZ solid electrolyte.

Since induced bipolar electrochemical promotion has not been done with small nanoparticles (< 10 nm), different mechanism is proposed to explain the phenomenon. As opposed to the in-plane polarization leading to the formation of galvanic cells, the increase in catalytic activity is explained by movement of ions from the O^{2-} flux. Upon application

of constant potential, O^{2-} ion concentration gradient is formed across the electrochemical cell. The flux of O^{2-} ions in solid electrolyte allows backspillover of O^{2-} ions form double layer on the surface of the supported nanoparticles, resulting in a change in work functions. Figure 7-10 illustrates the proposed mechanism of induced bipolar EPOC.

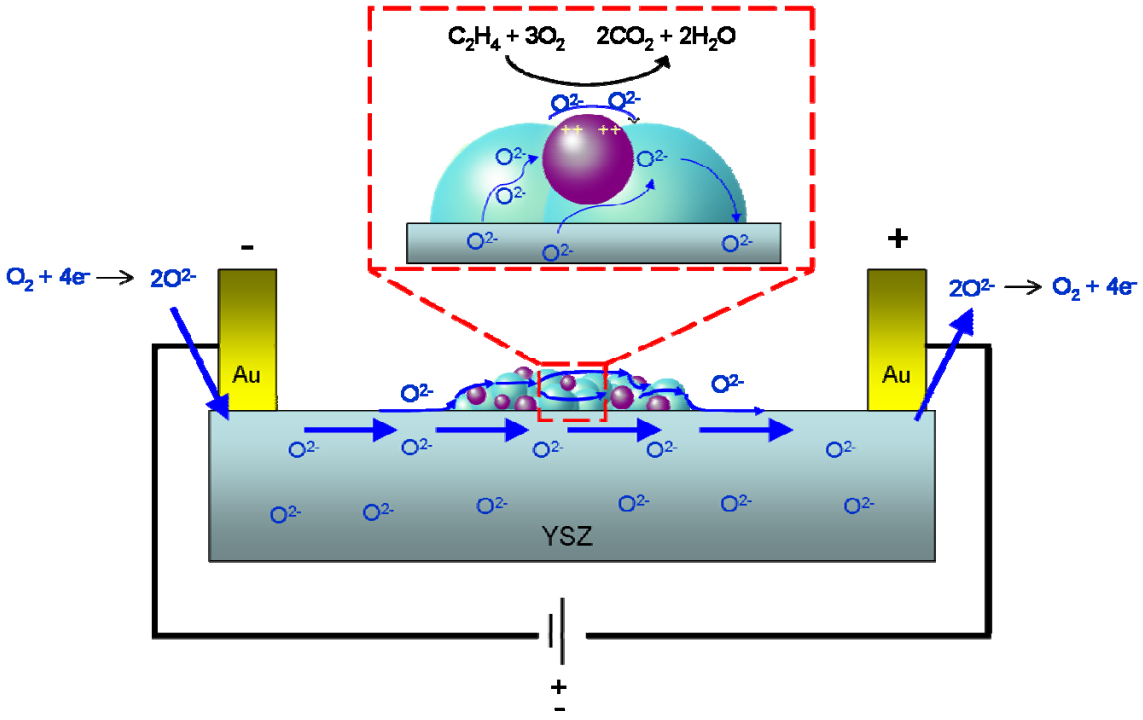

Figure 7-10 Proposed mechanism of induced bipolar EPOC of gold nanoparticles in complete oxidation of ethylene. Portion of the transported oxygen ions would polarize the gold nanoparticles.

However, some O^{2-} ions may bypass over the nanoparticles, thus having no effect on the change in work functions. Current bypass plays crucial role in successfully conducting EPOC experiments. The cell voltage of an electrochemical cell can be described as the sum of cathodic η_c and anodic η_a overpotentials (difference between the resultant

potential and each individual reaction equilibrium potential) and the ohmic drop IR across the cell [18]:

$$U_{cell} = \eta_c + IR + \eta_a \quad \text{(Eq. 7-4)}$$

The two overpotentials are associated with the charge transfer reactions at the cathode and anode, which are the reduction of oxygen and the oxidation of oxide ions in the case of an O^{2-} ion conductor like YSZ:

$$O_2 + 4e^- \leftrightarrow 2O^{2-} \quad \text{(Eq. 7-5)}$$

At high current, (Eq. 7-4) reduces to:

$$U_{cell} = IR^* \quad \text{(Eq. 7-6)}$$

Where R* is the ohmic resistance of cell voltages which includes the ohmic resistance of the solid electrolyte and the ohmic resistance of the charge transfer reactions. The feeding current (I_{feed}) of the system divides into the bypass current and the current crossing the bipolar electrode (I_{a+c}). The fraction of current constituting the bypass current depends on the relative size of the two total resistances between the two feeder electrodes [18]. Therefore, research into the modification of the design of EPOC cells, specifically with aims to minimize resistances and thus current bypass, is a viable area for future work. For example, a YSZ disk can have a groove in the middle for depositing the Au/YSZ-p catalyst to improve the O^{2-} ion conductivity and backspillover process.

In the current experiments, different amount of constant potentials have been applied to bipolar electrochemical cell to electrochemically promote gold nanoparticles for the complete oxidation reaction of ethylene. Also, the temperature, partial pressure of

oxygen and ethylene, total reactant flow rate and applied potential have been varied to determine the optimum condition at which EPOC effect is present.

7.4 **Conclusion**

Oxidation reactions of ethylene on Au1/YSZ-p under closed circuit conditions are studied in various conditions. The results obtained clearly demonstrate that Au nanoparticle catalysts can be effectively promoted electrochemically in the bipolar cell configuration upon application of constant potentials. When sufficient constant potential is applied, maximum conversion for ethylene increased approximately 70 to 80 % with maximum rate enhancement ratio and Faradaic efficiency of 1.79 and 6.5×10^5, respectively. Experiments at different experimental parameters show that higher electrochemical promotion can be achieved at the fuel-lean condition, given high enough temperatures above 350 ^{0}C where YSZ exhibits good ionic conductivity. Increase flow rate above 200 ml min^{-1} introduced external and/or internal mass transfer limitation, diminishing the effect of potential application.

The mechanism for the bipolar EPOC has been proposed as follows. Contrast to the mechanism proposed by Xia et al. [14, 19] of forming individual galvanic cells upon application of potential across the electrochemical cell, the proposed mechanism attempts to explain the wireless EPOC phenomenon through formation of O^{2-} ion concentration gradient across the electrochemical cell. The flux of O^{2-} ions in solid electrolyte allows

backspillover of ions to form double layer on the surface of gold nanoparticles, resulting in a change in their work functions.

The feasibility of electrochemically promoting Au nanoparticles supported on YSZ powder in the bipolar cell configuration has been demonstrated for the first time in this chapter. The promotion of C_2H_4 oxidation observed in the electrochemical cell with bipolar configuration is similar to that observed with isolated platinum film and platinum nanoparticles but different mechanism is proposed to explain the promotion effect.

7.5 **References**

[1] E. R. S. A. Wieckowski, C.G. Vayenas, *Catalysis and Electrocatalysis at Nanoparticle Surfaces*. New York: Marcel Dekker, Inc, 2003.

[2] M. Marwood, *et al.*, "Electrochemical promotion of electronically isolated and dispersed Pt catalysts," *Ionics,* vol. 4, pp. 207-214, 1998.

[3] M. Marwood and C. G. Vayenas, "Electrochemical promotion of a dispersed platinum catalyst," *Journal of Catalysis,* vol. 178, pp. 429-440, 1998.

[4] C. Koutsodontis, *et al.*, "The effect of catalyst film thickness on the electrochemical promotion of ethylene oxidation on Pt," *Topics in Catalysis,* vol. 39, pp. 97-100, 2006.

[5] E. Mutoro, *et al.*, "Electrochemical promotion of Pt(111)/YSZ(111) and Pt-FeOx/YSZ(111) thin catalyst films: Electrocatalytic, catalytic and morphological studies," *Applied Catalysis B: Environmental,* vol. 100, pp. 328-337, 2010.

[6] E. I. Papaioannou, *et al.*, "The role of TiO2 layers deposited on YSZ on the electrochemical promotion of C2H4 oxidation on Pt," *Journal of Applied Electrochemistry,* vol. 40, pp. 1859-1865, 2010.

[7] C. G. Vayenas, *et al.*, "Dependence of catalytic rates on catalyst work function," *Nature,* vol. 343, pp. 625-627, 1990.

[8] E. Varkaraki, *et al.*, "Electrochemical promotion of IrO2 catalyst for the gas phase combustion of ethylene," *Journal of Applied Electrochemistry,* vol. 25, pp. 978-981, 1995.

[9] J. Nicole and C. Comninellis, "Electrochemical promotion of IrO2 catalyst activity for the gas phase combustion of ethylene," *Journal of Applied Electrochemistry,* vol. 28, pp. 223-226, 1998.

[10] S. Wodiunig, *et al.*, "Electrochemical promotion of RuO2 catalyst dispersed on an yttria-stabilized zirconia monolith," *Electrochemical and Solid-State Letters,* vol. 2, pp. 281-283, 1999.

[11] H. Watanabe, *et al.*, "Properties of V2O5 thin films deposited by means of plasma MOCVD," *Thin Solid Films,* vol. 386, pp. 281-285, 2001.

[12] J. C. Badot, *et al.*, "Electrical properties of V2O5 thin films obtained by atomic layer deposition (ALD)," *Journal of Materials Chemistry,* vol. 14, pp. 3411-3415, 2004.

[13] C. Falgairette, *et al.*, "Solid electrochemical mass spectrometry (SEMS) for investigation of supported metal catalysts under high vacuum," *Journal of Applied Electrochemistry,* vol. 40, pp. 1893-1900, 2010.

[14] C. Xia, *et al.*, "Quantifying electrochemical promotion of induced bipolar Pt particles supported on YSZ," *Electrochemistry Communications,* vol. 12, pp. 1551-1554, 2010.

[15] C. G. Vayenas, S. Bebelis, C. Pilangos, S. Brosda, D. Tsiplakides, *Electrochemical Activation of Catalysis - Promotion, Electrochemical Promotion, and Metal-*

Support Interactions vol. 1. New York, Boston, Dordrecht, London, Moscow: Kluwer Academic Publishers, 2002.

[16] C. Pliangos*, et al.*, "Electrochemical promotion of conventional and bipolar reactor configurations for NO reduction," *Ionics,* vol. 8, pp. 372-382, 2002.

[17] D. Tsiplakides and S. Balomenou, "Milestones and perspectives in electrochemically promoted catalysis," *Catalysis Today,* vol. 146, pp. 312-318, 2009.

[18] S. Wodiunig*, et al.*, "Electrochemical promotion of bipolar electrodes: An estimation of the current bypass," *Electrochimica Acta,* vol. 46, pp. 357-363, 2000.

[19] C. Xia*, et al.*, "Electrochemical promotion of CO combustion over non-percolated Pt particles supported on YSZ using a novel bipolar configuration," *Electrochemistry Communications,* vol. 13, pp. 99-101, 2011.

Chapter 8 Conclusions and Recommendations

The study shows feasibility of using gold nanoparticles supported on yttria-stabilized zirconia for conventional heterogeneous catalysis, as well as induced bipolar electrochemical promotion of catalysis. Since the discovery of the high catalytic activity of gold nanoparticles by Haruta [1, 2], supported gold catalysts have been extensively studied [3-13]. The catalytic activity of gold has interested researchers not only because gold nanoparticles are such outstanding catalysts, but also because gold offers a classic example of chemistry on the nanoscale. This distinct difference in catalytic characteristics of gold at bulk and nanosize makes this metal unique and special.

Electrochemical Promotion of Catalysis (EPOC) is an alteration of catalytic properties of heterogeneous catalysis, which usually functions as working electrode in an electrochemical cell. It has been demonstrated that gold nanoparticles supported on yttria-stabilized zirconia (YSZ) can be electrochemically promoted using the "bipolar" configuration. In this configuration, application of constant electrical field between two feeder electrodes induces ionic flux across the electrochemical cell, resulting in backspillover of O^{2-} ions to the surface of the gold nanoparticles, modifying the work function of Au nanoparticles. This 'bipolar' configuration opens new opportunities for practical application of this phenomenon [14-19].

The novelty of the research is that there have been no reports on experimenting complete ethylene oxidation on gold nanoparticles supported on YSZ and also bipolar configuration of EPOC experiment is done for the first time on gold nanoparticles.

Catalytic performance of gold nanoparticles deposited on YSZ for complete ethylene oxidation is compared between open circuit (conventional heterogeneous catalysis) and closed circuit (electrochemical promotion of catalysis) conditions. Catalytic performances at two different distinct conditions allow determining the behaviour and characteristic of gold nanocatalysts.

8.1 Synthesis and Physiochemical Characterizations of Gold Nanoparticle Catalyst

The first chapter of results (Chapter 4) introduces a synthesis method for gold nanoparticles supported on YSZ. YSZ is an interesting support for catalyst because it possesses ionic conductivity at high temperatures and contains oxygen vacancies, and thus, can be used as solid electrolyte as well as heterogeneous catalyst. To synthesize YSZ supported Au nanoparticles, ethanol and water are used as reducing agent and PVP as stabilizer to the nanoparticles during reflux to prevent agglomeration. Similar synthesis method has been used to make colloidal platinum nanoparticles [20] but this method has never been used to synthesize supported gold nanoparticles. It is important to note that catalytic studies on YSZ supported Au nanoparticles has yet been reported in the literature.

Several types of analysis are used in order to characterize the physicochemical properties of nanoparticles. Morphological properties of the gold nanoparticles catalysts and their chemical surface composition are analyzed with Scanning electron microscopy (SEM), Transmission electron microscopy (TEM), X-ray diffraction (XRD) and X-ray

photoelectron spectroscopy (XPS). It follows from SEM, TEM and XRD analyses that the gold nanoparticles have average particle size of approximately 6 to 10 nm and face centered cubic structure. The particles are well dispersed on the YSZ support. The oxidation state of the catalyst is mainly pure metallic gold and might contain very little of gold with different oxidation state. XPS result of Au3/YSZ-p catalyst has revealed that the catalyst contains portions of gold oxide. These characteristics of the catalysts are often recalled in later Chapter 5, 6 and 7 in order to explain the electrochemical and catalytic behaviour of the catalysts.

Later chapters reveal that Au3/YSZ-p catalyst has the best performance out of the synthesized catalysts, due to having the smallest average particle size. Therefore, synthesis of supported gold nanocatalyst with smaller average particle size is recommended. Different synthesis method may be required to reduce the average particle size because adding further Polyvinylpyrrolidone (PVP) prevents from homogeneous mixing of the precursor solution. Martin method, which uses $NaBH_4$ as reducing agent, has shown to produce colloidal gold nanoparticles with average diameter of 3.2 to 5.2 nm [21]. Adapting the Martin method to synthesize gold nanoparticles supported on YSZ and conduct same experiment would give further information on the size effect of gold nanoparticles on oxidation of carbon monoxide and ethylene.

Though not clear, different compositions of gold and gold oxide of Au1/YSZ-p and Au3/YSZ-p may contribute to the difference in their catalytic activity. Controlling the oxidation states of gold nanoparticles during synthesis and calcination would also be another area needing an improvement.

Further physicochemical characterizations of supported gold nanoparticles are also recommended, in order to further understand their characteristics. Temperature programmed desorption (TPD) allows observing the desorbed molecules from a surface when the surface temperature is increased. Therefore, conducting TPD of ethylene and carbon monoxide can provide information on desorptivity of specific molecules, ethylene and carbon monoxide in this case, on the surface of gold nanoparticles.

8.2 **CO Oxidation Reaction on Gold Nanoparticle Catalyst**

In Chapter 5, catalytic activities of CO oxidation of the synthesized catalysts, Au1/YSZ-p and Au3/YSZ-p with the average particle size of 9 nm and 6 nm, respectively are compared to the commercial gold nanocatalyst, Au/γ-Al_2O_3-p (1-2 nm average size). The experiment confirms that both Au1/YSZ-p and Au3/YSZ-p are catalytically active toward CO oxidation, with Au3/YSZ-p having higher catalytic activity out of the synthesized catalysts, mainly due to smaller average particle size.

There may have been different factors that affect the catalytic activity of the gold nanoparticle samples, for example, their oxidation states. XPS analysis (Chapter 4) has shown that the synthesized gold nanoparticles contain various oxidation states of gold. Therefore, conducting experiments with controlled compositions of the gold's oxidation states are recommended to confirm the main cause of the difference in the catalytic activity.

8.3 **Ethylene Oxidation on Gold Nanoparticle Catalyst**

Chapter 6 discusses complete oxidation of ethylene over the synthesized gold nanocatalysts. Au3/YSZ-p shows better catalytic activity than Au1/YSZ-p for ethylene oxidation as well, also due to Au3/YSZ-p having smaller average particle size. When using the plug flow reactor, the oxidation of ethylene starts to occur even at room temperature at fuel-lean condition. It appears that two different conditions, fuel-rich and fuel-lean conditions exist for the reaction and they demonstrate different kinetics towards ethylene oxidation reaction [22]. It is shown that ethylene oxidation at high rates occurs when reactor operates under fuel-lean condition, suggesting that adsorption affinity of ethylene to the gold surface is stronger than for oxygen. However, on the fuel-rich side, the rate limiting step is the adsorption of oxygen because the oxygen coverage is scarce.

Conducting experiments with in-situ Fourier transform infrared spectroscopy (FTIR) is recommended. In-situ FTIR can be used along with gas chromatograph to provide infrared spectrum of the sample, which would provide exact compositions of the product at higher precision than the gas chromatograph. This technique would be useful for determining transient behavior of the ethylene oxidation reaction, which might be helpful in determining the exact mechanism behind the EPOC.

8.4 Electrochemical Promotion of C_2H_4 Complete Oxidation with Gold Nanoparticle Catalyst

Ethylene oxidation under closed circuit conditions is carried out with Au1/YSZ-p in Chapter 7. Evident increase in ethylene conversion proves that the electrochemical promotion of gold nanocatalysts can be achieved through bipolar configuration. When sufficient constant potential is applied, maximum conversion for ethylene has increased approximately 70 to 80% with maximum rate enhancement ratio and Faradaic efficiency of 1.79 and $6.5x10^5$, respectively. Contrast to the mechanism proposed by Xia et al. [18, 19], the proposed mechanism explains the wireless EPOC phenomenon through formation of O^{2-} ion concentration gradient across the electrochemical cell. The flux of O^{2-} ions in solid electrolyte allows backspillover of ions to form double layer on the gas exposed surface of Au nanoparticles, resulting in a change in work functions. The feasibility of electrochemical promotion of Au nanoparticles supported on YSZ powder in the bipolar cell configuration for complete oxidation of ethylene has been successfully demonstrated for the first time in this chapter.

In order to quantify the contributions from Faradaic reaction and non-Faradaic reaction, using isotopically labelled oxygen ($^{18}O_2$) as reactant gas and analyzing the product by in-situ mass spectroscopy is recommended. Using $^{18}O_2$ as reactant gas would lead to forming of CO_2 with different masses of oxygen, which are due to Faradaic reaction (^{16}O from YSZ) and non-Faradaic reaction (^{18}O from $^{18}O_2$) [18, 19].

8.5 **Reference**

[1] T. Kobayashi, *et al.*, "A selective CO sensor using Ti-doped α-Fe2O3 with coprecipitated ultrafine particles of gold," *Sensors and Actuators,* vol. 13, pp. 339-349, 1988.

[2] M. Haruta, *et al.*, "Gold catalysts prepared by coprecipitation for low-temperature oxidation of hydrogen and of carbon monoxide," *Journal of Catalysis,* vol. 115, pp. 301-309, 1989.

[3] M. Haruta, "Size- and support-dependency in the catalysis of gold," *Catalysis Today,* vol. 36, pp. 153-166, 1997.

[4] G. C. Bond and D. T. Thompson, "Catalysis by Gold," *Catalysis Reviews - Science and Engineering,* vol. 41, pp. 319-388, 1999.

[5] M. A. P. Dekkers, *et al.*, "Supported gold/MOx catalysts for NO/H2 and CO/O2 reactions," *Catalysis Today,* vol. 54, pp. 381-390, 1999.

[6] D. Thompson, "A golden future for catalysis," *Chemistry in Britain,* vol. 37, pp. 43-44, 2001.

[7] M. Haruta, "When gold is not noble: Catalysis by nanoparticles," *Chemical Record,* vol. 3, pp. 75-87, 2003.

[8] N. Lopez, *et al.*, "On the origin of the catalytic activity of gold nanoparticles for low-temperature CO oxidation," *Journal of Catalysis,* vol. 223, pp. 232-235, 2004.

[9] H. G. Ahn, *et al.*, "Complete oxidation of ethylene over supported gold nanoparticle catalysts," *Journal of Nanoscience and Nanotechnology,* vol. 6, pp. 3599-3603, 2006.

[10] M. Jia, *et al.*, "Preparation of Au/CeO2 catalyst and its catalytic performance for HCHO oxidation," *Journal of Rare Earths,* vol. 26, pp. 528-531, 2008.

[11] L. Q. Nguyen, *et al.*, "Performance of nano-sized Au/TiO2 for selective catalytic reduction of NOx by propene," *Applied Catalysis A: General,* vol. 347, pp. 94-99, 2008.

[12] M. Chun Yan, *et al.*, "Mesoporous co3o4 and AU/CO3o4 catalysts for low-temperature oxidation of trace ethylene," *Journal of the American Chemical Society,* vol. 132, pp. 2608-2613, 2010.

[13] Y. Zhang, *et al.*, "Gold catalysts supported on the mesoporous nanoparticles composited of zirconia and silicate for oxidation of formaldehyde," *Journal of Molecular Catalysis A: Chemical,* vol. 316, pp. 100-105, 2010.

[14] M. Marwood, *et al.*, "Electrochemical promotion of electronically isolated and dispersed Pt catalysts," *Ionics,* vol. 4, pp. 207-214, 1998.

[15] C. Pliangos, *et al.*, "Electrochemical promotion of conventional and bipolar reactor configurations for NO reduction," *Ionics,* vol. 8, pp. 372-382, 2002.

[16] D. Tsiplakides and S. Balomenou, "Milestones and perspectives in electrochemically promoted catalysis," *Catalysis Today,* vol. 146, pp. 312-318, 2009.

[17] S. Wodiunig, *et al.*, "Electrochemical promotion of bipolar electrodes: An estimation of the current bypass," *Electrochimica Acta,* vol. 46, pp. 357-363, 2000.
[18] C. Xia, *et al.*, "Electrochemical promotion of CO combustion over non-percolated Pt particles supported on YSZ using a novel bipolar configuration," *Electrochemistry Communications,* vol. 13, pp. 99-101, 2011.
[19] C. Xia, *et al.*, "Quantifying electrochemical promotion of induced bipolar Pt particles supported on YSZ," *Electrochemistry Communications,* vol. 12, pp. 1551-1554, 2010.
[20] S. R. Wang and W. J. Tseng, "Aggregate structure and crystallite size of platinum nanoparticles synthesized by ethanol reduction," *Journal of Nanoparticle Research,* vol. 11, pp. 947-953, 2009.
[21] M. N. Martin, *et al.*, "Charged gold nanoparticles in non-polar solvents: 10-min synthesis and 2D self-assembly," *Langmuir,* vol. 26, pp. 7410-7417, 2010.
[22] C. G. Vayenas, *et al.*, "The role of PtOx in the isothermal rate oscillations of ethylene oxidation on platinum," *Journal of Catalysis,* vol. 67, pp. 348-361, 1981.

List of Abbreviations and symbols

1. List of acronyms

AC	alternating current
ALD	atomic layer deposition
BSE	back-scattered electrons
CE	counter electrode
CVD	chemical vapor deposition
EPA	environmental protection agency
fcc	face-centered cubic
FWHM	full width at half maximum
HRTEM	high-resolution transmission microscopy
IAQ	indoor air quality
LCVD	laser-stimulated chemical vapor deposition
MSI	metal support interaction
NP	nanoparticle
PECVD	plasma enhancement chemical vapor deposition
PEEM	photoemission electron microscopy
PMVE	poly(methylvinylether)
PVA	polyvunyl alcohol
RE	reference electrode
rls	rate limiting step
STM	scanning transmission microscopy
THPC	tetrakis(hydroxymethyl)phosphonium chloride
TOF	turnover frequency
tpd	three phase boundary
VOC	volatile organic compound
WE	working electrode

2. List of Roman symbols

Symbols	Definitions	Units
a_{au}	surface area of one Au atom	2.29 x 10-19 m^2 $atom^{-1}$
d_{avg}	average atomic diameter	m
e	electron charge	1.6 x 10^{-19} C
E_a	catalytic activation energy	kJ mol^{-1}
E_C	energy at bottom of the conduction band	eV
E_F	Fermi level	eV
E_g	energy gap	eV
E_v	energy at top of the conduction band	eV
E_∞	vacuum energy	J
F	Faraday constant	96484.6 C
I	current	A
k	reaction rate constant	s^{-1}
K	Scherrer constant	0.89
k_b	Boltzmann constant	1.380 x 10^{-23} J K^{-1}
MW	molecular weight	g mol^{-1}
N_a	Avogadro's number	6.022 x 10^{23} atom mol^{-1}
n_{tot}	total number of Au moles in the catalytic reactor	Mol
P	partial pressure	Pa
r	catalytic rate	mol s^{-1}
R	gas constant	8.31441 J K^{-1} mol^{-1}
r_o	catalytic rate under open circuit condition, I=0	mol s^{-1}
T	temperature	K
U_{WR}	catalyst potential	V
V_b	attractive potential	eV
Z	atomic mass	g $atom^{-1}$
z_i	charge number	-

Symbols	Definitions	Units
α	NEMCA coefficient	-
α_e	real potential	kJ mol^{-1}
β	full width at half maximum (FWHM)	^{0}
θ	Bragg angle	^{0}
θ_i	surface coverage of reactant i	-
Λ	Faradaic efficiency	-
λ	x-ray wavelength	m
μ_e	chemical potential	kJ mol^{-1}
$\overline{\mu}_e$	electrochemical potential of electron	kJ mol^{-1}
ρ	rate enhancement ratio	-
ρ_{Au}	density of gold	19.43 g cm^{-3}
τ	grain size	m
Φ	work function	eV
ϕ	Galvani (inner) potential	V
χ	surface potential	V
χ_s	electron affinity	eV
Ψ	Volta (outer) potential	V